POLITECNICO DI TORINO

Corso di laurea magistrale
in Ingegneria Energetica e Nucleare

Tesi di Laurea Magistrale

Numerical modelling of HySun, an innovative hybrid air treatment technology within RE-COGNITION project

Relatori

Prof. Marco Simonetti
Dott. Vincenzo Maria Gentile
Dott. Francesco Neirotti

Candidato

Francesca Grillo

Anno Accademico 2020-2021

Abstract

The building sector has a remarkable importance on the overall EU final energy consumption and CO_2 emissions (with a share of 40% and 36% respectively), with about a third of the buildings constructed more than 50 years ago, meaning low energy efficiency and little or no renewable energy sources exploited. Simultaneously, EU has set challenging goals to achieve by 2030: curtailment of greenhouse gas emissions by, at least, 40% (with respect to 1990 levels), growth of the renewable energy share to 32%, improvement in energy efficiency by 32.5%. In order to improve the actual situation moving towards the targets set by EU, RE-COGNITION, a Horizon 2020 project, presents a solution which aims at employing on a large-scale Renewable Energy Sources (RES) in buildings, reaching zero-energy, or even energy positive buildings. One of the main objectives of RE-COGNITION project is to propose cutting-edge technology innovations using RES. This thesis will focus on one of the technologies presented in the project: HySun, a solar hybrid air cooling technology based on adsorption process. The core of the system is a finned heat exchanger coated with silica-gel, which exploits the desiccant material adsorption capacity to capture water vapor from air, dehumidifying it. When the adsorption process is terminated, silica-gel needs to be regenerated by supplying heat, which can be provided by a wide range of technologies (such as solar thermal collectors, heat pump, waste heat, district heating system). In this thesis, a numerical model of the adsorption heat exchanger is built by defining the energy and mass balances between the species involved in the process. Afterwards, the model is implemented on MATLAB in order to be able to simulate different working conditions. Firstly, a parametric study is carried out with the aim of understanding how the system performance varies with different operative conditions and configurations. Subsequently, dynamic simulations are accomplished with the purpose of analyzing the system performance in a real operating environment.

Ringraziamenti

Ci tengo a ringraziare il professor Marco Simonetti per avermi dato la possibilità di lavorare a questa tesi, Vincenzo Gentile e Francesco Neirotti per la loro grande disponibilità e per avermi aiutato nello svolgimento del lavoro.
Inoltre, un grazie particolare va ai miei genitori e a Enrico, che mi hanno dato la possibilità di intraprendere questo lungo percorso universitario e mi hanno sempre sostenuta.
Voglio, poi, ringraziare Andrea perchè insieme abbiamo affrontato tutti i momenti felici e difficili che questo percorso ci ha riservato.
Grazie anche alle mie compagne di corso Fabrizia, Erica, Greta e Cristina con cui ho condiviso i banchi delle aule e tante giornate al Politecnico.
Infine, un grazie va alle mie amiche di sempre Valeria, Elisa, Martina, Francesca e Martina con mi sono sempre potuta confrontare e che mi hanno sempre supportata durante questi anni.

Contents

List of Figures

List of Tables

Nomenclature

ΔP	pressure drop (Pa)
$\dot{G}$	mass transfer rate $(kg\ m^{-3}\ s^{-1})$
$\dot{m}$	mass flow rate $(kg\ s^{-1})$
$\dot{Q}_{cool}$	cooling power (W)
$\dot{V}$	volumetric flow rate $(m^3\ s^{-1})$
$\dot{W}_{el}$	electric power (W)
A	area (m^2)
a	specific area $(m^2\ m^{-3})$
A_o	minimum free flow area (m^2)
A_{hx}	heat exchange area (m^2)
COP_{el}	electric coefficient of performance (-)
COP_{th}	thermal coefficient of performance (-)
d_h	hydraulic diameter (m)
d_i	pipes inner diameter (m)
D_m	molecular diffusivity $(m\ s^{-1})$
D_o	surface diffusion constant $(m\ s^{-1})$
d_o	pipes outer diameter (m)
D_s	surface diffusivity $(m\ s^{-1})$

D_{eff} effective diffusivity ($m\ s^{-1}$)

D_{kn} Knudsen diffusivity ($m\ s^{-1}$)

dv Infinitesimal volume (m^3)

dz Infinitesimal length (m

e enthalpy ($J\ kg^{-1}\ K^{-1}$)

f friction factor (-)

h convective heat transfer coefficient ($W\ m^{-2}\ K^{-1}$)

h_m convective mass exchange coefficient ($kg\ m^{-2}\ s^{-1}$)

H_{ads} heat of adsorption ($J\ kg_w^{-1}$)

k thermal conductivity ($W\ m^{-1}\ K^{-1}$)

K_f mass transfer coefficient ($m\ s^{-1}$)

K_g overall mass transfer coefficient ($kg\ m^{-2}\ s^{-1}$)

L_p pipes length (m)

L_x adsorption battery width (m)

L_z adsorption battery height (m)

L_z adsorption battery length (m)

N_p number of pipes (-)

Nu Nusselt number (-)

P pressure (Pa)

p_f fin pitch (m)

R gas constant ($JK^{-1}mol^{-1}$)

r_p average pore radius (m)

Re Reynolds number (-)

RH relative humidity (-)

Sc Schmidt number (-)

Sh Sherwood number (-)

T temperature ($°C$)

t time (s)

t_s silica-gel layer thickness (m)

U global heat transfer coefficient ($W\ m^{-2}\ K^{-1}$)

v velocity ($m\ s^{-1}$)

W water uptake ($kg_w\ kg_s^{-1}$)

x specific humidity ($kg_v\ {kg_a}^{-1}$)

X_l longitudinal fin pitch (m)

X_t transversal fin pitch (m)

V volume (m^3)

Greek letters

α ratio of heat exchange area on air side to heat exchanger volume (m^{-1})

β friction factor (-)

η efficiency (-)

μ dynamic viscosity ($Pa\ s$)

ρ density ($kg\ m^{-3}$)

σ ratio of minimum free flow area to frontal area (-)

τ_s tortuosity factor (-)

ε porosity (-)

Subscripts

a air

b adsorption battery

o	initial condition
s	silca-gel
w	water

Chapter 1

Introduction

Buildings constitute one of the main sector in terms of CO_2 emissions and energy consumption worldwide. Buildings energy-related CO_2 emissions have lately increased after smoothing between 2013 and 2016. As reported by [19], direct and indirect emissions from electricity and commercial heat used in buildings reached 10 $GtCO_2$ in 2019, the highest of all times, covering a share of 28 % of global energy-related CO_2 emissions (38 % if considering also the building construction industry). This result depends on multiple factors, such as the continued use of fossil fuels together with higher activity levels in regions in which the electricity is still carbon-intensive (bringing to an increase in indirect emsissions), extreme weather events, increment in air-conditioners ownership, which led to a higher energy demand for both heating and cooling. In fact, final energy use in buildings increased from about 118 EJ in 2010 to 128 EJ in 2019, which represents the 30 % of global final energy use (35 % if buildings construction industry is included)[28].

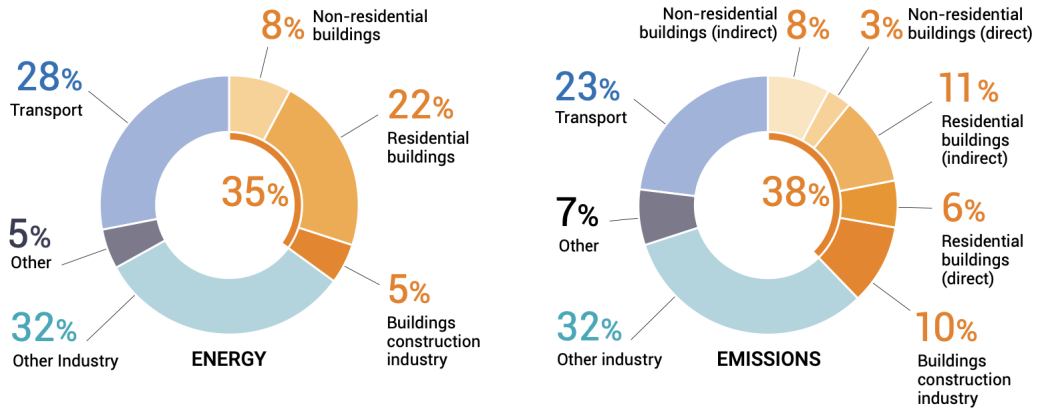

Figure 1.1: Global share of buildings and construction final energy and emissions, 2019 [28]

As previously mentioned, one of the main causes of the rise of CO_2 emissions and energy consumption is space cooling.
The energy demand for space cooling has had a great escalation throughout the years, in fact, it has more than tripled since 1990. In 2019, space cooling caused emissions of about 1 $GtCO_2$ and almost 8.5 % of total final electricity consumption and this growth is destined not to stop, since it is expected that the population will increase, the living standards will improve and heatwaves will be more recurrent and severe. According to [18], the number of air conditioners installed could increase by other two-thirds within 2030.
In order to limit the emissions and the energy consumption related to space cooling, high efficient equipment have to be used, otherwise, an increase of about 50% in electricity demand for cooling is expected by 2030.
Moreover, measures have been taken from country to country with the purpose of mitigating the impact of cooling on climate change, even if, in regions in which a fast cooling demand increase is expected, performance standards of cooling systems are absent or so.

1.1 Space cooling: State of the art

1.1.1 Vapor compression refrigeration cycle systems

The vapor compression refrigeration system is the most used technology for cooling systems thanks to high values of efficiency (COP), low quantities of refrigerant needed in order to remove large quantities of heat which means lower costs [40]. The cycle is based on four main stages, as can be seen in Figure 1.2.

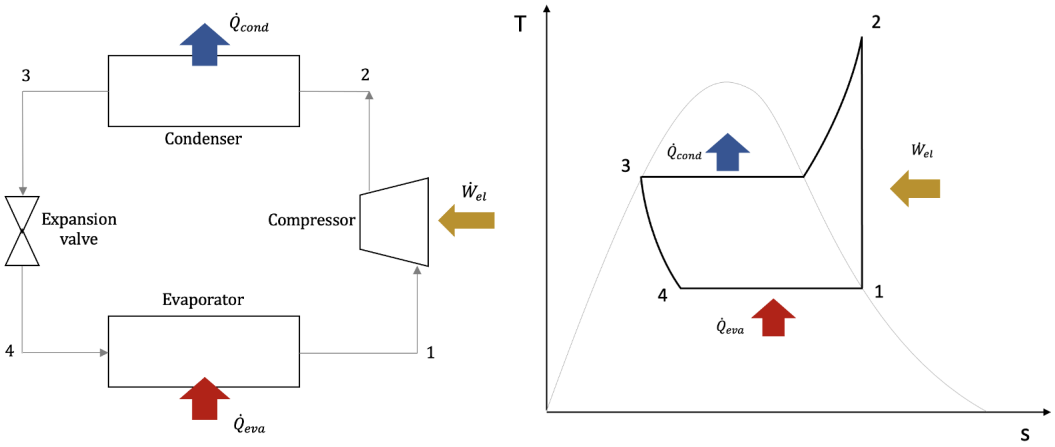

Figure 1.2: Vapor compression refrigeration cycle scheme and T-s diagram

The first step is the compression (1-2), during which, providing external work, the refrigerant, in the form of gas, is brought to higher pressure and temperature levels. Afterwards, the fluid is subjected to condensation (2-3), releasing heat to a warmer region and becoming liquid, and then, it passes through an expansion valve (3-4) lowering its pressure and, consequently, its temperature. Finally, the refrigerant enters the evaporator and starts absorbing heat from the air. At the end of the evaporation stage, the fluid exits the evaporator as lower-pressure vapor and is redirected to the compressor, so the cycle can restart. It is important to notice that the diagram reported in Figure 1.2 refers to an ideal cycle, in fact, it represents two isobaric transformations (condensation and evaporation), an isentropic transformation (compression) and an isenthalpic one. The real cycle is slightly different, since it is characterized by losses due to irreversibility and those, numerically less significant, caused by pressure drops in the ducts and the in the heat exchangers [25].

1.1.2 Evaporative cooling systems

The evaporative cooling systems are widely used in Middle East and Persian buildings, since this kind of technology is suitable in hot and dry climates. There are two types of evaporative cooling systems: direct and indirect systems. The first ones are based on the evaporation of liquid water through the hot ambient air. The hot dry ambient air stream flows through a wet surface made of a porous media containing water, makes the water evaporate, and exits the system as a wet cool air stream. The process is adiabatic, so, the sensible heat lost by the air is compensated by the latent heat coming from the water evaporation. Obviously, the efficiency of the system is closely related to the air wet bulb temperature. Normally a decrease in temperature of 2-3 °C is obtained.

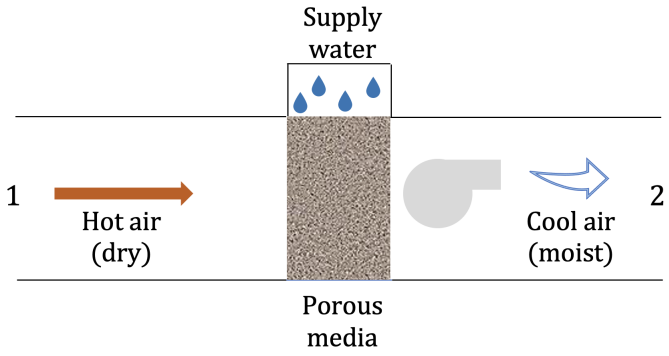

Figure 1.3: Direct evaporative cooling system

In the indirect systems, instead, the air flow passes through the so-called "dry channel", along which it cedes heat to an adjacent "wet channel" through a thin non-permeable channel wall, staying dry, and entering the room. A portion of the air flow is conveyed to the "wet channel" in order to make the evaporation process possible. Differently from the direct systems, the indirect ones allow to maintain the same content of moisture in the air [5].

1.1.3 Sorption refrigeration systems

Such systems are divided into:

- Closed sorption cycle systems: the environment and the thermal source can only exchange heat with the system. Absorption and desorption refrigeration systems belong to this category.
- Open sorption cycle systems: the environment and the thermal source exchange both heat and mass with the system. The main application is the desiccant cooling.

Absorption refrigeration systems

Absorption refrigeration systems differ from the traditional vapor compression ones because the cooling effect is not obtained through mechanical work, but, using heat, which can be found at very low price or even for free (solar energy, waste heat).
For applications such as air conditioning, in which chilled water is above 0 °C, typically, a liquid solution composed by water and lithium bromide is used with water as refrigerant.
The absorption chillers are composed by the following four principal components: the evaporator, the absorber, the generator and the condenser. The cooling effect is based on the evaporation of the refrigerant (water) in the evaporator at very low pressures due to the heat released by the water of the fan coils that needs to be chilled since it represents the cooling load.
At the end of this stage, the refrigerant (water), in the form of vapor, is directed to the absorber, where it dilutes the H20/LiBr strong solution coming from the generator. In this phase heat has to be removed, so, cooling water coming from cooling towers is used. The result is a weak solution which is pumped into the generator where is regenerated by applying heat through hot water coming, for examples, from solar collectors.

Then, the water vapor is extracted and sent to the condenser, in which cooling water makes the vapor condensate. Finally, the refrigerant (water) is sent again to the evaporator to restart the cycle [33].
These systems are characterized by lower performances compared to the vapor compression cycle but have some advantages such as the utilization of thermal energy instead of mechanical/electrical one which translates into lower costs, a noise-free system and a minimization of electricity consumption and of the overall impact on the environment, since they can use renewable energies as heat source.

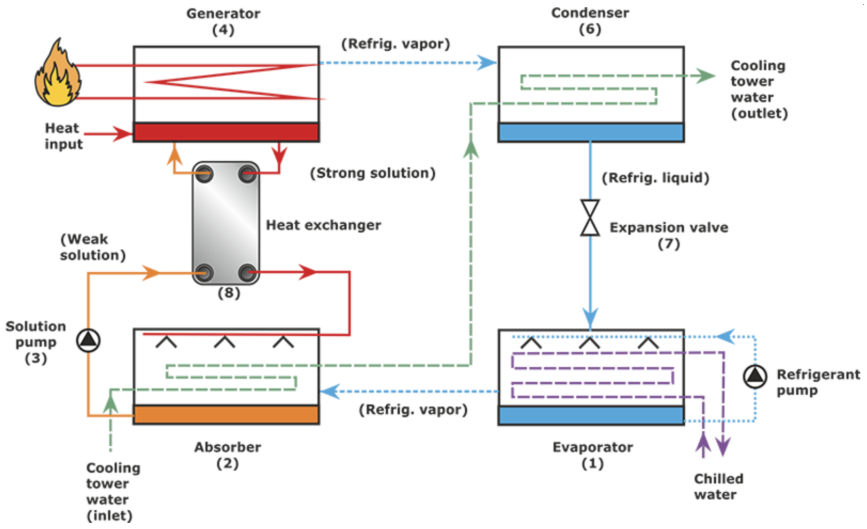

Figure 1.4: Absorption chiller scheme [37]

Adsorption refrigeration systems

The adsorption chillers are systems which use a refrigerant fluid and a solid or liquid sorption material. The commercial systems typically use water as refrigerant and silica gel as adsorbent. As can be seen in Figure 1.5, there are two parallel adsorption chambers. In the first one, the adsorption process takes place, which means the water vapor, contained in the stream passing through the chamber, is adsorbed by dry silica gel. In this phase, heat has to be removed from the chamber since the adsorption process is exothermic, so, water coming from a cooling tower is used.
In the second adsorption chamber, the adsorbent is rich in water and so regeneration occurs. In fact, the water contained in silica gel pores is desorbed by applying heat released by hot water flowing into a heat exchanger. Then, the water vapor is directed to the condenser where it releases heat to the cooling water. Afterwards, the condensed water is conveyed to the evaporator by mean of a throttling valve which lowers the fluid pressure, and it evaporates extracting heat from the chilled water circuit. This last process is the basis of the cooling effect of the system.

The advantage of such systems is that the heat needed to regenerate the adsorbent can be provided, for examples, by hot water heated up through solar collectors or through waste heat. Moreover, the driving temperature of the process, the regeneration temperature, is low, working in the range of 50-90 °C. This aspect allows to increase the number of sources which can supply heat.

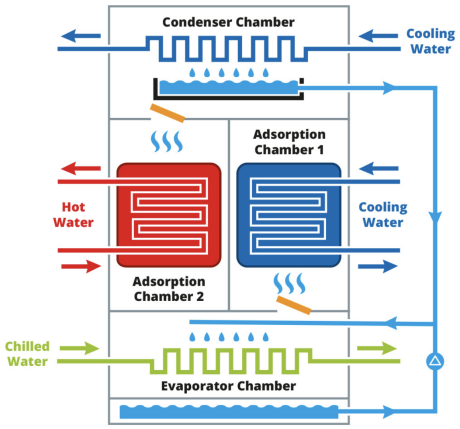

Figure 1.5: Absorption chiller scheme [34]

Desiccant cooling systems

These kind of systems exploit the characteristic of desiccant materials to remove water vapor from the air, lowering its moisture content. For this reason, these systems are convenient for building in areas with high humidity climates. Moreover these systems permit to make use of renewable energy sources or waste heat to drive the cooling cycle.
The main component of such systems is the desiccant wheel composed by two portions: a hygroscopic (or treatment) area and a regeneration one. Having two different processes (sorption and regeneration) occurring, two separate air streams are necessary. One is composed by air that needs to be dried before entering the indoor environment (process air), while, the other stream, flowing in the opposite direction, is that of the regeneration air.
The process air is fresh humid air taken from the external ambient, which, after passing through the desiccant wheel, becomes warm and dry. At this point, it can be cooled by using a heat exchanger (evaporator) and, then, sent to the indoor ambient.
The regeneration air is coming from the external ambient as well, and it usually needs to be heated up through a heat exchanger (condenser) before entering the

desiccant wheel. In fact, it is necessary that the regeneration air is at a temperature such as to allow the evaporation of the vapor condensed on the desiccant material [1].

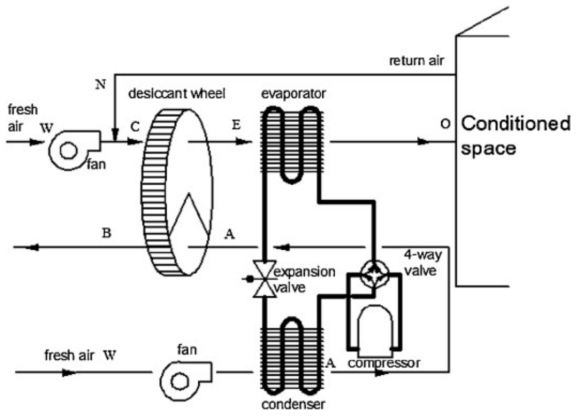

Figure 1.6: Desiccant wheel cooling system scheme [32]

1.2 The RE-COGNITION project

Focusing, now, on the European Union framework, the building sector is responsible for about 40% of the energy consumption and 36% of CO_2 emissions in the EU. One of the main reasons of this data can be addressed to the fact that about 30% of buildings in Europe have been constructed more than 50 years ago, meaning old systems are installed and little or no renewable energy sources are exploited.
But, on the other hand, EU has set challenging goals to achieve by 2030: curtailment of greenhouse gas emissions by at least 40% (from 1990 levels), growth of the renewables share to 32%, improvement of energy efficiency by 32.5% [10].
The only way possible to reach this targets is to implement new technologies, together with the introduction of strong policies, with the aim of encouraging investments for renewable energy technologies integration in buildings.

The RE-COGNITION project, part of Horizon 2020, has started from the challenge just explained, proposing a solution which, as stated in [29], "stands as an ICT integration framework, on-top of established and newly developed, innovative RE-based technologies, representing a highly inter-disciplinary concept for empowering the transition towards a renewable building landscape."

This means, it is a solution that aims at employing, on a large scale, Renewable Energy Sources (RES) in buildings, reaching zero-energy, or even energy positive buildings, which translates into reduction of greenhouses gases emissions and a higher share of renewables.
In order to do so, the project proposes a Renewable Energy Integration Framework capable of seamlessly putting together renewable energy sources systems, including both variable renewable energy sources (VRE), such as solar and wind, and dispatchable energy sources like bio-gas or geothermal, storage components and the load, thermal and electrical, represented by HVAC, chillers, EV chargers, etc.
It has to be considered that the load is different from building to building and varies along the day, so, the Integration Framework has to fulfill the user's electricity, heating, cooling and hot water demand whenever it is requested.

The project is based on the following two main ideas:

1. Development of Cross-Functional RES Integration Platform, constitued by the Automated Cognitive Energy Management Engine (ACEME) and the intelligent Gateway (iGateway), in order to efficiently exploit the energy coming from the RES according to the load necessity, storage state and grid conditions;

2. Advancement with respect to the ongoing State of the Art, on novel renewable technologies (Building Integrated Photovoltaics, Vertical-Axis Variable Geometry Wind Turbine) and more mature ones such as micro-CHP based on biogas, together with system peripherals like latent-heat thermal storage and hybrid system, solar cooling.

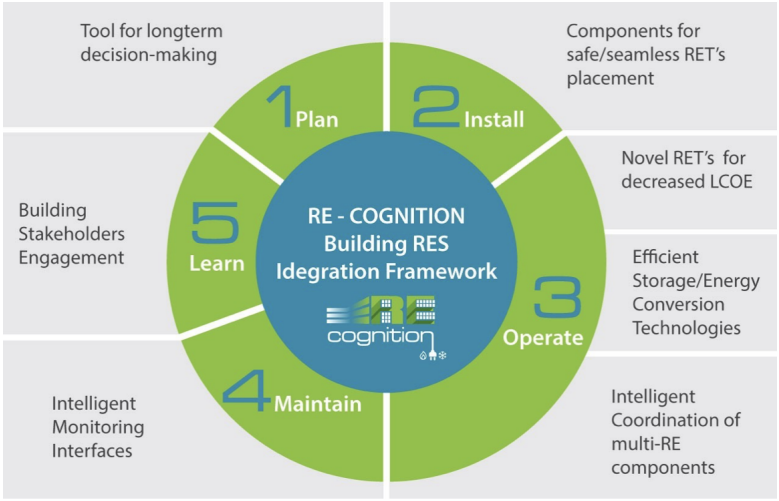

Figure 1.7: Enhancing RETs Integration through RE-COGNITION [29]

But, more specifically, the objectives of RE-COGNITION project are to:

- Develop an ICT-based Automated Cognitive Engine, which will control, predict, monitor and optimize the energy demand and supply sub-systems in order to leverage the RES deployment and building self-consumption;
- Propose cutting-edge technology innovations using RES, for European buildings;
- Improve interoperability, resiliency and scalability;
- guarantee optimal integration planning of RES and subsystems, using a tool (BE-PLATO), which involves a multi-objective optimization process based on the investment costs minimization and self-consumption maximization;
- Small-scales Testing and Validation of the components in close-to-real life conditions;
- Create and evaluate customer-centric business models;

1.2.1 HYSun: Hybrid Unit for Solar Cooling purposes

This thesis work will focus on one of the technologies included in the RE-COGNITION project: HYSun, a solar hybrid cooling technology.
As explained before, the cooling demand has risen significantly in the last years and it is going to increase even more in the near future. It has also already been said that the electricity consumption related to space cooling, is substantial, so, thermally driven technologies could be a great solution, in order to avoid peaks in electricity demand, leading to stress into the grid, and maximize the RES utilization. Concerning thermally driven technologies, solar dehumidification processes (open loop cycles), are deemed to be one of the most effective and convenient solutions.
The HYSun technology has two main purposes:

1. Improve efficiency with respect to the traditional compression cycles;
2. Use different sources to produce the required cooling power.

This technology is based on adsorption/desorption process, which exploits micro and macro porous materials in order to uptake water vapour from external ambient air (dehumidification) and lower its temperature, in order to meet the indoor required conditions.
The driving heat can be supplied by different sources such as solar thermal collectors,

cogeneration plants and waste heat. The lower is the temperature required for material regeneration, the higher is the number of the technologies that can be exploited.

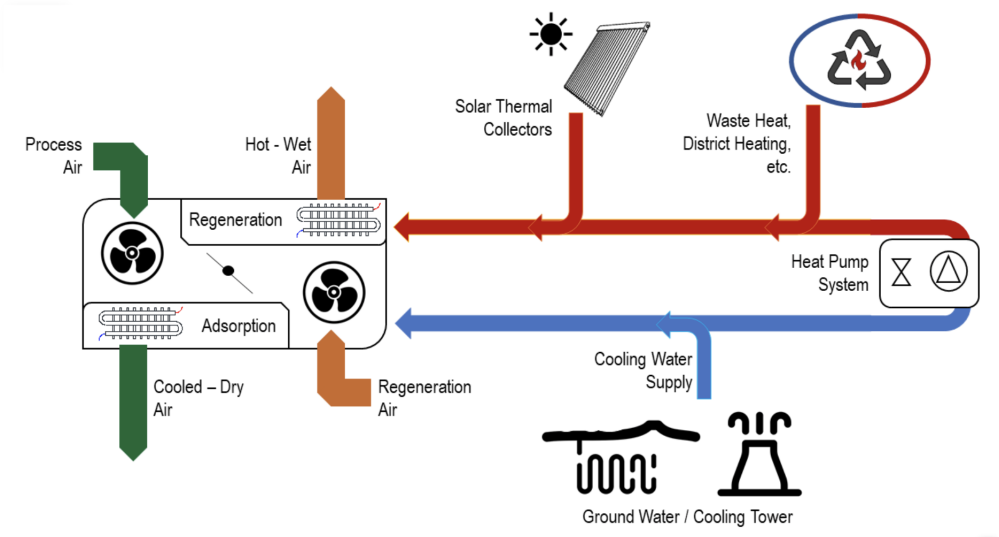

Figure 1.8: Block diagram of the Solar Hybrid Cooling System HYSun [30]

The configuration showed in Figure 1.8, represents the one available in the pilot site of the Energy Center in Turin, which comprehends a heat pump (HP) system, a solar thermal collector field and district heating (DH) system in parallel. This means that if there is an excess of electricity production from, for example, a local photovoltaic system or from the grid, the heat pump system can be used. Instead, if there is an excess of production from the solar collectors or from the district heating system, the HP can be switched off and the regeneration heat can be supplied by these sources.
In order to improve the system flexibility, thermal storage for cold and hot power can be added. Moreover, control systems will be introduced with the aim of managing the different sources and technologies integrated in the system.

Chapter 2

Adsorption

2.1 Fundamentals

Adsorption is a separation phenomenon whereby the surface of a solid substance, called adsorbent, fixes molecules coming from a gaseous or a liquid phase with which it is in contact. It is a spontaneous process, which means it goes along with a decrease in the free energy of the system; so, the process is exothermic, and the heat developed in the adsorption of one mole is called heat of adsorption.
There are two types of adsorption: physical adsorption, involving weak intermolecular forces, and chemical adsorption (or chemisorption), relating to chemical bonds. Physical adsorption is the most widespread along adsorptive separation processes and it is the one considered in this work.
The main forces taking place between the adsorbate and the adsorbent are the van der Waals forces; there are also electrostatic interactions, but they can be considered negligible in almost all the cases (they are significant in adsorption processes using zeolites as adsorbent), since they are present to a lesser extent.

Analyzing the intermolecular interaction, there are attractive and repulsive forces between two molecules. The attractive potential due to dispersion forces, can be expressed as:

$$\phi_D = -\frac{A_1}{r_{12}^6} - \frac{A_2}{r_{12}^8} - \frac{A_3}{r_{12}^{10}} \tag{2.1}$$

where r_{12} is the distance between the molecules and A_1, A_2, A_3 are constants. The terms of this expression represent, respectively, interactions between instantaneous induced dipoles, induced dipole-induced quadrupole and induced quadrupole-induced quadrupole. The repulsive potential, instead, occurs when the two molecules

are very close to each other and can be formulated as:

$$\phi_R = -\frac{B}{r_{12}^{12}} \tag{2.2}$$

where B is a constant. Through the Lennard-Jones potential, the attractive and the repulsive contributions are considered together (taking only the first term of the attractive potential expression, since it is the prevalent one), in order to have a single formulation to express the overall potential between two molecules as a function of their mutual distance [31]. The result is the following formulation:

$$\phi = V(r) = 4\epsilon \left[\left(\frac{\sigma}{r}\right)^{12} - \left(\frac{\sigma}{r}\right)^{6} \right] \tag{2.3}$$

where ε is the potential well depth, which corresponds to the equilibrium between attractive and repulsive forces. It indicates the strength of the attraction between the two particles. The symbol σ , instead, represents the distance between the two molecules at which the potential is equal to zero (intersection of the curve with the x-axis).

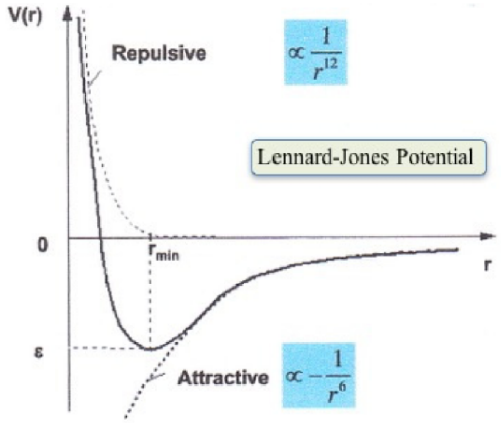

Figure 2.1: Lennard-Jones potential [17]

2.2 Thermodinamics of Adsorption

The analysis of the thermodynamics involving adsorption processes is based on the adsorption isotherms, that represent, at a fixed temperature, the load, which is the quantity of adsorbate on the solid (adsorbent) per unit mass of the solid itself, as a function of the relative pressure of the gaseous phase in equilibrium with the adsorbent at the set adsorption temperature.

According to the type of adsorbent material used and to the adsorbate involved in the process, the shape of the adsorption isotherm varies.
In conformity with IUPAC, in Figure 2.2 are illustrated the most important six isotherms, which represent both adsorption and desorption processes.

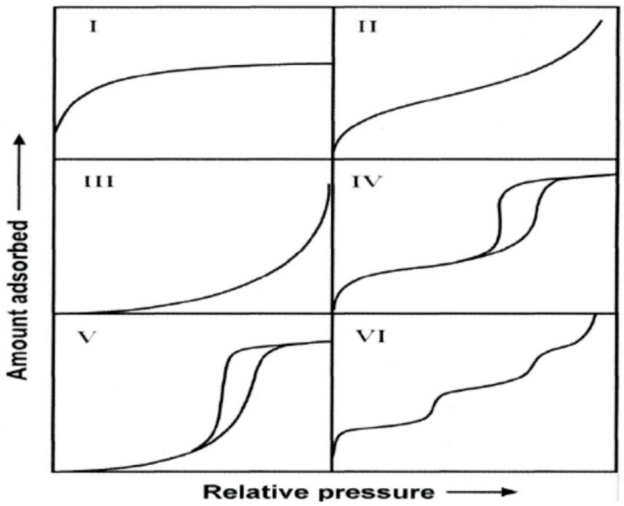

Figure 2.2: IUPAC Adsorption Isotherms [3]

It is possible to notice that, in some cases, the adsorption and the desorption curves do not coincide, meaning that hysteresis phenomenon occurs. Hysteresis typically takes place in adsorbent materials with pores larger than 2 nm [23].
In general, when the trend has an upward concavity, it signifies that the adsorbent material has a hydrophobic behavior, meaning it is necessary a large relative pressure increment to slightly increase the load. Instead, a downward concavity indicates a hydrophilic behavior, implying that rising the relative pressure a little bit, the load grows significantly. Finally, the isotherm could also show a linear trend.
Type I isotherm settles to a fixed value as the relative pressure increases; it is typical of microporous adsorbents. Types II and III isotherms are characteristic of macroporous materials and they differ from each other depending on the interaction strength between adsorbate and adsorbent (weak for Type II, strong for Type III) [13]. Types IV and V, instead, describe both monolayer and multilayer adsorption and are peculiar of mesoporous adsorbents and show hysteresis, due to capillary condensation. Generally speaking, hysteresis occurs, in equilibrium conditions, in pores of finite length. In fact, for such pores, the interface shape is supposed to be different during adsorption and desorption processes, and this causes hysteresis [12].
Type VI describes multilayer adsorption for non-porous materials [35].

2.3 Adsorption process models

2.3.1 Langmuir model

One of the models for the description of the adsorption process is the Langmuir model, which assesses the surface coverage in dynamic equilibrium conditions, balancing the relative rates of adsorption and desorption [4].
The model assumptions are the following:

- There is only one layer of adsorbate on the surface (monolayer adsorption);
- All the adsorption sites have the same energy;
- The process is reversible (both adsorption and desorption);
- The interactions between sorbate molecules are negligible.

The basic parameter of the Langmuir model is the coverage defined as the ratio between the occupied sites and the total number of sites available on the adsorbent surface.
This approach is a kinetic one, so, the process can be seen as a reversible reaction:

$$H_2O_{(g)} + \text{Free sites} \rightleftharpoons H_2O_{(l)} \tag{2.4}$$

The direct reaction represents the adsorption process (exothermic), while the inverse one the desorption process (endothermic). Both of them are associated with a reaction constant, useful in order to evaluate the reaction velocity. It is, then, defined an equilibrium constant, which is the ratio between the two single constants. Moreover, the equilibrium condition is realized when the adsorption velocity is equal to the desorption velocity. Basing on this definition of equilibrium between the two processes, it is possible to find the following law:

$$\theta(p,T) = \frac{H(T)p}{1 + H(T)p} \tag{2.5}$$

where

$$H(T) = \frac{K_{eq}}{RT} \tag{2.6}$$

which is a constant that for low coverage is precisely the Henry's constant, since the term $H(T)p$ at the denominator of the (2.9) is neglected (pressure tends to zero) and, so, the relation between the coverage and the pressure is linear.
The main drawback of Langmuir model is that it does not well describe the behaviour

of silica-gel at equilibrium (except for low coverage) because of its simplifying assumption of a homogeneous monolayer adsorption.

2.3.2 Dubinin-Polanyi model

The main idea behind this theory is that the porous material (adsorbent) is defined as a solid with a certain amount of available empty volume in the pores which can be filled by the adsorbate, considered as a continuous fluid. Consequently, the fundamental parameter at the core of the model is the specific volume of micropores, expressed as it follows:

$$W_0 = \frac{V}{m_{adsorbent}} \tag{2.7}$$

where V is the volume available for the adsorbate, and $m_{adsorbent}$ is the sorbent mass. The specific volume occupied by the adsorbate, instead, is given by:

$$W_s = \frac{V_{adsorbate}}{m_{adsorbent}} \tag{2.8}$$

Where $V_{adsorbate}$ is the volume occupied by the adsorbate. Under certain pressure and temperature conditions, it is possible to fill only a certain amount of volume. At the saturation pressure, the total volume is occupied so W_s is equal to W_0.
The variation of the free energy between the adsorbate in equilibrium with the adsorbent and the saturated fluid at a fixed temperature is named "adsorption potential" and it is formulated as:

$$A_{DB} = -\Delta g = -RT \ln \frac{p_s(T)}{p} \tag{2.9}$$

where $p_s(T)$ is the saturation pressure of the fluid and p is the equilibrium pressure of the adsorbed phase.
Each adsorbent-adsorbate pair is associated to a characteristic potential curve, since there is only one relation between adsorption potential and the volume of fluid adsorbed at a fixed temperature. Even if all the curves are different, there are analytical formulations for the characteristic curves. One of these is the Dubinin-Astakhov (DA) equation which is the following:

$$W = W_0 exp\left[-\left(\frac{RT \ln \frac{p_s(T)}{P}}{\gamma E_0}\right)^n\right] \tag{2.10}$$

where E_0 is the characteristic energy which depends only on the adsorbent, γ is the affinity constant depending on the adsorbate only, n takes count of the heterogeneity

of the pores. The interpretation of these fitting parameters is difficult and represent the biggest limitation of the DA equation [9].
Also the Dubinin-Polanyi model presents disadvantages. The main one is that this approach does not fit the Henry's Law, according to which, at low coverage, there is a linear relation between the adsorption capacity of the adsorbent and the pressure. Another drawback is that the estimation of the adsorbate molar volume is subject to significant uncertainty. Finally, the temperature-independent characteristic curve is not suitable for many systems [31].

2.4 Adsorbents

2.4.1 Silica gel

Silica gel is an incompletely dehydrated form of polymeric colloidal silicic acid. It is indicated as $SiO_2 * nH_2O$. It is produced synthetically starting from sodium silicate, and it comes as a granular, vitreous material, as can be seen in Figure 2.3.

Figure 2.3: Silica gel [6]

It is a highly porous material, in fact, it contains a large number of pores with diameter ranging from 2 to 20 nm and a porous volume between 0.35 and 1.15 cm^3/g. This characteristic allows such a material to present a very extent specific surface area that can go from 300 to 800 m^2/g.
The main advantages of this material that makes it a valid option for adsorption refrigeration systems are [26][14]:

- great water adsorption capacity up to 30-40% of its dry mass (in typical chiller working conditions);

- it can be regenerated at low temperatures ranging from 50 °C to 90 °C. This means it is possible to exploit a wider ranger of heat sources.

2.4.2 Zeolites

Zeolites are porous crystalline aluminosilicates. They are composed by SiO_4 and AlO_4 tetrahedra connected to each other through shared oxygen atoms forming a crystal lattice. This means that zeolites, having an ordered structure, are not characterized by a distribution of pore size. The Si/Al ratio in zeolites never goes under 1.0 but it has no upper limit. This characteristic makes the different types of zeolites starting from the aluminum rich sieves (hidrophilic) to silicalite, for example, which is hydrophobic. Generally, the zeolites which are hydrophobic are those with values of Si/Al ratio greater than or equal to 8-10 [31].
Common types of zeolites are the following:

- Type A: characterized by Si/Al ratio equal to 2-2.5, free diameters of 0.41 nm and specific surface of 800-1000 m^2/g;
- Type X and Y: have Si/Al ratio equal to 2-3, free diameters of 0.74 nm and specific surface of 800-1000 m^2/g [9].

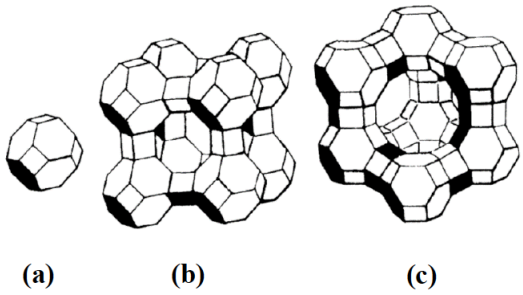

Figure 2.4: a) Primary unit of zeolites types A, X and Y; b) unit cell of zeolites type A; c) unit cell of zeolites types X and Y [8].

The desorption temperature needed is in the range 70-250 °C and the adsorption heat is higher than that of silica gel, bringing to lower COPs.

2.4.3 Activated carbon

Typically, it is derived from carbonaceous material through three phases: pelletization, carbonization and activation. This last process is made through steam or carbon dioxide at high temperatures between 700 °C and 1100 °C and is needed to

open the pores (micropores and mesopores). The structure obtained is composed by microcrystallites of graphite [31]. The main advantages of activated carbon are the following: the specific area and the pores volume are large, the regenerability is quite easy.
But, these materials are nonpolar, so, for water adsorption, they are not suitable as the other adsorbents [8].

2.4.4 Activated allumina

Activated alumina is obtained through dehydratation and recrystallization at high temperatures from bauxite or from the monohydrate. Compared to silica gel, at ambient temperature, the affinity for water is similar, while, at high temperatures it is stronger [31].

Figure 2.5: Activated carbon [7]

Figure 2.6: Activated alumina pellets [2]

The characteristic equilibrium adsorption isotherms for the adsorbent just presented, are shown in Figure 2.7.
The water uptake is indicated in terms of micro moles of water per unit surface of the adsorbent. The inserted graph represents the water uptake in terms of mass of water adsorbed per unit mass of adsorbent. The curves respectively refers to [39]:

- Curve A: zeolite (Type X);
- Curve B: silicaluminophosphate sieve;
- Curve C: activated alumina;
- Curve D: silica gel (at 28°C);
- Curve E: ionosilica (at 40°C);
- Curve F: activated carbon.

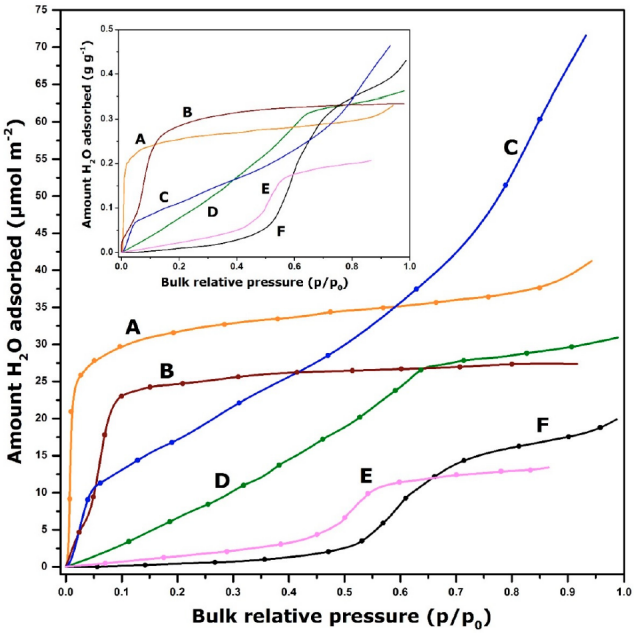

Figure 2.7: Typical equilibrium adsorption isotherms of water vapor for various adsorbent materials at 25°C [39]

Concerning the adsorbent materials previously presented, the equilibrium adsorption isotherm related to zeolite shows a trend similar to the Type I IUPAC adsorption isotherms already showed and discussed in Figure 2.2. In fact, it is characterized by a hydrophilic behaviour for low relative pressures, with a strong increase in water uptake; afterwards, as relative pressure rises, the curve flattens, meaning that, further increasing the relative pressure, the water uptake does not significantly change. Activated alumina, instead, exhibits a trend close to the one of Type II of IUPAC adsorption isotherms: except for the upward concavity corresponding to intermediate relative pressures, it shows strong affinity with water vapor.
Silica gel curve has an intermediate behaviour between IUPAC adsorption isotherms of Type I, IV and V: the water uptake increases almost linearly with the relative pressure until a certain point, then, the curve flattens, meaning that with higher relative pressure the growth of water uptake almost settles to a certain value.
Finally, the activated carbon adsorption isotherm is similar to the IUPAC Type V isotherm, with a trend which resembles a "S". It presents an upward concavity, corresponding to a hydrophobic behaviour, until intermediate values of relative pressure; then, the water uptake rapidly increases for low relative pressure increment, but, afterwards, the curve flattens.

Chapter 3

System description and Numerical Model

3.1 System description

The HYSun technology, as it has been previously explained, is based on a adsorption/desorption process, which allows to treat the air entering the indoor environment. So, the core of of such a system is the adsorption heat exchanger.

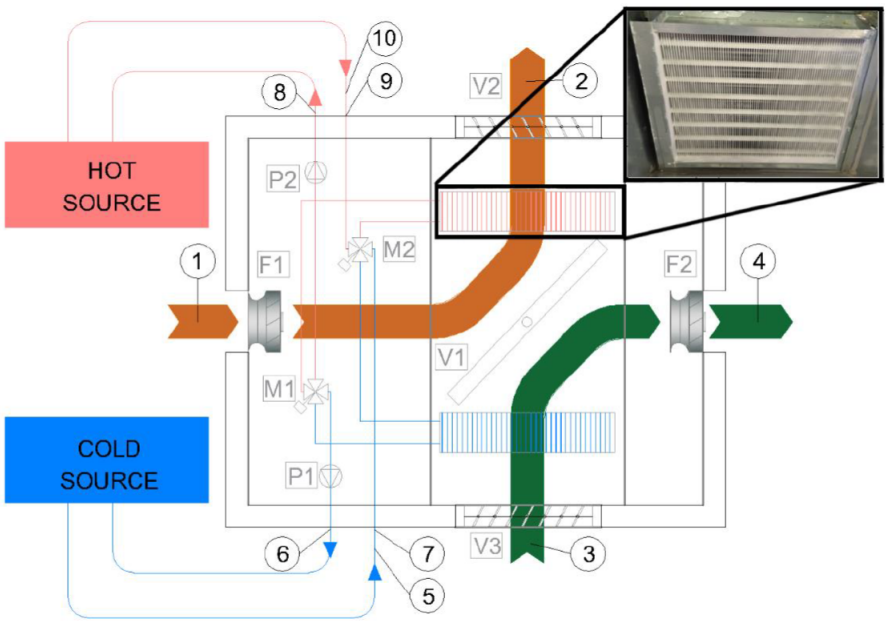

Figure 3.1: Adsorption module operating in batch mode [11]

As can be seen from Figure 3.1, the module is constituted by two adsorption batter-

ies placed in parallel, each of which consists of two finned coils coated with a silica gel layer with a thickness set to be equal to 0.55 mm.
When one of the batteries is working in adsorption mode, in the other one silica-gel is regenerated, removing the water vapor previously captured.
In both cases, the air flowing through the battery is taken from the external ambient, and it is conveyed to the battery thanks to a centrifugal fan (F1 is the regeneration fan, while F2 is the delivery fan). When the switch from one mode to another has to take place, the 4-way valve (V1) allows to change the two air flow directions. Concerning the air flows, also two other components have to be mentioned: the dumpers V2 and V3, which close the air loop when the system, or just one battery is not working.
Considering, now, the water loop, the water is sent to the pipes of the finned coil by using two pumps (P1 is the cold pump and P2 is the hot pump). Hot water (at a temperature level which can vary from about 50 to 90 °C) circulates between the hot source, representing the heat provided by the use of solar thermal collectors, latent heat storage, waste heat, district heating, or, as in the case analyzed, of the condenser of a heat pump, and the battery in regeneration mode. At the same time, cold water (which approximately ranges between 15-25 °C) circulates between the cold source, obtained from the integration in the system of ground water or an evaporative tower or, as in this case, the evaporator of a heat pump, and the battery working in adsorption mode. The 4-way valves M1 and M2 distribute, respectively, the delivery and the return water flows (hot and cold) to both the modules.
Finally, the numbers indicated in Figure 3.1, correspond to the sensors which measure the air temperature and relative humidity (1,2,3,4), the air velocity (1,3), the water temperature (6,7,8,9) and the water flow (5,10) [11].

3.2 Numerical model

The numerical model is built on mass and energy balances equations, considering the heat and mass exchanges between the main species involved: air, water vapor, silica gel and water flowing in the tubes.
In particular, mass transfer takes place between air, which contains the water vapor, and the adsorbent (silica gel). Heat transfers, instead, occur between all the species.

3.2.1 Assumptions

The assumptions on which the model is based are the following ones:

- the only species adsorbed and desorbed in the process is the water vapor;
- the heat of adsorption is generated within the pores of silica gel, since it derives from the water vapor condensation occurring inside them;
- there is an equilibrium condition close to the silica gel surface, since the adsorption phenomenon is faster than the diffusion one, so, it is possible to use the adsorption isotherms;
- it is a mono-dimensional model, which consider only the coordinate along with the air flow direction;
- the convective heat transfer mechanism is the dominant one, so, temperature gradients due to conduction in the flow direction are neglected;

3.2.2 Equations

After the assumptions are defined, it is possible to formulate the equations. As a reference, documents [20] and [15] are considered.
Afterwards, the analytical equations are implemented on MATLAB. In order to do so, both time and space domains need to be discretized. The time step chosen is equal to 1s (Δt=1s) and the method used to implement the time derivatives is the Backward Euler method, which is an implicit method that is defined as unconditionally stable, since the time step selected does not affect the convergence of the solution. So, defining n as the time step and i as the space element considered, the time derivative, becomes as it follows:

$$\frac{\partial T}{\partial t} = \frac{T_i^{n+1} - T_i^n}{\Delta t} \tag{3.1}$$

while, the space is set to be composed by finite elements along the z-axis, each of which has a length of 3mm (Δz=3mm). In this case, the Backward finite difference method is used:

$$\frac{\partial T}{\partial z} = \frac{T_i - T_{i-1}}{\Delta z} \tag{3.2}$$

Silica-gel water uptake

The equation accounting for the variation over time of the water uptake in the silica gel, is given by:

$$\rho_b \frac{\partial W}{\partial t} = K_g a_s (x_a - \bar{x}) = \dot{G} \quad [kg\, m^{-3} s^{-1}] \tag{3.3}$$

It is possible to notice that the variation of the water uptake is driven by the difference in moisture concentration between the air flow and the air in contact with the surface of silica-gel. As time passes by, this difference diminishes, since the water vapor adsorbed raises (while the moisture content in the air flow decreases), so, the driving force becomes increasingly weaker until the two concentration will be the same and the moisture transfer can not occur anymore (end of the process). The parameters of the equation (3.3) are:

- ρ_b is the bulk density of silica gel;
- K_g is the overall mass transfer coefficient, which takes into account the two mechanisms of moisture transfer rate: mass transfer rate on air side, driven by convection between air and desiccant surface; mass transfer rate on desiccant layer due to the intraparticle diffusion process.
  The mass transfer coefficient on air side can be evaluated through the correlation of the Sherwood number [41]:

$$Sh_a = \frac{K_f d_h}{D_m} = 0.079 {Re_a}^{0.71} {Sc_a}^{0.37} \quad [-] \tag{3.4}$$

  where K_f is the coefficient that needs to be found (then, it has to be multiplied by the air density in order to obtain the h_m coefficient in $kg\, m^{-2} s^{-1}$), d_h is the hydraulic diameter, Re_a is the Reynolds number of air and Sc_a is the Schmidt number calculated as the ratio between the dynamic viscosity of air and the air density multiplied by the molecular diffusivity of water vapor in air:

$$Sc_a = \frac{\mu_a}{\rho_a D_m} \quad [-] \tag{3.5}$$

with

$$\mu_a = 10^{-7}(2.43T + 157.5) \quad [Pa \cdot s] \tag{3.6}$$

$$\rho_a = \frac{P}{RT} = \frac{101325}{287(T + 273.15)} \quad [kg\ m^{-3}] \tag{3.7}$$

$$D_m = 1.735 * 10^{-9} \frac{(T_s + 273.15)^{1.685}}{P} \quad [m^2\ s^{-1}] \tag{3.8}$$

where T is the temperature in °C, P is the ambient pressure in Pa, R is the gas constant in $J\ kg^{-1}K^{-1}$,T_s is the silica gel temperature in °C [27].
The Reynolds number is evaluated as it follows:

$$Re_a = \frac{\rho_a v_a d_h}{\mu_a} \quad [-] \tag{3.9}$$

where v_a is the air flow velocity.
The hydraulic diameter is expressed as:

$$d_h = \frac{4\sigma}{\alpha} \quad [m] \tag{3.10}$$

with

$$\sigma = \frac{A_o}{A_b} \quad [-] \tag{3.11}$$

$$\alpha = \frac{A_{hx}}{V_b} \quad [m^{-1}] \tag{3.12}$$

where A_o is the minimum free flow area, A_b is the total frontal area, A_{hx} is the total exchange area, V_b is the total volume of the battery.

Concerning the intraparticle diffusion, it is characterized by three types of diffusion mechanism [27]:

1. Surface diffusion, which is the transport of adsorbed phase on the pores surface caused by a difference in the adsorbate concentration. It is evaluated as it follows:

$$D_s = \frac{D_0}{\tau_s} \cdot \exp^{-0.947 \frac{H_{ads}}{T_s + 273.15}} \quad [m^2\ s^{-1}] \tag{3.13}$$

where D_0 is a constant equal to $1.6 * 10^{-6}\ m^2/s$, τ_s is the tortuosity factor equal to 2 [41], T is the silica gel temperature in °C and H_{ads} is the heat

of adsorption calculated as a function of the water uptake [27]:

$$H_{ads} = 3500 - 13400W \quad for \quad W \quad \leq 0.05 \quad [kJ\ kg^{-1}] \tag{3.14}$$

$$H_{ads} = 2950 - 1400W \quad for \quad W > 0.05 \quad [kJ\ kg^{-1}] \tag{3.15}$$

2. Molecular diffusion, which is related to the gas phase diffusion due to the molecular collision within the pores, that needs to be larger than the mean free path of the molecules. It has already been expressed in equation (3.8).
3. Knudsen diffusion, which is linked to the gas phase as well, and represents the interaction between the gas molecules and the silica gel surface. It mainly occurs when the pores diameters are small enough (can be compared with the mean free path). It is formulated as it follows:

$$D_{kn} = \bar{r}_p 22.86(T_s + 273.15)^{0.5} \quad [m^2\ s^{-1}] \tag{3.16}$$

where $\bar{r}_p$ is the average radius of the pores, which, in the case analyzed, is equal to 10 nm.

The contribution of the diffusion process related to the gas phase can be represented by the series of molecular and Knudsen diffusion resistances. The resulting resistance is, then, in parallel with that associated with the surface diffusion. The consequent effective diffusion coefficient is equal to:

$$D_{eff} = D_s + \frac{\varepsilon_p}{\tau_s}\left(\frac{1}{D_m} + \frac{1}{D_{kn}}\right)^{-1} \quad [m^2\ s^{-1}] \tag{3.17}$$

where ε_p is the silica gel porosity.
Finally, the convective and the diffusive resistances are put in series, giving the overall resistance of the mass transfer mechanism, from which is possible to obtain K_g [41]:

$$\frac{1}{K_g} = \frac{1}{h_m} + \frac{t_s}{2D_{eff}\rho_a} \tag{3.18}$$

where t_s is the silica gel coating thickness.

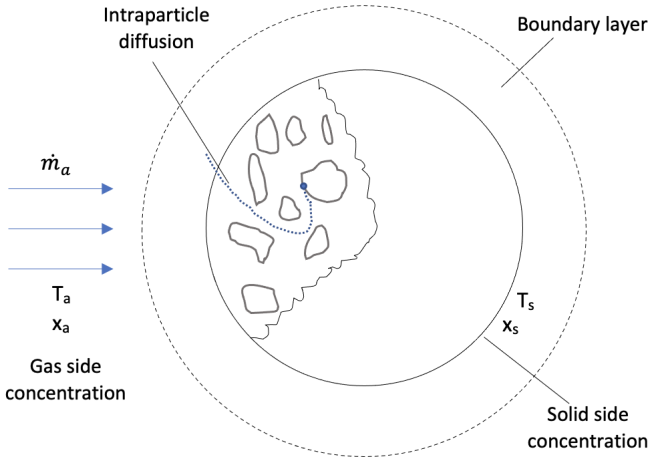

Figure 3.2: Mass diffusion scheme

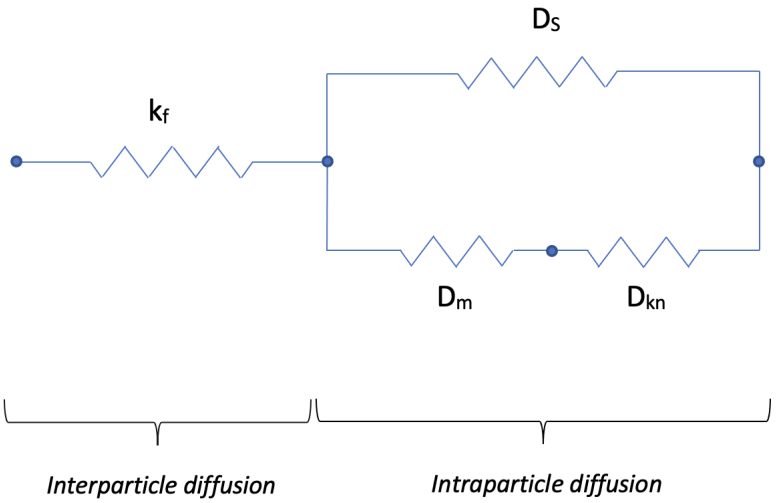

Figure 3.3: Mass transfer resistances

- a_s is the specific area of silica gel defined as:

$$a_s = \frac{A_s}{V_s} \qquad [m^{-1}] \tag{3.19}$$

where A_s is the total exchange surface of silica gel and V_s is the total volume of silica gel.

- x_a is the specific humidity ratio of air calculated as a function of the ambient pressure (P_{amb}) in Pa, the saturation pressure of water vapor at a certain temperature (P_{sat}) in Pa and the relative humidity of air (RH_a):

$$x_a = 0.622 \frac{RH_a P_{sat}}{P_{amb} - RH_a P_{sat}} \qquad [kg_v\ kg_a^{-1}] \tag{3.20}$$

The saturation pressure of water vapor P_{sat} is expressed as a function of air temperature:

$$P_{sat} = 0.0004677T^4 + 0.02444T^3 + 1.359T^2 + 45.98T + 604.6 \quad [Pa] \quad (3.21)$$

- $\bar{x}$ is the air humidity ratio in equilibrium with silica gel. In order to evaluate it, the equations used above for the air moisture content are also exploited now, having as input the silica gel temperature and its relative humidity. The latter one is calculated using the adsorption isotherm obtained from measurements on how the relative changes at different values of water uptake W and silica gel temperature T_s. The correlation obtained is the following:

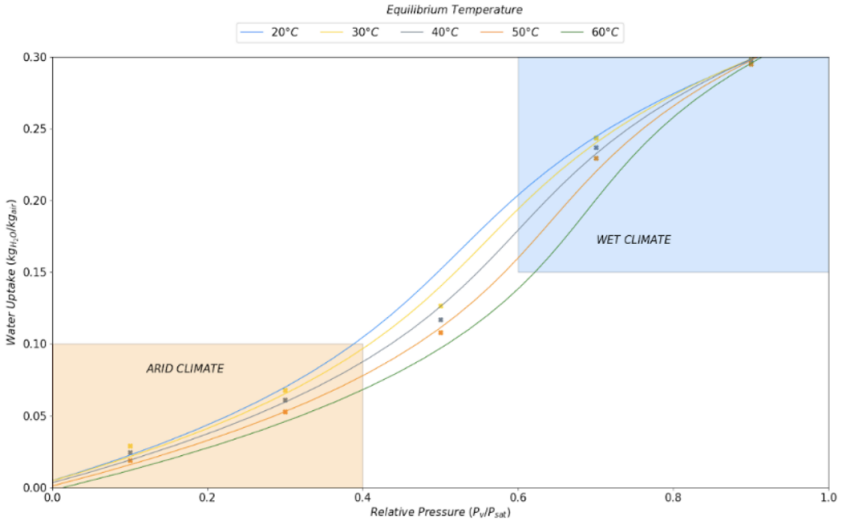

Figure 3.4: Adsorption Isotherm

$$RH_s = s_1 \cdot T + s_2 \cdot T^2 + s_3 \cdot W + s_4 \cdot W \cdot T + s_5 \cdot W \cdot T^2 + s_6 \cdot W^2 + s_7 \cdot T \cdot W^2 + s_8 \cdot W^3 + s_9 \cdot T^3 \quad (3.22)$$

where the coefficients are respectively: s_1=-0.00249434; s_2=0.0000529632; s_3=5.65527; s_4=0.0360887; s_5=-0.0000713679; s_6=-24.9044; s_7=-0.112424; s_8=54.8088; s_9=-0.000000123558.

It is possible to notice from Figure 3.2 that the different curves, related to different temperatures, converge into the same point corresponding to a water uptake of 0.3 $kg_w kg_s^{-1}$, meaning that the maximum increment in weight due to water adsorption by dry silica gel is equal to 30 % for the temperatures considered.

As mentioned before, the analytical equation of water uptake (3.3) has to be written in a numerical form in order to be implemented on MATLAB:

$$\rho_b \frac{W^{n+1} - W^n}{\Delta t} = K_g a_s ({x_a}^n - \bar{x}^n) \tag{3.23}$$

from which it is possible to find and update the water uptake:

$$W^{n+1} = W^n + \frac{\Delta t K_g a_s ({x_a}^n - \bar{x}^n)}{\rho_b} \tag{3.24}$$

It is, then, defined the initial condition:

$$W(z, t = 0) = W_0 \tag{3.25}$$

Air-water mass balance

The equation governing the mass balance between the air stream and the silica gel coating is the following one:

$$\varepsilon_b \rho_a \frac{\partial x_a}{\partial t} dv = -\dot{m}_a \frac{\partial x_a}{\partial z} dz - \dot{G} dv \quad [kg\ s^{-1}] \tag{3.26}$$

It can be observed that the variation of air moisture content over time is due, basically, to a variation of air specific humidity ratio along the z-axis caused by convection, and to the mass transfer rate $\dot{G}$.
The equation is written considering the infinitesimal volume of the battery expressed as:

$$dv = A_b dz \quad [m^3] \tag{3.27}$$

The coefficient ε_b is the void volume fraction, namely the ratio between the void volume and the void and silica gel volume:

$$\varepsilon_b = \frac{V_{void}}{V_{void} + V_s} \quad [-] \tag{3.28}$$

The term $\dot{m}_a$ is the air mass flowrate and it is given by:

$$\dot{m}_a = \rho_a A_b v_a \quad [kg\ s^{-1}] \tag{3.29}$$

where A_b is the battery total cross section in m^2. The correspondent numerical equation is the following:

$$\varepsilon_b \rho_a \frac{{x_{a_i}}^{n+1} - {x_{a_i}}^n}{\Delta t} dv = -\dot{m}_a \frac{{x_{a_i}}^{n+1} - {x_{a_{i-1}}}^n}{\Delta z} dz - K_g a_s ({x_{a_i}}^{n+1} - \bar{x_i}^n) dv \tag{3.30}$$

defining M_A the bidiagonal sparse matrix of the coefficients and Q_A the matrix of the known terms, the equation (3.30) can be rewritten as:

$$x_a{}^{n+1} = M_{X_a}{}^{-1} Q_{X_a} \tag{3.31}$$

where

$$M_{X_a} = \begin{bmatrix} 1 + \Delta t(A_1 + A_2) & ... & ... \\ -\Delta t A_1 & 1 + \Delta t(A_1 + A_2) & ... \\ ... & -\Delta t A_1 & 1 + \Delta t(A_1 + A_2) \end{bmatrix} \tag{3.32}$$

$$Q_{X_a} = x_a{}^n + \Delta t A_2 \bar{x}^n \tag{3.33}$$

$$A_1 = \frac{v_a}{\varepsilon_b \Delta z} \tag{3.34}$$

$$A_2 = \frac{K_g a_s}{\varepsilon_b \rho_a} \tag{3.35}$$

In this case, since the spatial derivative appears, it is necessary to define also a boundary condition (for z=0), in addition to an initial condition (for t=0):

$$x_a(z, t = 0) = x_{a_0} \tag{3.36}$$

$$x_a(z = 0, t) = x_{a_{in}} \tag{3.37}$$

which corresponds to:

$$M_{X_a}(1, 1) = 1 \tag{3.38}$$

$$M_{X_a}(1, 2) = 0 \tag{3.39}$$

$$Q_{X_a}(1) = x_{a_{in}} \tag{3.40}$$

In this analysis x_{a0} is set equal to $x_{a_{in}}$.

Air thermal balance

The air thermal balance accounts for the temperature variation of air during the process, and it is expressed as:

$$\varepsilon_b \rho_a cp_a \frac{\partial T_a}{\partial t} dv = -\dot{m}_a cp_a \frac{\partial T_a}{\partial z} dz + h_a a_f (T_s - T_a) dv - U_l a_l (T_a - T_{amb}) dv \quad [W] \tag{3.41}$$

Observing the right hand side of the equation, the first term represents the spacial temperature gradient along the z-axis due to the air flowing through the battery. Then, there is the term accounting for convective heat exchange between the silica gel coating and the air and the term related to the air heat losses through the casing, which can be neglected.
The specific heat for air is calculated as:

$$cp_a = 1884x_a + 1005(1 - x_a) \quad [J\ kg^{-1}\ K^{-1}] \tag{3.42}$$

The convective heat transfer coefficient h_a is calculated through the definition of Nusselt number and by using the correlation reported in [36]:

$$Nu_a = \frac{h_a d_h}{k_a} = 0.722 Re^{0.43} Pr^{0.3} \quad [-] \tag{3.43}$$

where k_a is the air thermal conductivity set at $0.027\ Wm^{-1}K^{-1}$ and Pr is the Prandtl number equal to 0.7055. Both these terms are assumed to be constant during the simulation, since their variation is negligible.
Then, in the equation (3.41), appears the a_f, which is the specific exchange area between air and silica gel, supposed to be equal to the specific total exchange surface, i.e. the ratio between the total exchange surface (sum of fins and tubes) and the total volume of the battery:

$$a_f = \frac{A_{hx}}{V_b} \quad [m^{-1}] \tag{3.44}$$

The term accounting for the losses through the battery casing is be calculated as:

$$\frac{1}{U_l} = \frac{1}{h_{amb}} + \frac{t_c}{k_{al}} + \frac{1}{h_a} \quad [m^2\ K\ W^{-1}] \tag{3.45}$$

where h_{amb} is the convective heat transfer coefficient between the external surface of the casing and the ambient air, t_c is the casing thickness, k_{al} is the thermal conductivity of aluminium. While a_l is equal to the casing surface divided by the battery volume:

$$a_l = \frac{A_c}{V_b} \quad [m^{-1}] \tag{3.46}$$

The numerical equation corresponding to the analytical one just presented, is the following:

$$\varepsilon_b \rho_a cp_a \frac{{T_{a_i}}^{n+1} - {T_{a_i}}^{n}}{\Delta t} dv = -\dot{m}_a cp_a \frac{{T_{a_i}}^{n+1} - {T_{a_{i-1}}}^{n+1}}{\Delta t} dz + h_a a_f ({T_{s_i}}^{n} - T_{a_i}^{n+1}) dv \\ -U_l a_l (T_{a_i}^{n+1} - T_{amb}) dv \tag{3.47}$$

Defining the matrix of coefficients and known terms, it becomes:

$${T_a}^{n+1} = {M_{T_a}}^{-1} Q_{T_a} \tag{3.48}$$

where the sparse matrix M_{T_a} is equal to:

$$M_{T_a} = \begin{bmatrix} 1 + \Delta t(B_1 + B_2 + B_3) & ... & ... \\ -\Delta t B_1 & 1 + \Delta t(B_1 + B_2 + B_3) & ... \\ ... & -\Delta t B_1 & 1 + \Delta t(B_1 + B_2 + B_3) \end{bmatrix} \tag{3.49}$$

while, the known term matrix Q_{T_a} is given by:

$$Q_{T_a} = {T_a}^{n} + \Delta t B_2 {T_s}^{n} + \Delta B_3 T_{amb} \tag{3.50}$$

with

$$B_1 = \frac{v_a}{\varepsilon_b \Delta z} \tag{3.51}$$

$$B_2 = \frac{h_a a_f}{\varepsilon_b \rho_a cp_a} \tag{3.52}$$

$$B_3 = \frac{U_l a_l}{\varepsilon_b \rho_a cp_a} \tag{3.53}$$

The initial condition and the boundary condition are set:

$$T_a(z, t = 0) = T_{a_0} \tag{3.54}$$

$$T_a(z = 0, t) = T_{a_{in}} \tag{3.55}$$

corresponding to:

$$M_{T_a}(1, 1) = 1 \tag{3.56}$$

$$M_{T_a}(1, 2) = 0 \tag{3.57}$$

$$Q_{Ta}(1) = T_{a_{in}} \tag{3.58}$$

Similarly to the air mass balance, the initial value of the air temperature is imposed equal to the air temperature at the entrance of the battery: $T_{a_0} = T_{a_{in}}$.

Silica gel thermal balance

The equation expressing the evolution of silica gel as time passes by, is the following:

$$(1 - \varepsilon_b)\rho_s cp_s \frac{\partial T_s}{\partial t} = H_{ads}\dot{G} - h_a a_f (T_s - T_a) - U a_f (T_w - T_s) \quad [W] \tag{3.59}$$

The first term on the right-hand side accounts for the change of the adsorption heat released by the adsorption process, since it varies with the quantity of water vapor adsorbed. The second term is the one already seen for the air thermal balance, that is related to the convective heat exchange between silica gel and air. The last term represents the heat exchange between the silica gel coating and the water flowing in the tubes of the heat exchanger.

The specific heat is considered dependent on the water uptake and, so, evaluated through the correlation:

$$cp_s = 4178w + 921 \quad [J\ kg^{-1}\ K^{-1}] \tag{3.60}$$

The heat transfer coefficient between silica gel coating and water is calculated using the electrical analogy for heat transfer, considering the overall thermal resistance as a series of different thermal resistances. The first one is represented by the conductive resistance of the silica gel layer, the second one is due to the conduction through the tubes walls and the last one expresses the convective thermal resistance caused by the water flowing in the pipes [24]:

$$R_{s-w} = R_{cond_s} + R_{cond_{tube}} + R_{conv_w} \tag{3.61}$$

which corresponds to

$$\frac{1}{UA_{hx}} = \frac{t_s}{\eta_0 k_s A_{hx}} + \frac{ln(d_o/d_i)}{2\pi L_p k_{cu}} + \frac{1}{h_w A_w} \quad [K\ W^{-1}] \tag{3.62}$$

where t_s is the thickness of the silica gel coating, η_0 is the fins efficiency, k_s is the thermal conductivity of silica gel, assumed to be constant and equal to 0.2 $W\ m^{-1}\ K^{-1}$, d_o and d_i are, respectively, the outer and the inner diameters of the

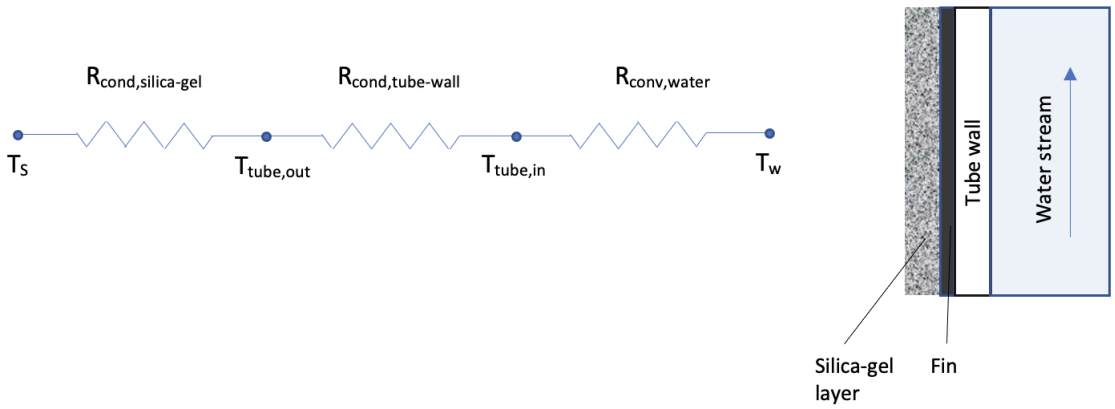

Figure 3.5: Electric analogy for thermal resistances between silica gel and water

tubes, L_p is the total length of the pipes, k_{cu} is the thermal conductivity of copper, A_w is the total inner surface of the tubes, h_w is the thermal convective coefficient of water, evaluated from the water Nusselt number correlation:

$$Nu_w = \frac{h_w d_i}{k_w} = 0.023 Re_w^{0.8} Pr_w^{0.4} \quad [-] \tag{3.63}$$

setting the thermal conductivity of water equal to 0.6 W/mK, the Prandtl number Pr_w equal to 6.9 and the Reynolds number Re_w given by:

$$Re_w = \frac{\rho_w v_w d_i}{\mu_w} \quad [-] \tag{3.64}$$

being ρ_w the density of water and μ_w the dynamic viscosity of water.
The fin efficiency is calculated through the following equations:

$$\eta_0 = 1 - \frac{A_{fin}}{A_{hx}}(1 - \eta_f) \quad [-] \tag{3.65}$$

$$\eta_f = \frac{tanh(mL_f)}{mL_f} \quad [-] \tag{3.66}$$

$$m = \sqrt{\frac{2h_a}{k_{al}\delta_f}} \quad [m^{-1}] \tag{3.67}$$

where a_f is the finned surface, L_f is taken as half the distance between two tubes (assuming adiabatic ends), δ_f is the fin thickness, k_{al} is the thermal conductivity of aluminum.

The numerical equation corresponding to the (3.59) is:

$$\begin{aligned}(1-\varepsilon_b)cp_s\rho_s\frac{{T_{s_i}}^{n+1}-{T_{s_i}}^{n}}{\Delta t} =& H_{ads}K_g a_s({x_{a_i}}^{n}-\bar{x_i}^{n})-h_a a_f({T_{s_i}}^{n+1}-{T_{a_i}}^{n})\\ &-Ua_f({T_{s_i}}^{n+1}-{T_{w_i}}^{n})\end{aligned} \tag{3.68}$$

from which is possible to obtain and update the silica-gel temperature:

$${T_{s_i}}^{n+1}=\frac{{T_{s_i}}^{n}+\Delta tC_1({x_{a_i}}^{n}-\bar{x_i}^{n})+\Delta tC_2{T_{a_i}}^{n}+\Delta tC_3{T_{w_i}}^{n}}{1+\Delta tC_1+\Delta tC_2+\Delta tC_3} \tag{3.69}$$

where

$$C_1=\frac{H_{ads}K_g a_s}{(1-\varepsilon_b)cp_s\rho_s} \tag{3.70}$$

$$C_2=\frac{h_a a_f}{(1-\varepsilon_b)cp_s\rho_s} \tag{3.71}$$

$$C_3=\frac{Ua_f}{(1-\varepsilon_b)cp_s\rho_s} \tag{3.72}$$

Since there is only a time derivative, in this case, only the initial condition is imposed:

$$T_s(z,t=0)=T_{s0} \tag{3.73}$$

the value of T_{s0} is set to be equal to the inlet air temperature $T_{a_{in}}$.

Water loop thermal balance

The temperature of the water flowing in the tubes of the finned heat exchanger is not constant over time, since it is affected by a space gradient along the z-axis direction as it progressively passes through the battery. Moreover water exchanges heat with the silica gel layer coating the heat exchanger.
This terms are accounted in the analytical equation:

$$\rho_w cp_w\frac{\partial T_w}{\partial t}dv=-\dot{m}_w cp_w\frac{\partial T}{\partial z}dz-Ua_f(T_w-T_s)dv \tag{3.74}$$

where cp_w is the specific heat of wate. The mass flowrate is evaluated as it follows:

$$\dot{m}_w=\rho_w A_{w_{cross}}v_w \quad [kg\ s^{-1}] \tag{3.75}$$

where $A_{w_{cross}}$ is the cross section of each pipe.

The correspondent numerical equation is:

$$cp_w\rho_w\frac{{T_{w_i}}^{n+1}-{T_{w_i}}^{n}}{\Delta t}dv=-cp_w\dot{m}_w\frac{{T_{w_i}}^{n+1}-{T_{w_{i-1}}}^{n+1}}{\Delta z}dz-Ua_f({T_{w_i}}^{n+1}-{T_{a_i}}^{n})dv \tag{3.76}$$

introducing the matrix of the coefficient and the known term, the equation (4.72) can be rewritten as:

$${T_{w_i}}^{n+1}=Q_w{M_w}^{-1} \tag{3.77}$$

The sparse matrix M_w is given by:

$$M_w=\begin{bmatrix}1+\Delta t(C_1+C_2) & ... & ... \\ -\Delta tC_1 & 1+\Delta t(C_1+C_2) & ... \\ ... & -\Delta tC_1 & 1+\Delta t(C_1+C_2)\end{bmatrix} \tag{3.78}$$

The known term matrix Q_w is equal to:

$$Q_w={T_w}^{n}+\Delta tC_2{T_s}^{n} \tag{3.79}$$

with

$$C_1=\frac{\dot{m}_w}{\rho_w A_b\Delta z} \tag{3.80}$$

$$C_2=\frac{Ua_f}{\rho_w cp_w} \tag{3.81}$$

Since both the spacial and the temporal derivatives are present, an initial condition and a boundary condition need to be set:

$$T_w(z=0,t)=T_{w_{in}} \tag{3.82}$$

$$T_w(x,t=0)=T_{w0} \tag{3.83}$$

which translates into:

$$M_w(1,1)=1 \tag{3.84}$$

$$M_w(1,2)=0 \tag{3.85}$$

$$Q_w(1)=T_{w_{in}} \tag{3.86}$$

Again, the value of the temperature at the beginning of the simulation T_{w0} and at inlet temperature $T_{w_{in}}$ are set to be the same.

3.3 Convergence analysis

In this section a convergence study is carried out in order to check if the numerical model developed is convergent, meaning if the model reaches a fixed value as space and time domains are refined [38]. Consequently, at the same time, it is possible to find out if the time step and the size of the finite space elements utilized allow to obtain an accurate solution.
Moreover, a comparison among the computational times for the various domain definitions is executed with the purpose of understanding if there are significant differences.

3.3.1 Space convergence

In order to accomplish the space convergence, a range of different Δz to discretize the space domain is defined: $\Delta z = 0.5mm$, $\Delta z = 1mm$, $\Delta z = 3mm$, $\Delta z = 5mm$, $\Delta z = 10mm$, $\Delta z = 30mm$ and $\Delta z = 50mm$.
Then, a chosen output is selected and calculated using the different Δz. In this case the maximum outlet air temperature in adsorption mode, during the first cycle, is used for the study.
The results obtained are presented in Figure 3.6.

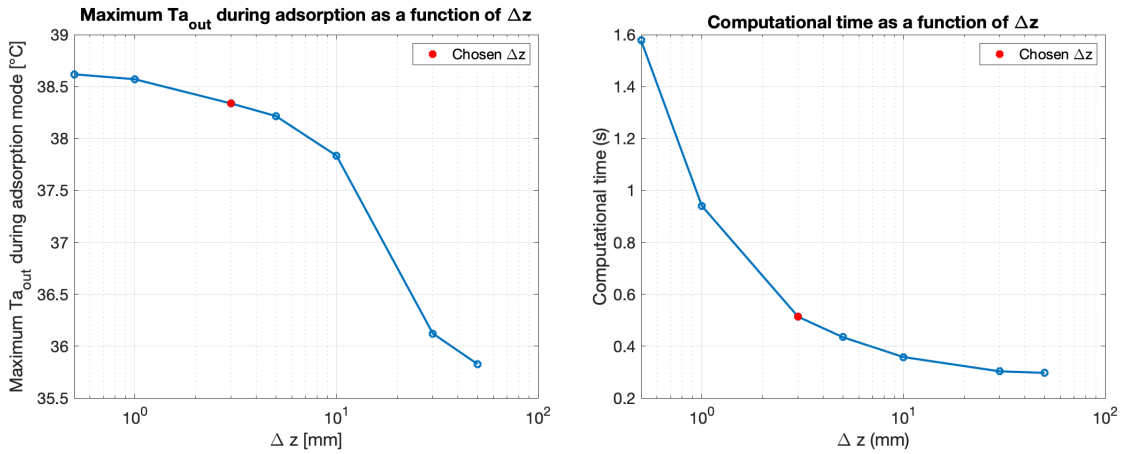

Figure 3.6: Maximum air outlet temperature during adsorption and computational time as a function of Δz

It can be observed that, as the Δz decreases, the trend of the temperature becomes flat, converging to a certain value, that, in this case, is equal to about 38.6 °C. The chosen Δz gives a value approximately equal to 38.3 °C with a relative error with respect of the most refined solution of 0.73%.

Concerning the computational time, which is calculated over the first adsorption phase, it significantly decreases shifting from $\Delta z = 0.5mm$ to $\Delta z = 3mm$ and, then, it settles, reaching a duration around 0.3 s.
Therefore, the solution given by the chosen Δz is a good compromise between an accurate solution and a limited computational time (equal to 0.54 s).

3.3.2 Time convergence

Similarly to what has been done for the space convergence, in order to execute the time convergence study, a range of time step is set: $\Delta t = 0.1s$, $\Delta t = 0.5s$, $\Delta t = 1s$, $\Delta t = 5s$, $\Delta t = 10s$, $\Delta t = 15s$, $\Delta t = 20s$.
Once more, the maximum outlet air temperature during the first adsorption cycle is considered with the purpose of comparing the solutions obtained through the definition of different time domains.
The results are shown in Figure 3.7.

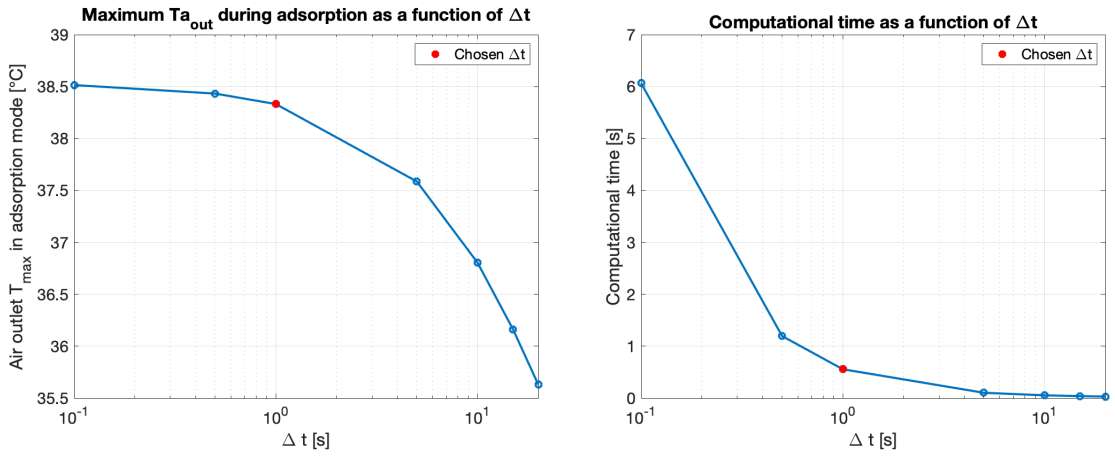

Figure 3.7: Maximum air outlet temperature during adsorption and computational time as a function of Δt

Again, as the time step reduces, the temperature converges to a fixed value (about 38.5 °C). The chosen Δt gives the same solution as before, since, in both cases, the Δz is equal to $3mm$ and the Δt is equal to $1s$. The relative error relating to the most refined solution is equal to 0.47%.
The computational time has a trend which flattens as the Δt increases (reaching almost 0.03 s when $\Delta t = 20s$), with a substantial reduction passing from $\Delta t = 0.1s$ to $\Delta t = 0.5s$.
Even in this case, the used Δt can be considered a good choice for the same reasons previously explained for the space convergence.

3.4 Model validation

The model just defined is validated by comparing its output with experimental results for silica-gel coated fin-tube heat exchangers obtained by [16] and [21].
The experimental conditions are used as input parameters for the model; in case data are missing, hypothetical reasonable values are set.

The input data for the first reference experiment are the ones of Table 3.1.

Input data reference [16]	
Silica gel type	Macro pore, ZCX-II
HX length	50 mm
HX height	200 mm
HX width	160 mm
Fin thickness	0.15 mm
Fin pitch	1.5 mm
Tube inner diameter	7 mm
Inlet air temperature	30 °C
Inlet air humidity ratio	14.5 $g_v \ kg_a^{-1}$
Inlet air velocity	1 $m \ s^{-1}$
Cooling water temperature	25 °C
Hot water temperature	60 °C
Water flowrate	160 $l \ h^{-1}$
Adsorption duration	367 s
Regeneration duration	253 s

Table 3.1: Experimental conditions, reference [16]

Some data are missing, such as the silica-gel layer thickness and porosity, the tubes pitch and outer diameter.
The results obtained for the outlet air temperature and specific humidity ratio are compared in Figure 3.8. It may be noted that time begins at 620 s. This is because the model output is taken starting from the second cycle, since the first cycle is affected by the initial conditions which make it not representing well the system at regime.
Looking at Figure 3.8, it can be observed that the curves are fairly coupled in both cases. Concerning the outlet air temperature, the minimum values resulting from the model and the reference are, respectively equal to 27.7°C and 26.5°C, while the maximum air temperatures are 54.2°C and 55°C. The average outlet air temperature during adsorption obtained from the model (31.6 °C) is about 7.85% higher than

that of the experiment(29.3 °C), during regeneration, instead, the model average outlet air temperature (46.7 °C) is about 6.58% lower than the experimental one (49.9 °C).

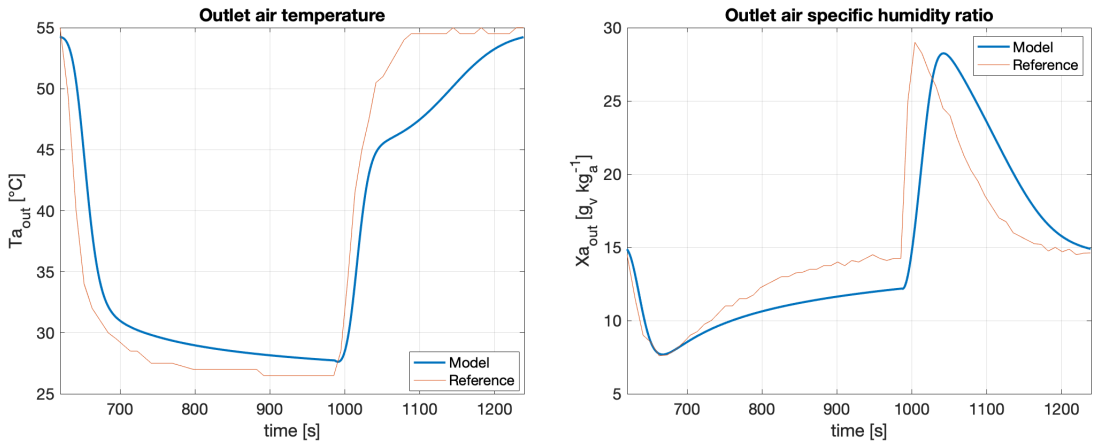

Figure 3.8: Outlet air temperature and specific humidity ratio

Considering now the outlet air specific humidity ratio, the minimum value attained through the model is coincident with that of the experiment, equal to 7.6 $g_v kg_a^{-1}$, while, the maximum values are 28.3 $g_v kg_a^{-1}$ for the model and about 29 $g_v kg_a^{-1}$ for the reference. The average value of the difference between the inlet and the outlet air specific humidity ratio obtained by the model (3.9 $g_v kg_a^{-1}$) is about 25.8% greater than experiment (3.1 $g_v kg_a^{-1}$) during adsorption. These discrepancies are associated to the lack of information about the silica gel material, meaning its density, pores radius, porosity, layer thickness and adsorption isotherm.
However, the maximum and minimum values of the model for both outlet air temperature and outlet air specific humidity ratio are almost coincident and the relative errors of the average values are quite small.

Another experiment has been considered in order to validate the model. The input data are reported in Table 3.2. The lacking data, in this case, are the thickness and the properties of silica-gel used (pore radius, porosity, adsorption isotherm, density), the tubes and fins pitch.

Input data reference [21]	
Silica gel type	Mesopore
HX length	45 mm
HX height	280 mm
HX width	200 mm
Fin thickness	0.15 mm
Tube outer diameter	9.52 mm
Tube inner diameter	7.85 mm
Inlet air temperature	30 °C
Inlet air relative humidity	60 %
Inlet air velocity	1.54 $m\ s^{-1}$
Cooling water temperature	25 °C
Hot water temperature	50 °C
Water flowrate	200 $l\ h^{-1}$
Adsorption duration	600 s
Regeneration duration	600 s

Table 3.2: Experimental conditions, reference [21]

The results are shown in Figure 3.9. As in the previous case, the results are considered starting from the second cycle.
The model outcome of the outlet air temperature shown in Figure 3.9, is quite different from that of the experiment. This can be explained by the fact that the temperature sensors are placed at a certain distance from the end of the heat exchanger, so the thermal inertia of the ducts and casings, as well as the heat exchange between air exiting the heat exchanger and the ducts walls, cause a discrepancy among the actual temperature at the end of the adsorption battery and the temperature detected by the sensors. Despite this, the trend is similar and the maximum and minimum values are almost the same. In fact, the highest outlet air temperature reached through the model simulation and the experiment are respectively equal to 41 °C and 40 °C, while the minimum temperatures during adsorption are 27.6 °C for the model and 26.6 °C for the reference. The average value of air outlet temperature during adsorption corresponds to 29.1 °C for the model and 29.8 °C for the experiment, during regeneration, instead, the air outlet temperature of the model is

equal to 39.3 °C, while, for the reference, it is equal to 36.2 °C.
The curves showing the air outlet specific humidity ratio have quite the same trend, but there are some discrepancies. This can be due to the fact that the information about the silica-gel used are incomplete. The minimum and the maximum value obtained by the model simulations are equal to 11.8 $g_v kg_a^{-1}$ and 23.4 $g_v kg_a^{-1}$, while the ones resulting from the experiment corresponds to about 12 $g_v kg_a^{-1}$ and 22.2 $g_v kg_a^{-1}$. The average moisture removal given by the model coincides with 1.51 $g_v kg_a^{-1}$, while, the one obtained by the experiment is equal to 0.98 $g_v kg_a^{-1}$.

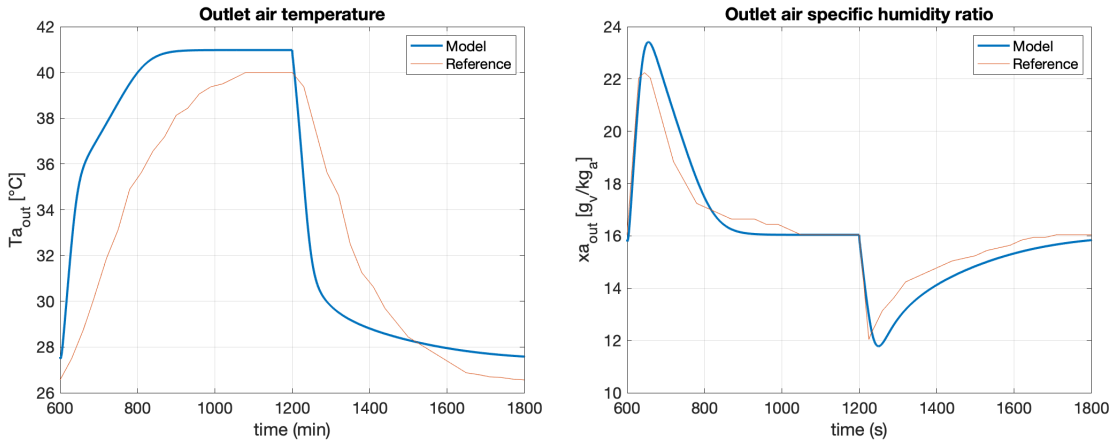

Figure 3.9: Outlet air temperature and specific humidity ratio

In conclusion, the dissimilarities between the model simulation and the experiments are, in general, addressed to the fact that some data are missing, in particular the ones relating to the silica-gel used and the silica gel layer thickness. Moreover, the curves related to the experiments are reproduced basing on the graphs represented in the references, so, some errors of measure and trasposition could occur. In addition, the experiment outputs are affected by uncertainties and the sensors measuring the air conditions are, in some cases, located not immediately after the heat exchanger exit.
Concerning the model used, it makes some simplifying assumptions, such as considering the problem mono-dimensional, some properties constant and neglecting some contributions in heat transfer (conduction in air flow rate direction).
Considering all these aspects, since the trends and the minimum and maximum values of the parameters considered are quite similar, the model can be reputed validated.

Chapter 4

Parametric analysis

In this chapter, a parametric analysis is undertaken in order to find out what are the best operative conditions and battery configurations which maximise the system performance.
The parameters that are changed are the following:

- Heat exchanger length (from 5 cm to 30 cm);
- Hot water temperature (from 50 °C to 70 °C);
- Cold water temperature (from 15 °C to 25 °C);
- Air stream velocity (from 0.2 ms^{-1} to 1.6 ms^{-1}).

4.1 Performance coefficients

In order to evaluate the performance of the system under different conditions and configurations, performance coefficients are defined.

4.1.1 COP_{el} - Electric Coefficient of Performance

The first parameter considered is the COP_{el}, which is the ratio between the useful effect, that, in this case, is the cooling power, and the electric power needed to run the system, which is evaluated as the sum of the power required by the fan, the water pump and the heat pump:

$$COP_{el} = \frac{\dot{Q}_{cool}}{\dot{W}_{el_{fan}} + \dot{W}_{el_{pump}} + \dot{W}_{el_{HP}}} \quad [-] \tag{4.1}$$

where the cooling power is calculated as the air mass flow rate multiplied by the variation of the air enthalpy between the inlet and the outlet sections [20]:

$$\dot{Q}_{cool} = \dot{m}_a(e_{a_{in}} - e_{a_{out}}) \quad [W] \tag{4.2}$$

with the air enthalpy obtained as a function of the air temperature and specific humidity:

$$e_a = 10^3(1.006T + x(2501 + 1.86T) \quad [Jkg^{-1}] \tag{4.3}$$

The $\dot{W}_{el_{fan}}$ is given by:

$$\dot{W}_{el_{fan}} = \frac{\dot{V}_a \Delta P_a}{\eta_{is_{fan}} \eta_{el_{fan}}} \quad [W] \tag{4.4}$$

where $\dot{V}_a$ is the volumetric air flow rate in $m^3 s^{-1}$, $\eta_{is_{fan}}$ and $eta_{el_{fan}}$ are the isentropic and electric efficiencies (set to be equal to 0.45 and 0.95 respectively), ΔP_a represents the pressure losses along the battery on air side, evaluated as:

$$\Delta P_a = f_a \rho_a \frac{{v_a}^2}{2} \frac{L}{d_h} \quad [Pa] \tag{4.5}$$

with v_a being the air flow velocity in $m\, s^{-1}$, L the battery length in m and f_a the friction factor, which, for laminar flows is equal to $\frac{64}{Re_a}$.

Similarly, $\dot{W}_{el_{pump}}$ is calculated as:

$$\dot{W}_{el_{pump}} = \frac{\dot{V}_w \Delta P_w}{\eta_{is_{pump}} \eta_{el_{pump}}} \quad [W] \tag{4.6}$$

where $\dot{V}_w$ is the volumetric water flowrate in $m^3 s^{-1}$, $\eta_{is_{pump}}$ and $\eta_{el_{pump}}$ are set to be equal to 0.65 and 0.95. The pressure loss $\Delta \mathrm{P}_w$ is the sum of the distributed and concentrated pressure drops:

$$\Delta P_w = f_w \rho_w \frac{{v_w}^2}{2} \frac{L_p}{d_i} + N_{pass} \beta \rho_w \frac{{v_w}^2}{2} \quad [Pa] \tag{4.7}$$

where the friction coefficient f_w, neglecting the pipes roughness, is evaluated as [20]:

$$f_w = \left(-1.8 log \left(\frac{6.9}{Re_w} \right) \right)^{-2} \quad [-] \tag{4.8}$$

while the friction factor for concentrated losses β is put equal to 2.5 and N_{pass} is the number of tube passes.

The electric power needed by the heat pump, $\dot{W}_{el_{HP}}$ is derived from the definition of COP for the heat pump, that, for example, in the case of adsorption is given by:

$$COP_{HP} = \frac{\dot{Q}_{cond}}{\dot{W}_{el_{HP}}} \quad [-] \tag{4.9}$$

where $\dot{Q}_{cond}$ is the heat power exchanged in the condenser.
A simplification for the calculation of the COP can be done, assuming it is equal to the inverse Carnot cycle efficiency corrected through a factor set equal to 0.5:

$$COP_{HP} = \frac{T_{cold}}{T_{hot} - T_{cold}} \quad [-] \tag{4.10}$$

where T_{cold} is the temperature of the cold source and T_{hot}, the one of the hot source. Similarly the COP_{HP} for the regeneration case can be calculated.

It can be noticed that the COP_{el} just introduced in (4.1) is defined in terms of power, meaning it is an instant value. In order to evaluate the average electric COP for the entire process, it needs to be integrated over time. This implies that the COP has to be expressed in terms of energy:

$$COP_{el} = \frac{\sum_{i=1}^{n_{ads}} \dot{Q}_{cool} \Delta t}{\sum_{i=1}^{n_{tot}} \dot{W}_{el_{fan}} \Delta t + \sum_{i=1}^{n_{tot}} \dot{W}_{el_{pump}} \Delta t + \sum_{i=1}^{n_{tot}} \dot{W}_{el_{HP}} \Delta t} \quad [-] \tag{4.11}$$

where n_{ads} is the final timestep of the adsorption process, while n_{tot} is the final timestep of the entire process (both adsorption and regeneration). Δt is the duration of each timestep.

4.1.2 COP_{th} - Thermal Coefficient of Performance

The second performance coefficient introduced in the analysis is the thermal Coefficient of performance COP_{th}. It differs from the previous COP for the fact that it accounts for thermal power only. It is given by the ratio between the cooling capacity during adsorption and the heat exchange rate of water during regeneration, both integrated over time [21].
It can be deduced that, in this case, it is not possible to evaluate an instant value of the COP_{th}, since the two terms belongs to different periods of time. So, only the average value of COP_{th} can be calculated:

$$COP_{th} = \frac{\sum_{i=1}^{n_{ads}} \dot{Q}_{cool} \Delta t}{\sum_{i=1}^{n_{rig}} \dot{Q}_{heat} \Delta t} \quad [-] \tag{4.12}$$

with n_{rig} corresponding to the final timestep of the regeneration process and $\dot{Q}_{heat}$ to the water thermal power equal to:

$$\dot{Q}_{heat} = \dot{m}_w cp_w (T_{w_{in}} - T_{w_{out}}) \quad [W] \tag{4.13}$$

4.1.3 Moisture removal effectiveness

The last coefficient considered is the moisture removal effectiveness, defined as the average moisture removal during adsorption. It is evaluated as (taking into account only the positive values of Δx):

$$\bar{\Delta x} = \frac{\sum_{i=1}^{n_{ads}} (x_{a_{in}} - x_{a_{out}}) \Delta t}{t_{ads}} \quad [g_v kg_a^{-1}] \tag{4.14}$$

4.2 Results of the analysis

The input data used for simulations are reported in Table 4.1 and Table 4.2, while the heat exchanger configuration is shown in Figure 4.1.

Silica gel properties and conditions	
Density ρ_s	1129 kg/m^3
Porosity ε_s	0.35
Pore radius $\bar{r}_p$	100 nm
Initial water uptake W_0	0.005 kg_w/kg_s
Geometrical parameters of the heat exchanger	
Longitudinal fin pitch X_l	21.65 mm
Transversal fin pitch X_t	25 mm
Battery length L_z	50-300 mm
Battery width L_x	500 mm
Battery height L_y	500 mm
Outer pipe diameter d_o	9.52 mm
Inner pipe diameter d_i	8.62 mm
Fin pitch p_f	2.5 mm
Silica gel coating thickness t_s	0.55 mm
Fin thickness δ_f	0.1 mm

Table 4.1: Silica-gel and geometrical input parameters

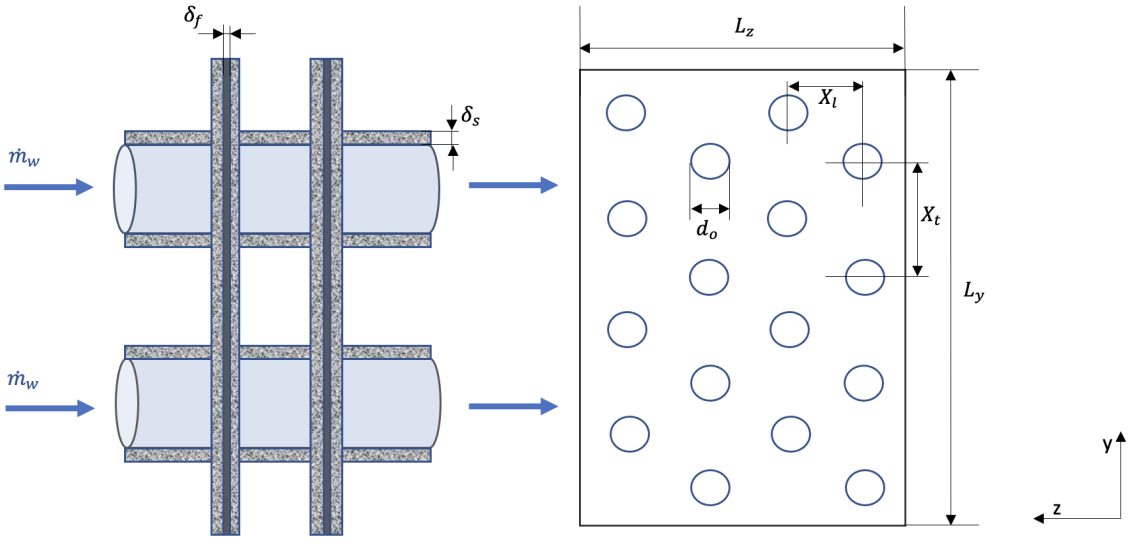

Figure 4.1: Adsorption heat exchanger configuration

Air flow conditions	
Average velocity v_a	0.2-1.6 m/s
Inlet temperature $T_{a_{in}}$	30 °C
Inlet relative humidity RH_{a_in}	70%
Water flow conditions	
Adsorption mass flowrate $\dot{m}_{w_{ads}}$	0.08 kg/s
Regeneration mass flowrate $\dot{m}_{w_{ads}}$	0.05 kg/s
Cold inlet water temperature T_{w_c}	15-25 °C
Regeneration inlet water temperature T_{w_h}	50-70 °C

Table 4.2: Air and water flows conditions

Concerning the time of the simulation, it is imposed that the adsorption and the regeneration have the same duration, set to be equal to 1 hour, resulting in an adsorption-regeneration cycle of 2 hours.
All the performance calculations are made starting from the second cycle, in order to evaluate the performance when the system is fully operational, excluding the initial conditions.

4.2.1 Influence of the heat exchanger length

Firstly, the performance is evaluated varying the length of the battery. This is done fixing the average v_a at 0.8 m/s, T_{w_c} at 20 °C and T_{w_h} at 50 °C.
The outlet air temperature, specific humidity ratio and the silica gel mean water uptake in time are reported in Figure 4.2.

Concerning the outlet air temperature during adsorption, it is lower as the length of the heat exchanger decreases: the outlet air temperature at the end of the adsorption phase is equal to 29.3 °C for $L_z = 30cm$ and reaches 25.3 °C when $L_z = 5cm$ with a decrement related to the average outlet temperature of 12.6%. The regeneration temperature, instead, is higher as the length decreases, achieving 38.3 °C at the end of the regeneration for $L_z = 5cm$ and 34.7 °C when $L_z = 30cm$, with a reduction in the average outlet air temperature of 5.5%. This trend is explained by the fact that as the length increases, more moisture is removed from air, but, also, more adsorption heat is released, so, the water flowing into the tubes can cool down air to a lesser extent.
It can be noticed that the difference of the outlet temperature is strongly affected by the heat exchanger length, especially when it varies from $L_z = 5cm$ to $L_z = 15cm$ (with average values of outlet air adsorption and regeneration temperature increasing

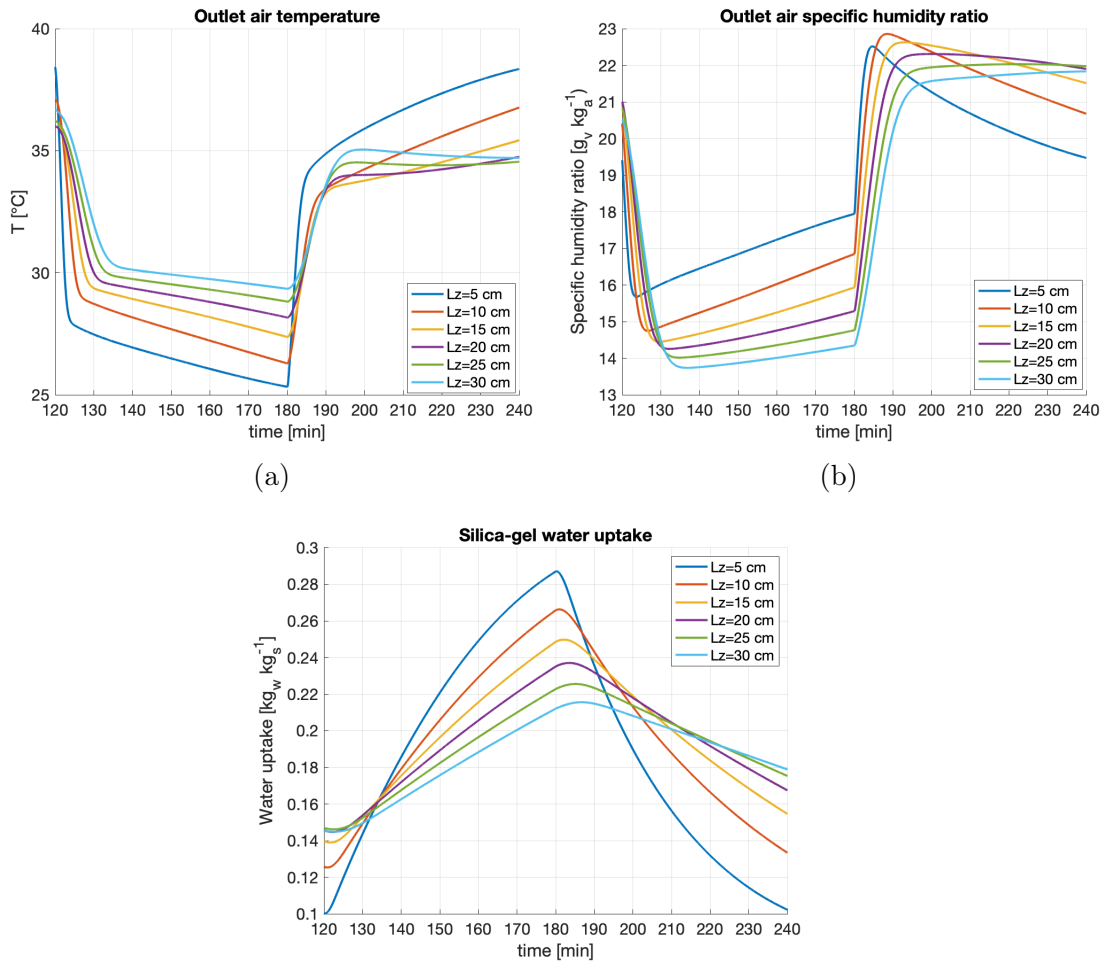

Figure 4.2: Temperature, specific humidity of outlet air and silica-gel water uptake for different heat exchanger lengths

respectively by 4.92% and lowering by 4.70% passing from $L_z = 5cm$ to $L_z = 10cm$), then, it begins to settle, slightly changing, in fact, from $L_z = 25cm$ to $L_z = 30cm$ the average adsorption outlet temperature of air varies only by 1.69% and the regeneration one by 1.03%.

Considering the air outlet specific humidity, it can be noticed that the silica-gel is closer to saturation when $L_z = 5cm$, in fact, the outlet air humidity at the end of the adsorption cycle, in this case, is equal to 18.0 $g_v kg_a^{-1}$ while the inlet air specific humidity ratio is 18.8 $g_v kg_a^{-1}$. As the length of the heat exchanger increases, the air outlet specific humidity ratio lowers, since the amount of silica-gel grows, meaning the ability of the battery of adsorbing water vapor raises. In fact, the outlet air specific humidity ratio at the end of adsorption process for $L_z = 30cm$ is equal to 14.4 $g_v kg_a^{-1}$. For the same reason, if the heat exchanger is longer, the time of silica-gel regeneration will be higher.

Looking at the average water uptake, as the length diminishes, the average silica-gel water uptake increases reaching around 0.29 $kg_w kg_s^{-1}$ at the end of adsorption phase and 0.10 $kg_w kg_s^{-1}$ at the end of regeneration with $L_z = 5cm$. When $L_z = 30cm$, instead, the water uptake when adsorption terminates is equal to 0.22 $kg_w kg_s^{-1}$, while it goes down to 0.18 $kg_w kg_s^{-1}$ when regeneration finishes. Again, this is explained by the fact that the quantity of silica-gel is higher as the length of the heat exchanger increases, so, there is more adsorbent material. Moreover, it may be noticed from Figure 4.1, that the peaks of water uptake is reached during regeneration rather than during adsorption. This happens because the saturation of the material is not achieved, and the water flowing in the tubes gradually reaches the regeneration temperature, so, the silica-gel is still able to capture water in the first part of the regeneration cycle.

$\mathbf{COP}_{el}$

The instant and the average COP_{el} are reported in Figure 4.3. The instant COP_{el} is considered only for the adsorption cycle, since during regeneration there is no cooling effect.

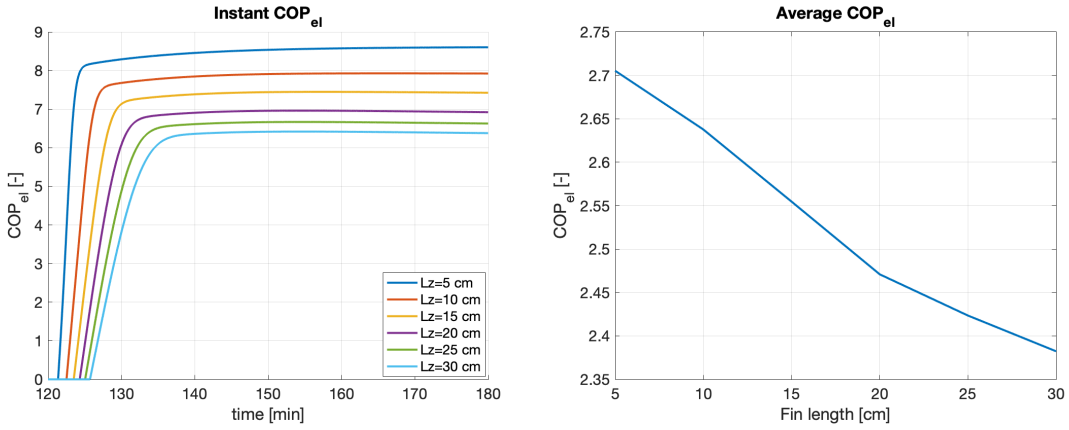

Figure 4.3: Instant and average COP_{el} as a function of heat exchanger length

As the heat exchanger length lowers, both the instant and average COP_{el} increase. The instant COP_{el} starts to be greater than zero after a certain time because, at the beginning of adsorption, the water flowing in the tubes takes some minutes to reach the temperature set. The maximum instant COP_{el} for $L_z = 5cm$ is equal to 8.6, while, for $L_z = 30cm$ it corresponds to 6.42. Concerning the average COP_{el}, the one obtained with $L_z = 5cm$ is approximately equal to 2.71 and drop to about 2.38 for $L_z = 30cm$, with a reduction of 12.2%.

This can be explained looking at the result of single contributions. The latent, sensible and global cooling power are showed in Figure 4.4 (considering the adsorption process only).

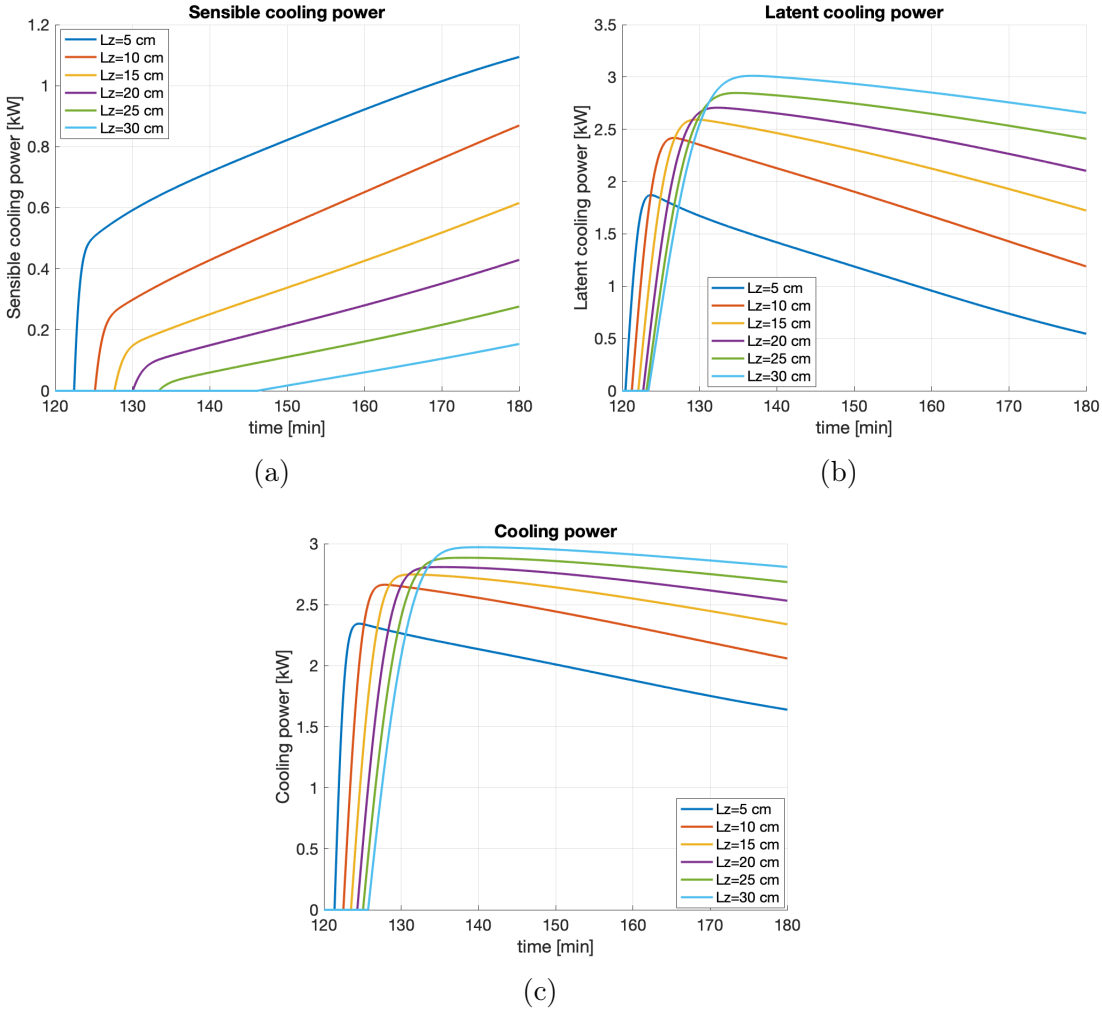

Figure 4.4: Sensible, latent and global cooling power for different heat exchanger lengths

In general, the sensible cooling power increases as time passes by, while the latent cooling power diminishes. This is explained by the fact that the latent cooling power has the same trend of the air moisture removal, which decreases as the silica-gel water uptake raises. At the same time, the sensible cooling power grows, since the cold water has to remove less adsorption heat as time goes on and, so, can cool down air. The global trend of the cooling power follows the one of the latent cooling power since it represents the most significant contribution.
The maximum value of cooling power is obtained for $L_z = 30cm$ with a value of 2.97 kW, while the minimum results from the simulation with $L_z = 5cm$ with a cooling power equal to 2.35 kW (20.9% lower). There is a significant difference passing from

$L_z = 5cm$ to $L_z = 10cm$ (the maximum value increases of 13.6%), afterwards, the maximum values are all around 2.8 kW.

The electric power contributions are shown in Figure 4.5.

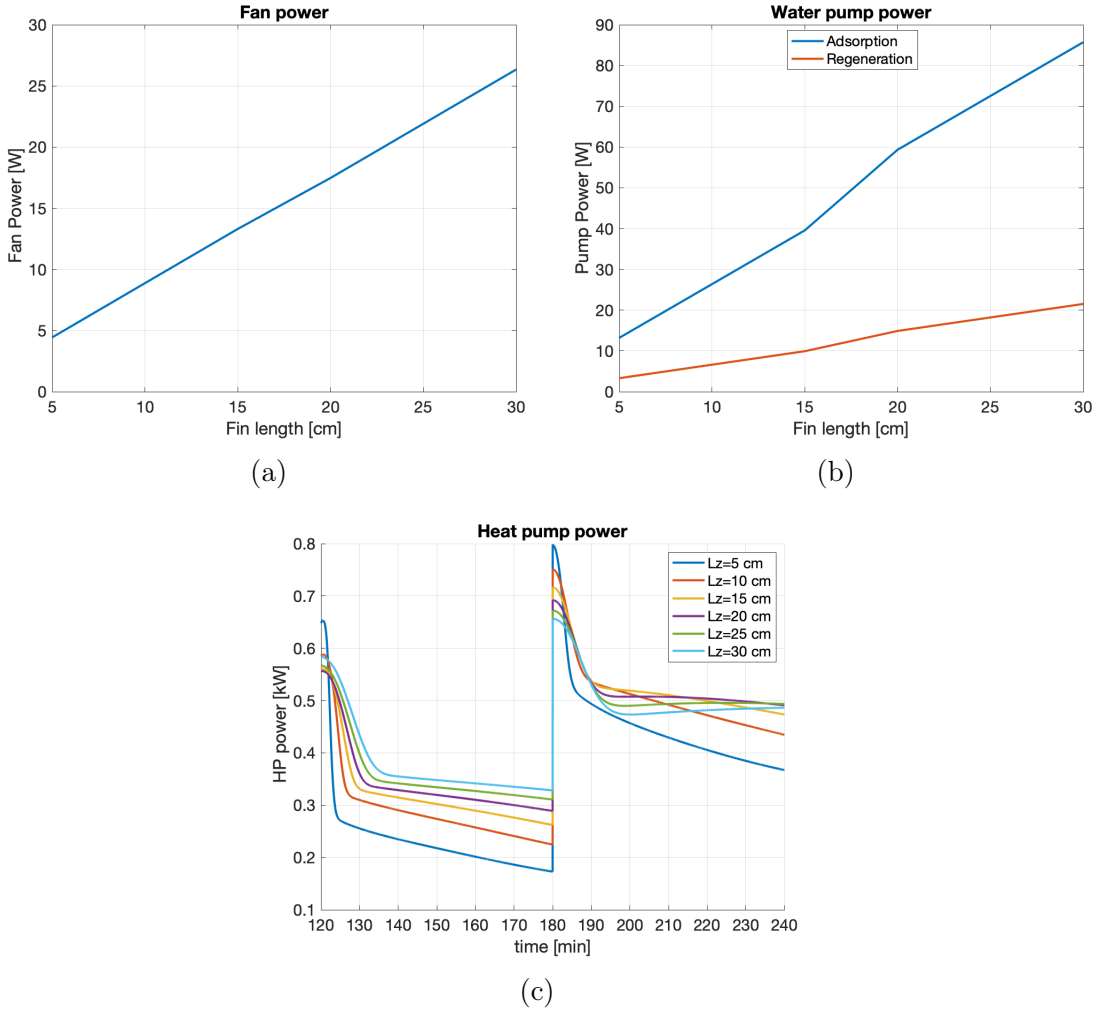

Figure 4.5: Fan, water pump and heat pump electric power for different heat exchanger lengths

The fan power linearly increases as the length of the heat exchanger grows, passing from 4.44 W with $L_z = 5cm$ to 26.4 W for $L_z = 30cm$.
The water pump power changes between adsorption and regeneration because the water mass flow rates are different. The trend is almost linear with the increment of the battery length. The electric power required when $L_z = 5cm$ is 13.2 W during adsorption and 3.31 W during regeneration and reaches 85.7 W during adsorption and 21.5 W during regeneration using $L_z = 30cm$.
The heat pump, then, consumes more power at the beginning of adsorption when

$L_z = 5cm$ because the water temperature, from the previous regeneration cycle, is higher than for the other cases and it needs to be cooled down to 20 °C. Similarly, as regeneration starts, the water flowing in the tubes is at a lower temperature level with respect to the other cases, so, more power from the heat pump is needed to bring water up to 50 °C. But afterwards, since the temperature of water for lower values of L_z is closer to the set point, the power required to the heat pump is inferior. It may be noted that the heat pump electric power change significantly passing from $L_z = 5cm$ to $L_z = 10cm$, with an increment in the total energy required of 16.9%. Then, it approaches almost the same value, with a slight increase of electric energy between $L_z = 25cm$ and $L_z = 30cm$ (0.68%).
So, even if the cooling power is lower for $L_z = 5cm$, at the same time, the electric power required for the system functioning is much lower. This results in a higher COP_{el}.

$\mathbf{COP}_{th}$

The resulting COP_{th} is reported in Figure 4.6.

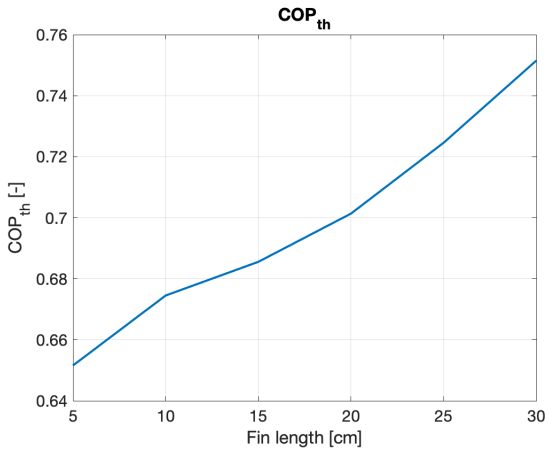

Figure 4.6: COP_{th} as a function of heat exchanger length

The maximum COP_{th} is obtained with $L_z = 30cm$ ($\text{COP}_{th} = 0.75$), then, as the length decreases, it almost linearly diminishes reaching the value of 0.65 when $L_z = 5cm$.
The cooling power is the one previously reported in Figure 4.4c , while the water thermal power exchanged during regeneration is shown in Figure 4.7.
It can be observed that the heating power for $L_z = 5cm$ is lower than that of the other lengths, with an amount of heat exchanged equal to 2.95 kWh. Then, the other values are quite similar, in the range of 3.3-3.45 kWh with a decrement between the values corresponding to $L_z = 30cm$ and $L_z = 5cm$ of 10.6%.

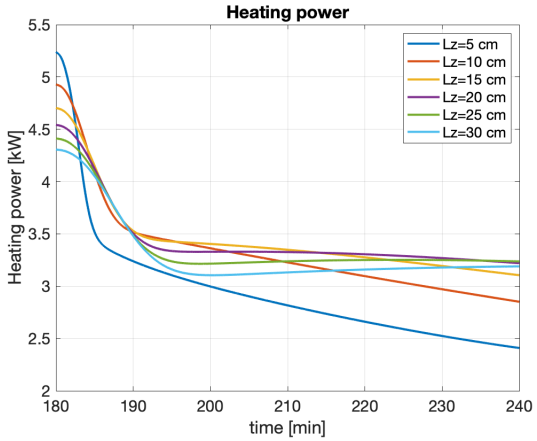

Figure 4.7: Water heating power

Considering the cooling energy, instead, it is maximum for $L_z = 30cm$ with a value of 2.48 kWh, and it diminishes to 1.92 kWh when $L_z = 5cm$ (22.5 % lower).
So, since the diminishing of cooling energy is greater than the heating energy supplied by water as the length decreases, the COP_{th} raises with the length.

Moisture removal effectiveness

The resulting moisture removal effectiveness as a function of the heat exchanger length, is shown in Figure 4.8.

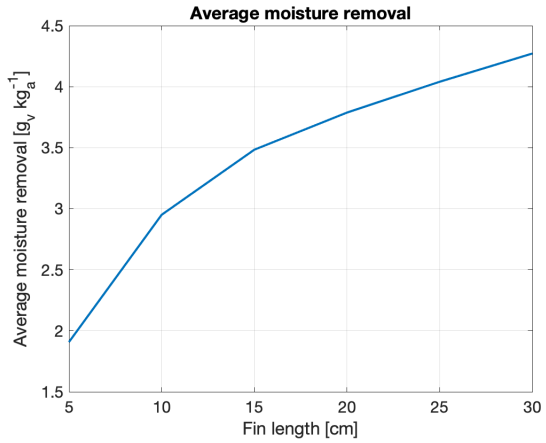

Figure 4.8: Average moisture removal as a function of heat exchanger length

It is possible to notice that the average value of moisture removal raises as the length increases. In particular, between $L_z = 5cm$ to $L_z = 10cm$, the value significantly increases, passing from an average moisture removal of 1.91 $g_v kg_a^{-1}$ to a value of 2.95 $g_v kg_a^{-1}$ (54.4% higher) with $L_z = 10cm$, then, it grows up to the maximum value, equal to 4.27 $kg_v kg_a^{-1}$, when $L_z = 30cm$.

This trend is justified by the fact that as the length increases, the silica-gel quantity raises and so the capacity of the system of removing moisture from air grows.

4.2.2 Influence of the hot water temperature

In this section, the performance is evaluated varying the hot water temperature in the range 50-70 °C. This is done fixing the average v_a at 0.8 m/s, T_{w_c} at 20 °C and the heat exchanger length at 100 mm.
The outlet air temperature, specific humidity and the silica gel average water uptake over time are reported in Figure 4.9.

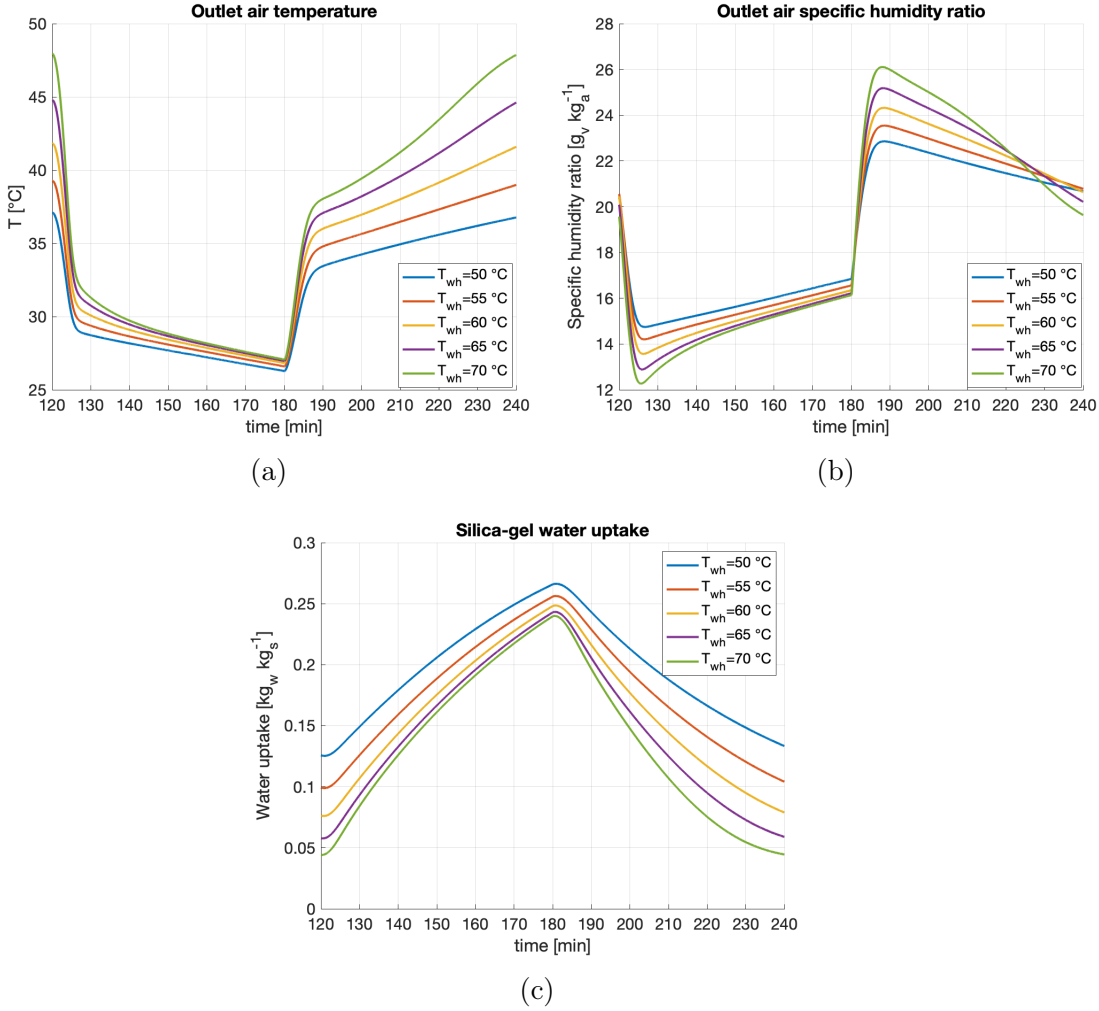

(a) (b)

(c)

Figure 4.9: Temperature, specific humidity of outlet air and silica-gel water uptake for different hot water temperatures

Considering the outlet air temperature, its main variation, as the hot water set point changes, occurs throughout regeneration, during which, it reaches the value of about 36.8 °C when T_{w_h} is equal to 50 °C and 47.9 °C when T_{w_h} corresponds

to 70 °C, with an increment of 30.2%. The average outlet air temperature during regeneration, instead, increases by 19.4% passing from 50 °C to 70°C with values respectively equal to 34.5 °C and 41.2 °C. During adsorption, instead, the average value of the outlet air temperature for all the hot water temperature used is around 29.2 °C.

Then, observing the plot of the outlet air specific humidity, the results obtained during adsorption are similar, but as the hot water temperature grows, the minimum value reached decreases. In fact, when T_{w_h} is equal to 50 °C, the minimum value of outlet air specific humidity is equal to 14.8 $g_v kg_a^{-1}$, while, for T_{w_h} =70°C, it corresponds to 12.3 $g_v kg_a^{-1}$ with a decrement of 16.9%. This is explained by the fact that, for lower hot water temperatures, the amount of water vapor desorbed, during regeneration, diminishes and, consequently, the capacity of the material of removing moisture from air is reduced. In fact, the average water uptake at the end of regeneration, when T_{w_h} is set to 50 °C, is equal to 0.13 $kg_w kg_s^{-1}$, instead, for T_{w_h}=70 °C, it corresponds to 0.04 $kg_w kg_s^{-1}$ (more than three times lower). Moreover, at the end of regeneration cycle, it can be noticed that the outlet air specific humidity almost coincides with the inlet value as the hot water temperature raises, meaning silica-gel is close to be completely regenerated. The maximum value of outlet air specific humidity diminishes together with the hot water temperature, passing from 26.1 $g_v kg_a^{-1}$ when T_{w_h}=70°C to 22.9 $g_v kg_a^{-1}$ for T_{w_h}=50 °C with a decrement of 12.3%. This means that with higher hot water temperatures is possible to regenerate the silica-gel more rapidly.

$\mathbf{COP}_{el}$

The instant and the average electric COP are reported in Figure 4.10.

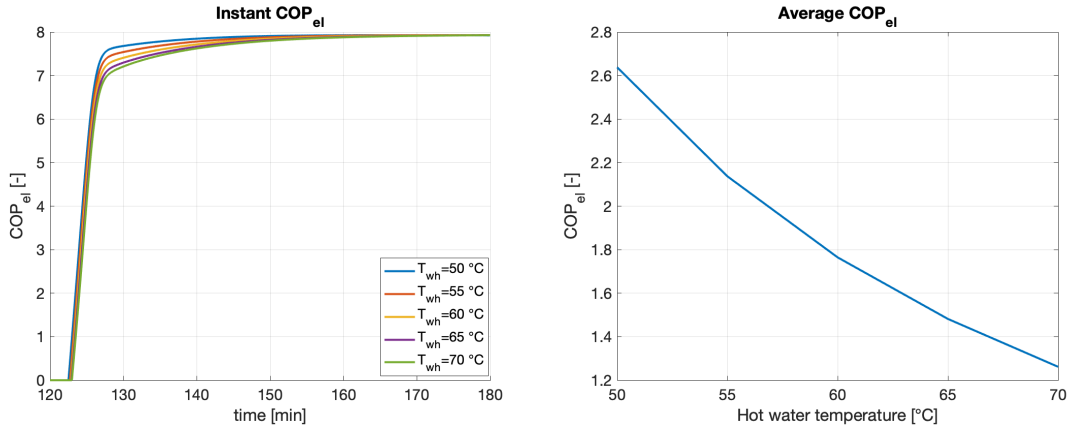

Figure 4.10: Instant and average COP_{el} as a function of hot water temperature

The instant COP_{el} is quite the same for all the hot water temperatures (it reaches a maximum value around 8 for all the cases considered), since it depends on adsorption process, so, it is slightly affected by the regeneration water temperature. The average COP_{el}, instead, considers the entire cycle and it reduces as the hot water temperature grows, decreasing from 2.64 for T_{w_h}=50 °C to 1.26 for T_{w_h}=70 °C (decrement of 52.3%). This can be addressed analysing the output of all the contributions.

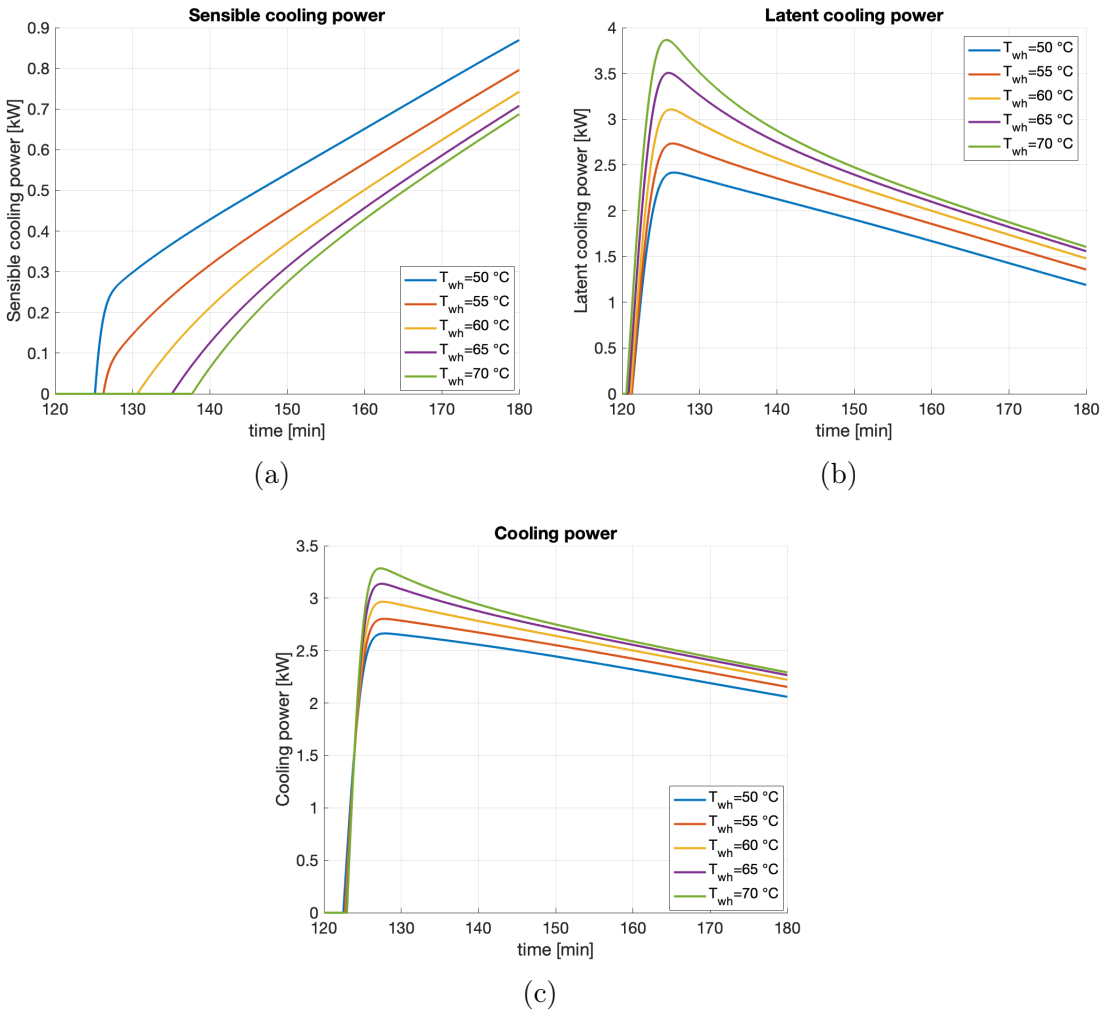

Figure 4.11: Sensible, latent and total cooling power as a function of hot water temperature

Figure 4.11 shows the cooling power and the relative sensible and latent share. Again, the total cooling power follows the trend of the latent one, since its contribution is higher than that of sensible cooling power. The trends are similar for all the hot water temperatures, but the values are different. The maximum sensible cooling power decreases, raising the hot water temperature, from 0.87 kW to 0.69 kW. In particular, the difference between two consecutive hot water temperatures is

higher between T_{w_h}=50 °C and T_{w_h}=55 °C, with a maximum sensible cooling power decreasing by 8.6%.
The peak of latent cooling power varies significantly increasing T_{w_h} from 50 °C to 70 °C, with values respectively equal to 2.42 kW and 3.87 kW, corresponding to an increment of 59.9%.
The resulting total cooling power is higher as the hot water temperature raises, with a maximum value increasing from 2.66 kW when T_{w_h}=50 °C to 3.29 kW for T_{w_h}=70 °C (23.7% higher).
In conclusion, a higher latent cooling power is associated with higher regeneration temperatures, since the capacity of moisture removal increases, for the same reason, the sensible cooling power has the opposite trend as the amount of adsorption heat to be removed is higher.

Considering now the electric power required by the fan and the water pump, they do not change with the hot water temperature and are equal to $\dot{W}_{el_{fan}}$=8.87 W, $\dot{W}_{el_{pump}}$=26.4 W during adsorption and $\dot{W}_{el_{pump}}$=6.62 W during regeneration.
Instead, the trend of the electric power required by the heat pump is reported in Figure 4.12.

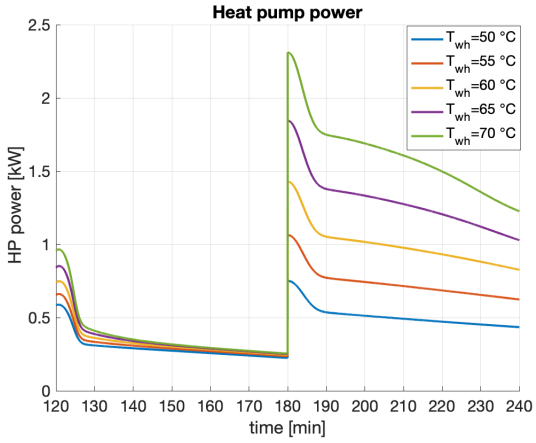

Figure 4.12: Heat pump electric power as a function of hot water temperature

It can be noticed that there is a big difference of heat pump electric power during regeneration as the hot water temperature varies: the maximum value for T_{w_h}=70 °c is equal to 2.31 kW, while, for T_{w_h}=50 °C, it correspond to 0.75 kW with a decrement of 67.5%. This is explained by the fact that, when the hot water temperature set point is higher, more heat power has to be supplied to the water in order to bring it and to maintain it at the fixed value.
In conclusion, increasing the hot water temperature means enhancing the cooling

effect of the heat exchanger, but also requiring more electric power in order to run the heat pump. The contribution of the heat pump is the dominant one, since it significantly varies with hot water temperature, while, the cooling power changes to a lesser extent, so, the average COP_{el} will decrease as the hot water temperature grows.

COP_{th}

The resulting COP_{th} is reported in Figure 4.13.

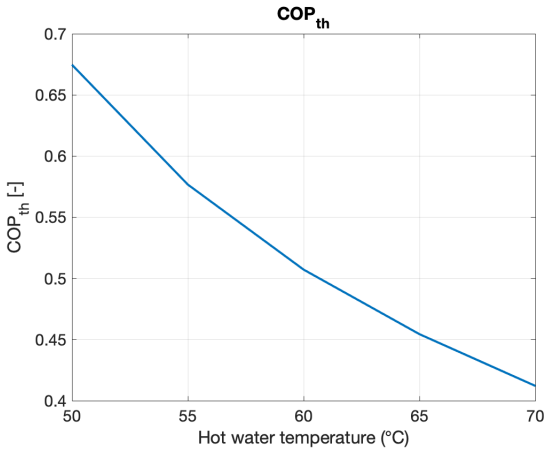

Figure 4.13: COP_{th} as a function of hot water temperature

It decreases as the hot water temperature raises, passing from 0.67 for T_{w_h}=50 °C to 0.41 for T_{w_h}=70 °C, with a correspondent decrement equal to 38.8%.

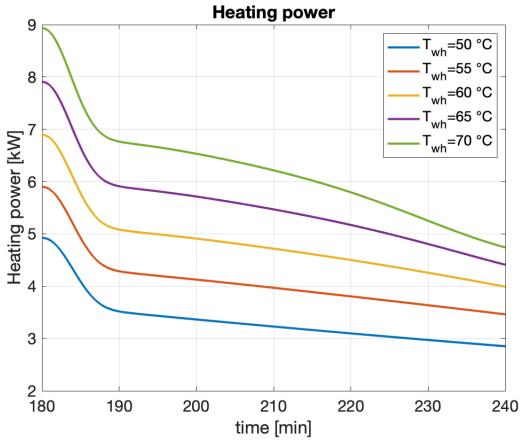

Figure 4.14: Water heating power for different hot water temperatures

The cooling power has already been reported and discussed in Figure 4.11c, while, the water thermal power exchanged during regeneration is shown in Figure 4.14. It reduces with time, as the regeneration process goes on, and significantly varies with

the set point of hot water temperature. In fact, as the temperature level rises, the ΔT between water and air expands, allowing more heat exchange. The correspondent heat supplied by water goes from 3.33 kWh for T_{w_h}=50 °C to 6.21 kWh with T_{w_h}=70 °C (increment of 86.3%). Since the cooling power does not considerably change with hot water temperature as the heating power does, the heating power has a strong impact on the resultant COP_{th}.

Moisture removal effectiveness

The resulting moisture removal effectiveness as a function of the regeneration hot water temperature is reported in Figure 4.15.

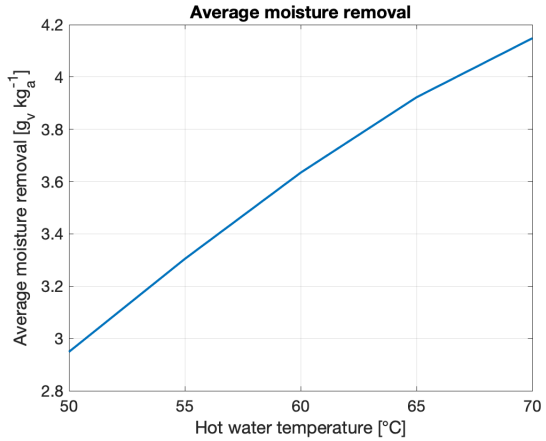

Figure 4.15: Average moisture removal as a function of hot water temperature

Differently from the other two performance coefficients, COP_{el} and COP_{th}, the moisture removal effectiveness increases with higher hot water temperatures because it has been seen before that the outlet specific humidity presents the minimum value in the case in which the water temperature is equal to 70 °C. So, the average moisture removed from air grows together with the hot water temperature, increasing from 2.95 $g_v kg_a^{-1}$ (T_{w_h}=50 °C) to 4.15 $g_v kg_a^{-1}$ (T_{w_h}=70 °C), which corresponds to an increment of 40.7%.

4.2.3 Influence of cold water temperature

In this step, the performance coefficients are evaluated varying the adsorption cold water temperature from 15 °C to 25 °C, fixing the average v_a at 0.8 m/s, T_{w_h} at 50 °C and the heat exchanger length at 100 mm.
The outlet air temperature, specific humidity and the silica-gel average water uptake over time are reported in Figure 4.16.

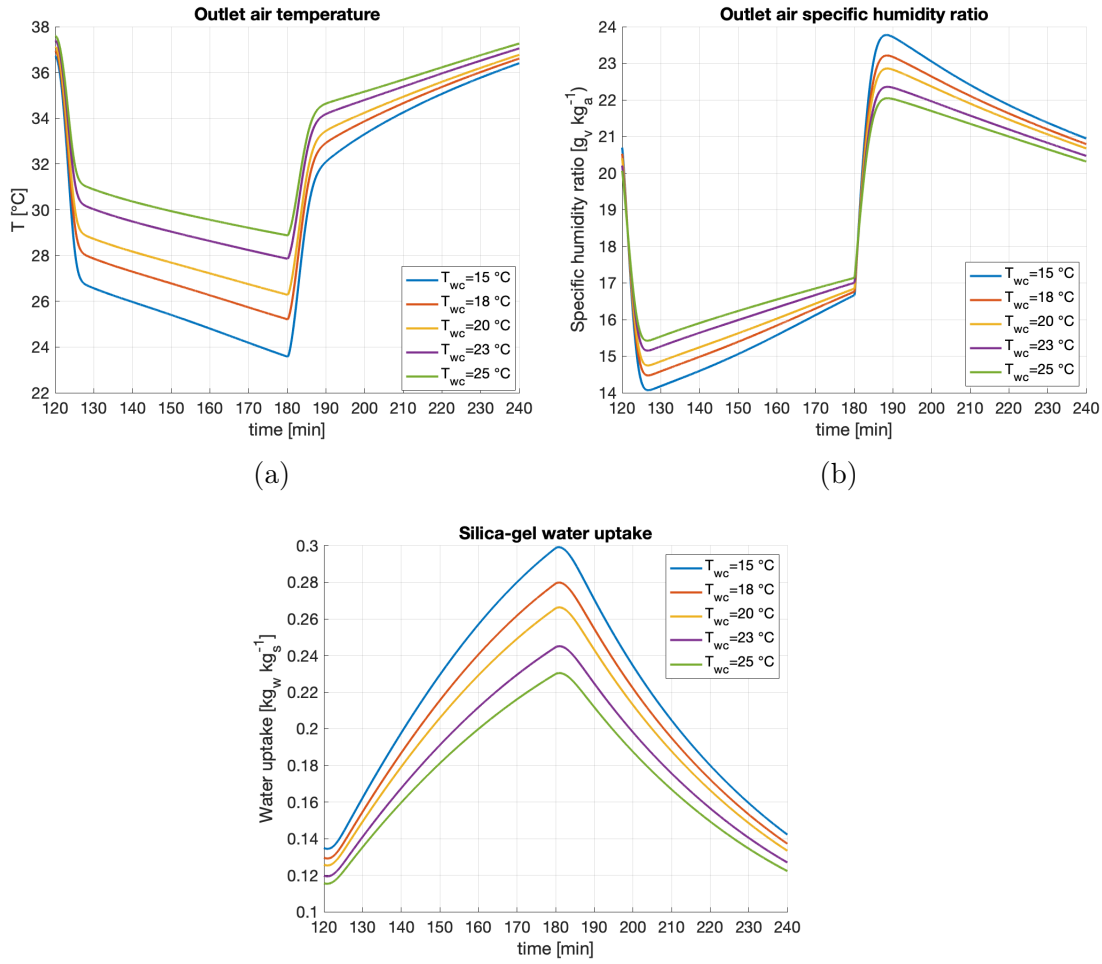

Figure 4.16: Temperature, specific humidity of outlet air and silica-gel water uptake for different cold water temperatures

The lower is the cold water temperature, the higher are the heat and the moisture removed from air. In fact, the outlet air temperature at the end of adsorption is equal to 28.9 °C when T_{w_c}=25 °C and reduces until 23.6 °C for T_{w_c}=15 °C (18.3% lower). The average values of temperature during adsorption for T_{w_c}=15 °C and T_{w_c}=25 °C are, instead, respectively equal to 25.9 °C and 30.4 °C. Afterwards, during regeneration, even if the starting temperatures of air are very different, then, they converge to a temperature approximately correspondent to 36.5 °C.
Considering the outlet air specific humidity, it diminishes as the temperature lowers, but then converges to almost the same value (16.8 $g_v kg_a^{-1}$). The minimum value coincides with 14.0 $g_v kg_a^{-1}$ when T_{w_c}=15 °C and increases to 15.4 $g_v kg_a^{-1}$ with T_{w_c}=25 °C (10.0% higher). During regeneration, instead, the maximum value corresponds to the minimum cold water temperature (23.8 $g_v kg_a^{-1}$), while, the lowest outlet air specific humidity peak is obtained with T_{w_c}=25 °C (22.1 $g_v kg_a^{-1}$), with a reduction

of 11.3%.
Accordingly to the fact that for lower cold water temperatures, the moisture removed from air is higher, the silica-gel water uptake almost reaches 0.30 $kg_w kg_s^{-1}$ for the coldest water temperature and decreases up to 0.23 $kg_w kg_s^{-1}$ when T_{w_c}=25 °C with a decrement of 23.3%.

$\mathbf{COP}_{el}$

The instant and the average COP_{el} are reported in Figure 4.17.

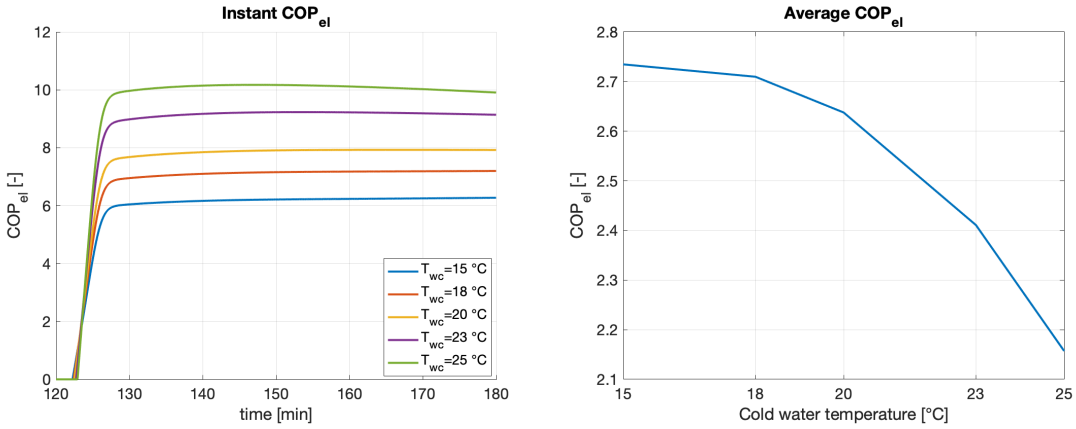

Figure 4.17: Instant and average COP_{el} for different cold water temperatures

The instant COP_{el} significantly changes from temperature to temperature: it is much lower in the case of the lowest cold water temperature. The maximum value for T_{w_c}=15 °C, in fact, is equal to 6.27, while, for T_{w_c}=25 °C, it reaches 10.2, with an increment of 62.7%. But, at the same time, the average value of COP_{el} is higher for lower cold water temperatures: it remains the same until 20 °C an then rapidly diminishes. It corresponds to 2.73 for T_{w_c}=15 °C and decreases until 2.16 when T_{w_c}=25 °C (20.9% lower). In order to understand these results, the single contributions have to be analyzed.

In Figure 4.18, sensible, latent and total cooling power are shown.
Cooling power significantly changes as the cold water temperature varies. The sensible share results in a correspondent sensible cooling energy equal to 1.02 kWh when T_{w_c}=15 °C and diminishes up to 71 Wh for T_{w_c}=25 °C, with a reduction of 68.6%. Considering the latent cooling power obtained from each temperature, it almost converges, at the end of adsorption, to a value in the range of 1-1.3 kW. Its peak, instead, considerably changes together with the cold water temperature variation. In fact, when T_{w_c}=15 °C the maximum latent cooling power is equal to 2.83 kW,

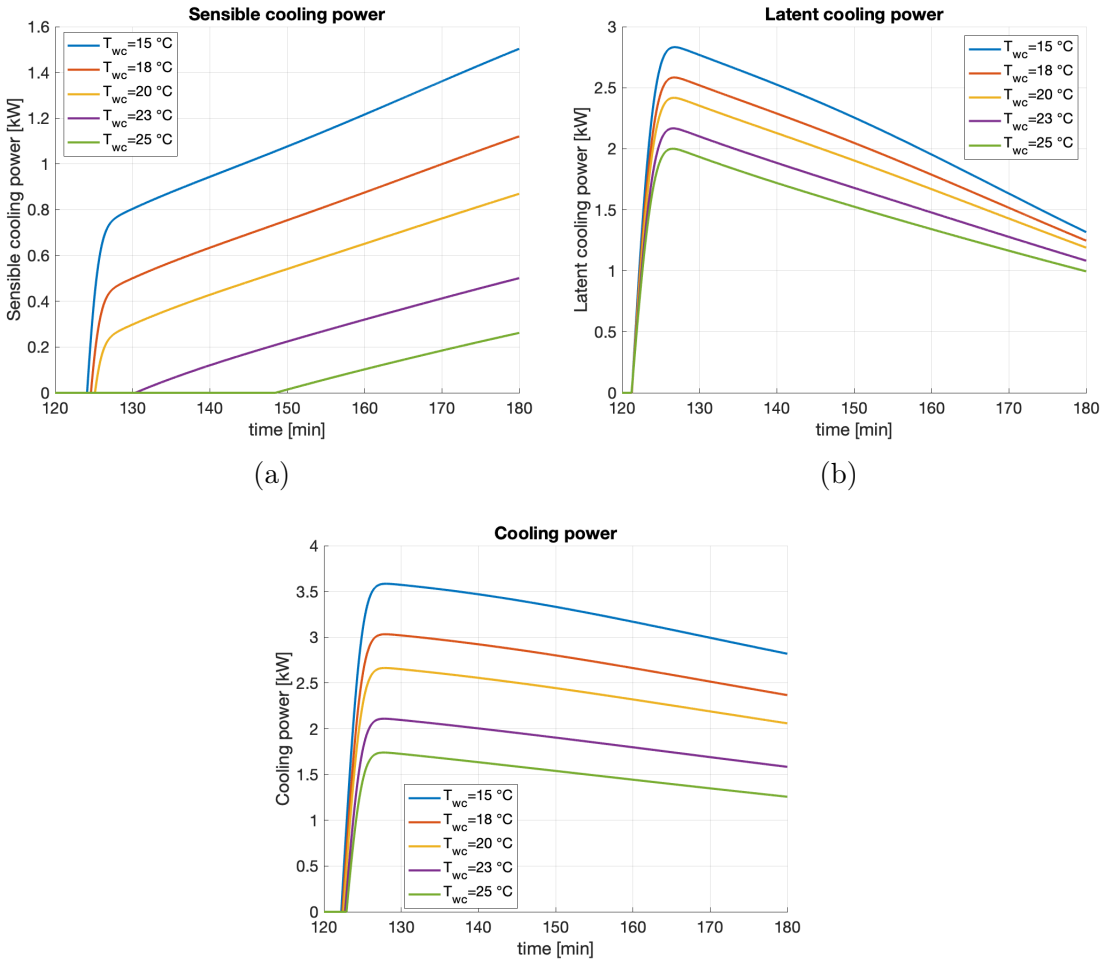

Figure 4.18: Sensible, latent and total cooling power for different cold water temperatures

while, for T_{w_c}=25 °C it corresponds to 2.00 kW (29.3% less).
The resulting total cooling power follows the trend of the latent cooling power, since it represents the major contribution, even if at the end of adsorption, the total power does not converge to a certain value. When T_{w_c}=15 °C, the peak value reached is equal to 3.58 kW and the cooling energy obtained is equal to 3.07 kWh, while, for T_{w_c}=25 °C they are respectively equal to 1.74 kW and 1.41 kWh.

Considering now the electric power contributions, the fan and water pump electric powers are respectively equal to $\dot{W}_{el_{fan}}$=8.87 W, $\dot{W}_{el_{pump}}$=26.4 W during adsorption and $\dot{W}_{el_{pump}}$=6.62 W during regeneration. The trend of the electric power required by the heat pump, instead, is reported in Figure 4.19.
The heat pump electric power is higher at the beginning of the two cycles (adsorption and regeneration) because the water flowing in the tubes has to be brought to the

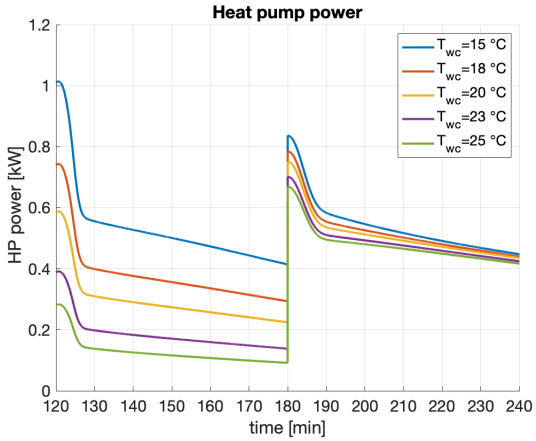

Figure 4.19: Heat pump electric power for different cold water temperatures

new set point temperature. Moreover, the power required when the cold water temperature is lower, is much higher. In fact, it reaches 1.01 kW when T_{w_c}=15 °C and reduces to 0.28 kW for T_{w_c}=25 °C, with a decrement of 72.3%. In energy terms, with a total cycle of 2 h, the electric energy required by the heat pump corresponds to 1.07 kWh in the case T_{w_c}=15 °C and to 604 Wh when T_{w_c}=25 °C (reduction of 43.6%). During regeneration, the values of the electric power are almost coincident, except for the first minutes, when the temperature of water, being at different temperature levels at the end of adsorption for the different cases, has to be raised up to the regeneration temperature.

From the results just reported, the instant COP_{el} trend is explained by the fact that, even if the cooling power for lower cold water temperatures is higher, also the electric power required by the heat pump is much higher for lower temperatures. The average COP_{el}, instead, considers the entire cycle (adsorption and regeneration), integrating all the power contribution over time, so, the resultant value is higher as the cold water temperature diminishes.

COP_{th}

The COP_{th} obtained is reported in Figure 4.20.
It may be noticed that the thermal COP almost linearly lowers as the cold water temperature raises, passing from 0.87 when T_{w_c}=15 °C to 0.45 for T_{w_c}=25 °C, decreasing by 48.3%.
The cooling power has already been shown in Figure 4.18, instead, the water thermal power exchanged during regeneration is shown in Figure 4.21.
It can be observed that the water heating power is higher in the case of the cold

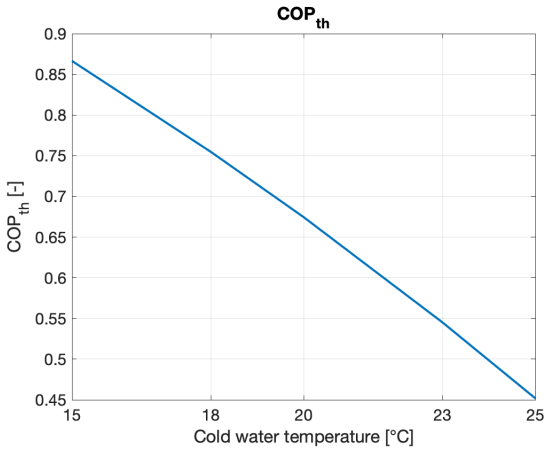

Figure 4.20: COP_{th} as a function of cold water temperature

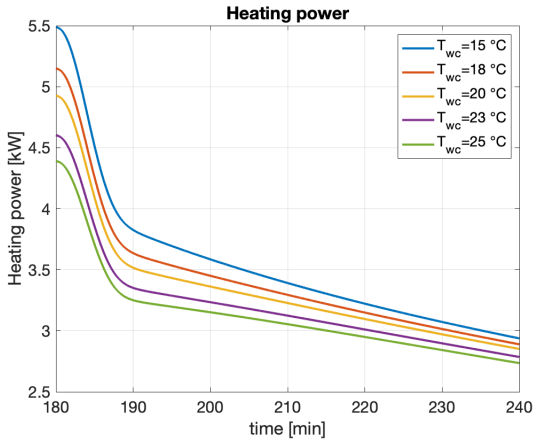

Figure 4.21: Water heating power for different cold water temperatures

water temperature equal to 15 °C with a maximum value correspondent to 5.49 kW, while, for T_{w_c}=25 °C, the maximum power is equal to 4.39 kW with a decrement of 20.0%. But, afterwards, the curves for the different temperatures, as time passes by, almost converge. Instead, the heat exchanged throughout regeneration for T_{w_c}=15 °C and T_{w_c}=25 °C are respectively equal to 3.54 kWh and 3.13 kWh (11.7% lower). Therefore, both cooling and heating power are higher for lower cold water temperatures, but, the cooling power contribution is dominant, so, the resulting thermal COP, increases as the cold water temperature diminishes.

Moisture removal effectiveness

The average moisture removed from air as a function of the regeneration cold water temperature is reported in Figure 4.22.
The average moisture removed from air decreases as the cold water temperature increases, passing from a value equal to 3.43 $g_v kg_a^{-1}$ for T_{w_c}=15 °C and 2.42 $g_v kg_a^{-1}$

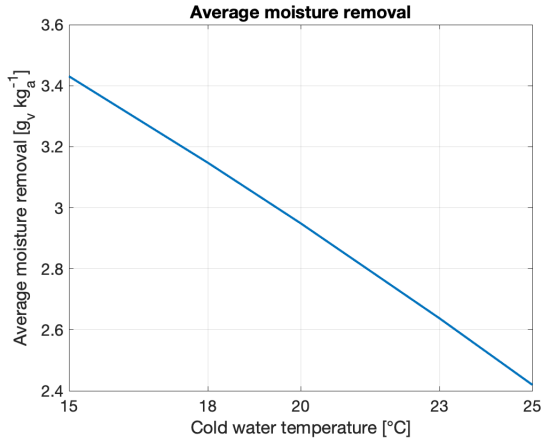

Figure 4.22: Average moisture removal as a function of cold water temperature

for T_{w_c}=25 °C (29.4% lower).
This is explained by the fact that, with a colder water temperature, both the mass and heat transfer mechanism are enhanced.

4.2.4 Influence of air stream velocity

In this step, the simulations are carried out changing the air stream velocity, with T_{w_c} at 20 °C, T_{w_h} at 50 °C and a battery length equal to 100 mm.
The outlet air temperature, specific humidity and the silica-gel water uptake over time are reported in Figure 4.23.
It can be noticed that, during adsorption, for lower velocity values, the air exits at a higher temperature at the beginning, because of higher temperatures reached during regeneration, but then, it rapidly diminishes with the lowest value correspondent to a velocity of 0.2 ms^{-1}. At the end of adsorption, in fact, the outlet air temperature is equal to 25.0 °C with v_a fixed at 0.2 ms^{-1} and reaches 26.9 °C when v_a=1.6 ms^{-1} (increment of 7.6%). It can be observed that the result obtained with the lowest v_a is significantly different from the others, while, even increasing v_a to 0.4 ms^{-1}, the output is quite similar to the ones relative to the other velocities. In fact, the average outlet air temperature during adsorption increases by 4.05% as v_a raises from 0.2 ms^{-1} to 0.4 ms^{-1}, while it grows by only 1.15% between v_a=0.4 ms^{-1} and v_a=0.6 ms^{-1}. The same behaviour occurs throughout regeneration, during which, the average outlet air temperature is much higher than the others when v_a=0.2 ms^{-1} (equal to 38.8 °C for v_a=0.2 ms^{-1}, 36.2 °C for v_a=0.4 ms^{-1} and 33.3 °C for v_a=1.6 ms^{-1}).
Concerning the outlet air specific humidity, the trend is similar of that of the outlet air temperature. The minimum value of it, 9.16 $g_v kg_a^{-1}$, is obtained with v_a=0.2

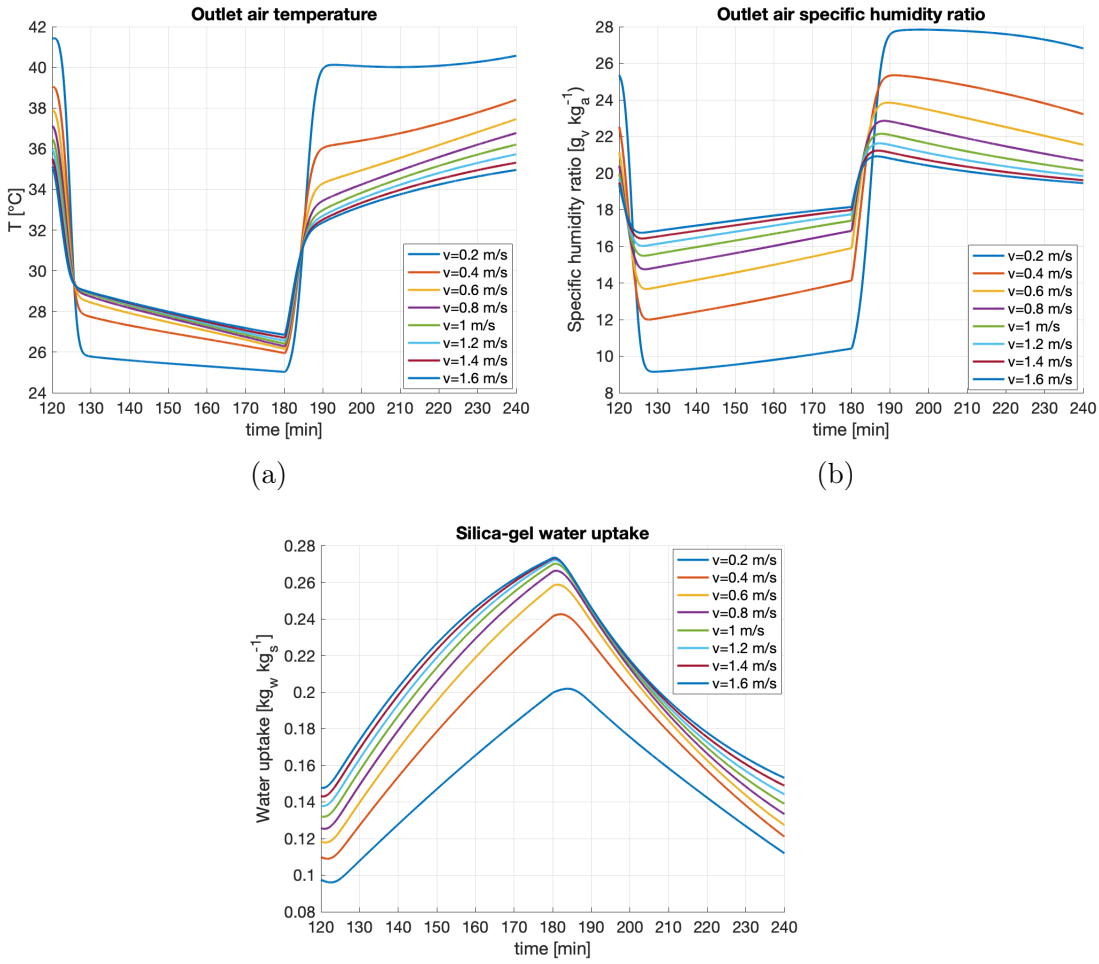

Figure 4.23: Temperature, specific humidity ratio of outlet air and silica-gel water uptake as a function of air velocity

ms^{-1}. The minimum value correspondent to v_a=1.6 ms^{-1}, instead, is equal to 16.7 $g_v kg_a^{-1}$, which is 82.3% higher. This occurs because a higher air velocity coincides with a larger air flow rate, meaning, more air enters the heat exchanger, so, there is a higher amount of water vapor to remove. In fact, observing the results of the silica-gel water uptake, it is higher as the air velocity increases, because, even if the outlet air specific humidity is higher, the amount of water captured is larger with respect to lower air velocities. The maximum average water uptake for v_a=0.2 ms^{-1} is equal to 0.20 $kg_w kg_s^{-1}$, while, for v_a=1.6 ms^{-1} it reaches 0.27 $kg_w kg_s^{-1}$ with an increment of 35%.

$\mathbf{COP}_{el}$

Instant and average COP_{el} are reported in Figures 4.24.

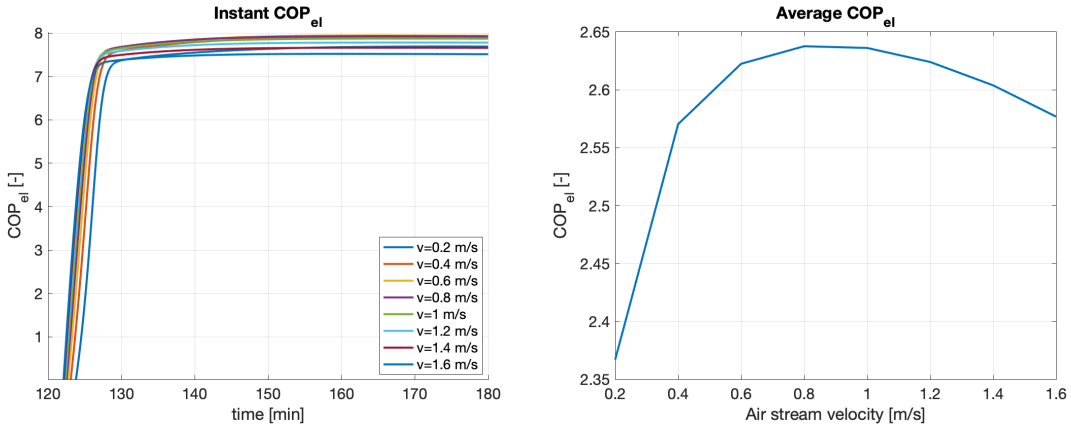

Figure 4.24: Instant and average COP_{el} as a function of air velocity

It may be observed that the instant COP_{el} is similar for all the velocities analyzed, achieving a maximum value approximately in the range of 7.5-7.9. The average value, instead, rapidly increases passing from 0.2 ms^{-1} (equal to 2.37) to 0.4 ms^{-1} (correspondent to 2.57), then continues to raise until a value of 2.64 when v_a=0.8 ms^{-1}. Afterwards it slightly decreases until 2.58 for v_a=1.6. ms^{-1}. The increment between the values obtained with v_a=0.2 ms^{-1} and v_a=0.8 ms^{-1} is equal to 11.4%.

In order to understand these trends, the single contributions are assessed starting from the cooling power, showed in Figure 4.25.
The sensible cooling power rises with higher air velocity values, reaching 0.29 kW for v_a=0.2 ms^{-1} and 1.47 kW for v_a=1.6 ms^{-1} (about 5 times higher). This great difference is due to the fact that, even if the difference in temperature (and so the sensible enthalpy) between inlet and outlet air rises as the velocity diminishes, the sensible cooling power is much lower because the air flow rate strongly reduces.
The latent cooling power considerably varies between v_a=0.2 ms^{-1} and v_a=0.6 ms^{-1}, then, it becomes more stable for the other velocities. The maximum values correspondent to v_a=0.2 ms^{-1}, v_a=0.4 ms^{-1} and v_a=0.6 ms^{-1} are respectively equal to 1.44 kW, 2.03 kW (50.0% higher) and 2.29 kW (12.8% greater than the value with v_a=0.4 ms^{-1}). The other velocities reach a value approximately equal to 2.5 kW. Moreover, it can be observed that the curves relative to v_a=0.2 ms^{-1} and v_a=0.4 ms^{-1}, are above the others starting from a certain time. This is explained by the fact that for low air velocities the outlet air humidity ratio is far from the inlet value, meaning silica-gel is not close to saturation, so, it still has a good capacity of

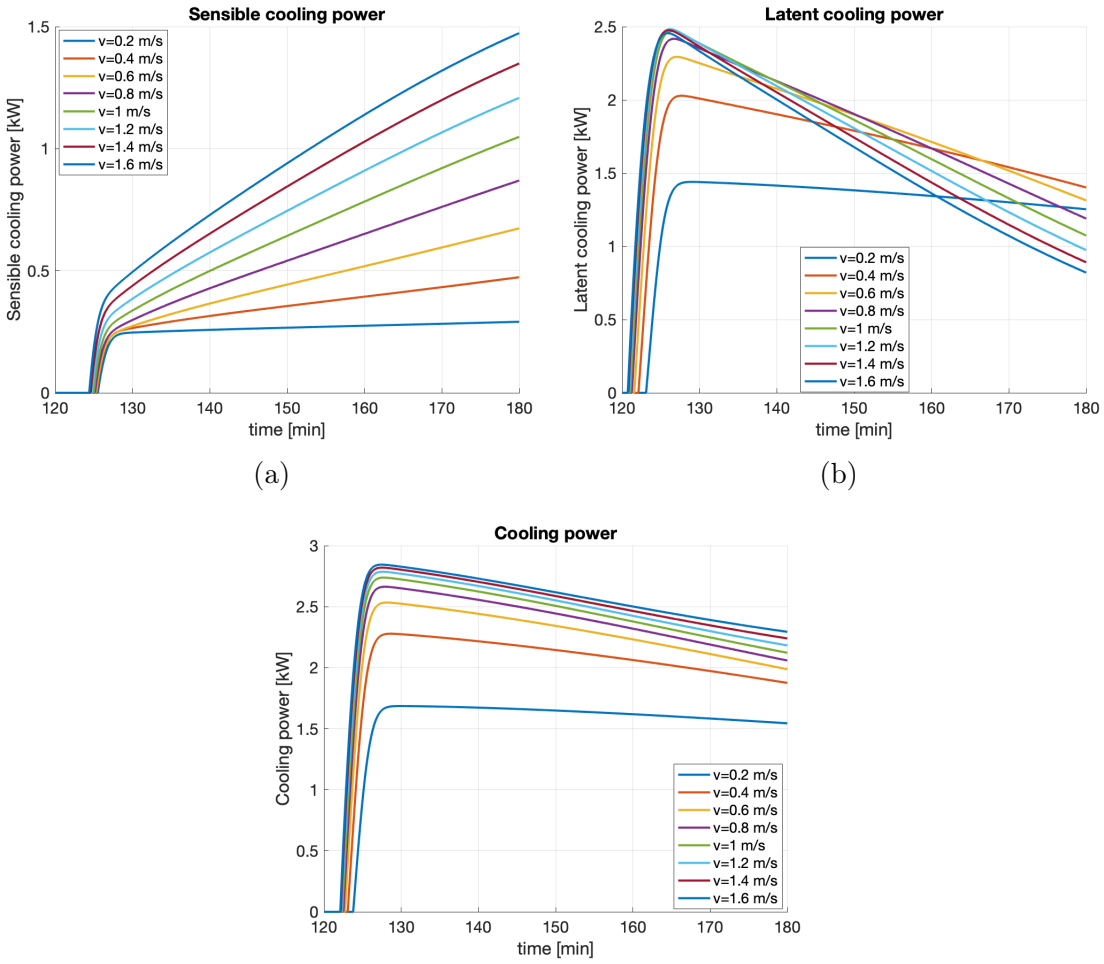

Figure 4.25: Sensible, latent and total cooling power as a function of air velocity

moisture removal.
The total cooling power increases as the air velocity grows, reaching almost a maximum fixed value (2.8 kW) as the air velocity is greater than 0.8 ms^{-1}. For v_a=0.2 ms^{-1} the maximum value coincides with 1.69 kW, which is 40.7% lower than that obtained with v_a=1.6 ms^{-1} (equal to 2.85 kW). The cooling energy, during adsorption, obtained with v_a=0.2 ms^{-1} is equal to 1.50 kWh, while, for v_a=1.6 ms^{-1} is equal to 2.44 kWh (63.8% greater).

Considering now the electric power terms, the water pump electric power is constant and equal to $\dot{W}_{el_{pump}}$=26.4 W during adsorption and to $\dot{W}_{el_{pump}}$=6.62 W during regeneration. Instead, the trends of electric power required by the fan and the heat pump are reported in Figure 4.26.
The electric power required by the fan increases as the air velocity (and, consequently, the air flow rate) raises, passing from 0.55 W, when v_a=0.2 ms^{-1}, to 35.5

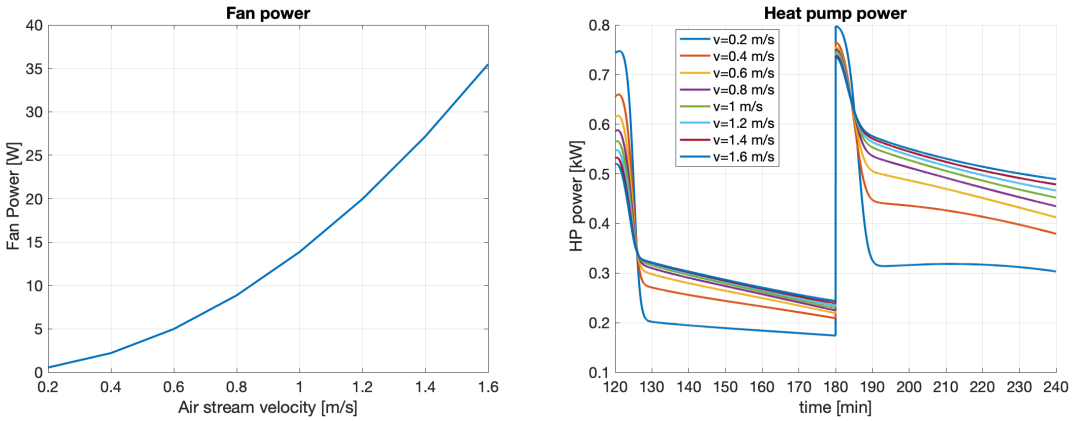

Figure 4.26: Fan and heat pump electric power for different air stream velocities

W with v_a=1.6 ms^{-1}.
The heat pump electric power, instead, is higher at the beginning of both adsorption and regeneration as air velocity lowers, afterwards, it rapidly decreases. The peaks values during adsorption are equal to 0.75 kW for v_a=0.2 ms^{-1} and to 0.52 kW for v_a=1.6 ms^{-1}, while, during regeneration, the maximum value is achieved with v_a=0.2 ms^{-1} (0.80 kW), instead, for the other air velocities, the maximum heat pump electric power approach a fixed value (0.75 kW). It can be noticed that the curve correspondent to v_a=0.2 ms^{-1} shows the greatest discrepancy with respect to the others. In fact, the electric heat pump energy required when v_a=0.2 ms^{-1}, for the entire cycle (adsorption and regeneration) is equal to 598 Wh, increasing to 724 Wh for v_a=0.4 ms^{-1} and, then, growing until a value of 845 Wh when v_a=1.6 ms^{-1}. The increment of the heat pump electric energy passing from v_a=0.2 ms^{-1} to v_a=0.4 ms^{-1} is equal to 21.1%, while increasing the air velocity from v_a=0.4 ms^{-1} to v_a=0.6 ms^{-1}, it is equal to 7.1%.

In conclusion, the average COP_{el} increases with air velocity because the cooling power contribution prevails. The flattening of the curve is due to the fact that for air velocity over 0.6 ms^{-1} the trends of all the contributions are quite similar. The fan power is the only term that varies considerably as the air velocity grows, but its absolute value is almost negligible with respect to the others.

$\mathbf{COP}_{th}$

The resulting COP_{th} is reported in Figure 4.27.
It can be seen that the thermal COP grows as the air velocity increases, starting from a value of 0.63 for v_a=0.2 ms^{-1} and reaching a value of 0.68 when v_a=1.6 ms^{-1},

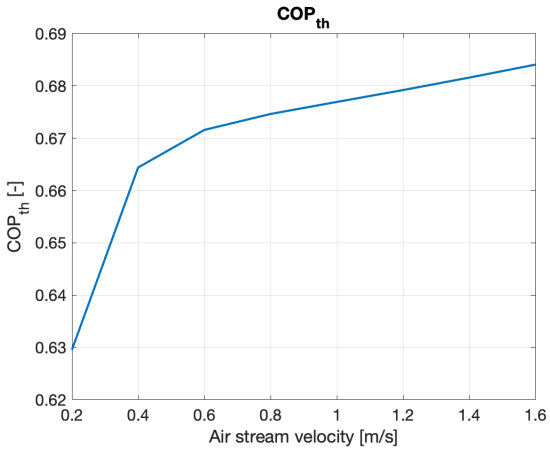

Figure 4.27: COP_{th} as a function of air velocity

with an increment of 7.9%. In particular, the COP_{th} significantly augments varying v_a between 0.2 ms^{-1} and 0.4 ms^{-1} (with an increase of 4.8%), then the curves tends to flatten.
The cooling power has been shown before, while, the water thermal power exchanged during regeneration is reported in Figure 4.28.

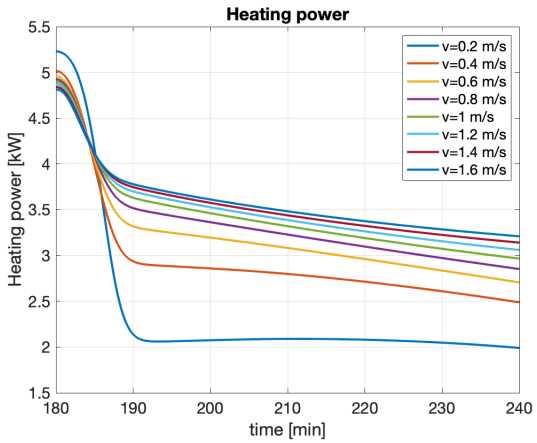

Figure 4.28: Water heating power as a function of air velocity

The water heating power is higher for lower air velocities at the beginning of regeneration, but, as time goes on, the trend is the opposite, with lower values correspondent to lower air velocities. Again, the curve obtained from v_a=0.2 ms^{-1} presents a significant discrepancy with respect to the others. Its maximum value is equal to 5.23 kW, while, for the other air velocities it approaches a value around 4.9 kW. The water heat exchanged is equal to 2.38 kWh when v_a=0.2 ms^{-1}, to 2.95 kWh for v_a=0.4 ms^{-1} (23.9% greater) and then it rises up to 3.58 kWh with v_a=1.6 ms^{-1}.

Therefore, the trend of the thermal COP is explained by the fact that, even if both cooling energy and water heat raise with air velocity, the value of cooling energy grows faster than that of the exchanged water heat.

Moisture removal effectiveness

The resulting average moisture removed from air is shown in Figure 4.29.

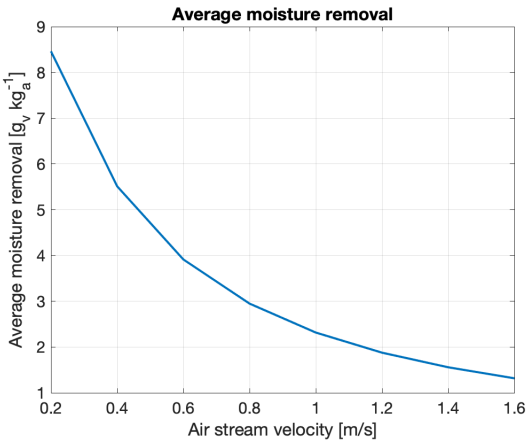

Figure 4.29: Average moisture removal as a function of air velocity

In this case, the average moisture removal diminishes significantly as the air velocity increases, with a value equal to 8.46 $g_v kg_a^{-1}$ when v_a=0.2 ms^{-1}, that reduces until 1.32 $g_v kg_a^{-1}$ for v_a=1.6 ms^{-1} (84.4% lower).
This results can be explained by the fact that the maximum difference between inlet and outlet specific humidity ratio occurs for the lowest air velocity, because the quantity of air crossing the heat exchanger is smaller, so more moisture can be removed.

Chapter 5

Dynamic simulations

In this chapter, dynamic simulations are carried out in order to analyze the system performance in a real operating environment.
The system is supposed to be located in Turin (Italy) and the simulations have been accomplished for a summer day characterized by high temperatures.
Afterwards, the influence of different switching times and air flow rates is assessed, with the purpose of understanding which is the best operating point in such external conditions.

5.1 Simulations input data

As previously mentioned, the location selected is the city of Turin. Meteorological data from [22] are used as input for the simulations, in particular the ones relating to the ambient temperature and relative humidity.
The climate files utilized collect, for each day of the year, average values derived from the years going from 2004 to 2018. So, in order to perform the simulations, a certain day has is chosen and it is one of the worst days, in terms of ambient temperature, of the month of June. Moreover, only the central hours of the day are considered (11.00 a.m. to 9.00 p.m), meaning the ones during which the ambient temperature overcomes 28 °C. The correspondent data are reported in Table 5.1.
Since the ones reported are hourly data, it is assumed that, during each hour, the values are constant, obtaining the curves reported in Figure 5.1.
It can be noticed that, during the time period considered of the day chosen, the ambient air which will enter the system, varies from 30 °C to 32 °C, while the relative humidity changes between 0.31 and 0.47.
Running the numerical model of the heat exchanger, these values are set, for each time step, as boundary and initial conditions for the inlet air stream.

Hour of the day	T_{amb} (°C)	RH (%)
11:00	30	38
12:00	31	36
13:00	30.8	42
14:00	32	31
15:00	32	34
16:00	32	36
17:00	32	36
18:00	31	40
19:00	31.7	47
20:00	30	35

Table 5.1: Ambient conditions

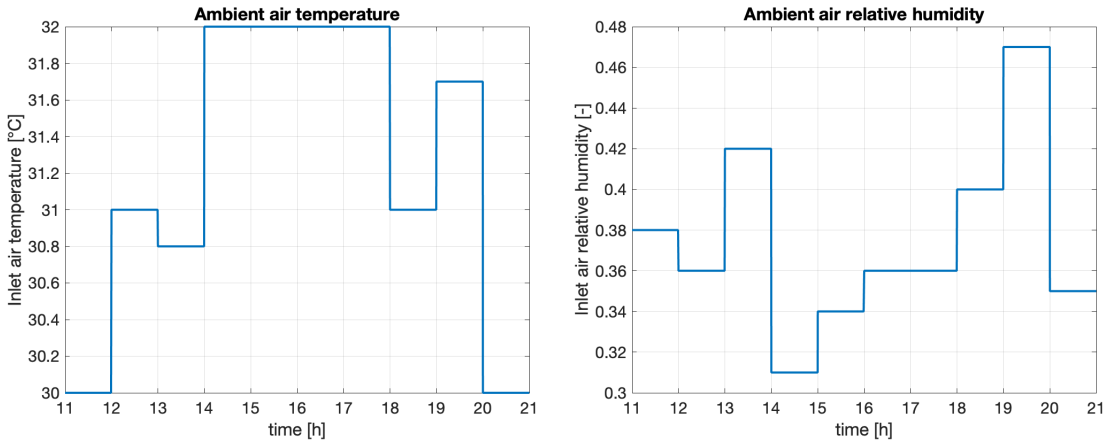

Figure 5.1: Temperature and relative humidity of ambient air

The switching time is set at 30 minutes, meaning a complete cycle (adsorption and regeneration) lasts 1 hour. The configuration of the heat exchanger and the silica gel properties and conditions are the ones reported in the previous chapter, in Table 4.1, setting the length of the battery equal to 200 mm. The air and water flow conditions are, instead, reported in Table 5.2.

Air and water flow conditions	
Average air velocity v_a	0.8 ms^{-1}
Adsorption water mass flow rate $\dot{m}_{w_{ads}}$	0.08 kgs^{-1}
Regeneration water mass flow rate $\dot{m}_{w_{ads}}$	0.05 kgs^{-1}
Cold inlet water temperature T_{w_c}	15 °C
Hot inlet water temperature T_{w_h}	50 °C

Table 5.2: Air and water flow conditions

5.2 Simulations results

In these section the simulations results are assessed. As the cycle switch time is set to be equal to 30 minutes, the operating mode alternation along the day is reported in Figure 5.2. The mode "1" corresponds to regeneration, while "0" coincides with adsorption mode.

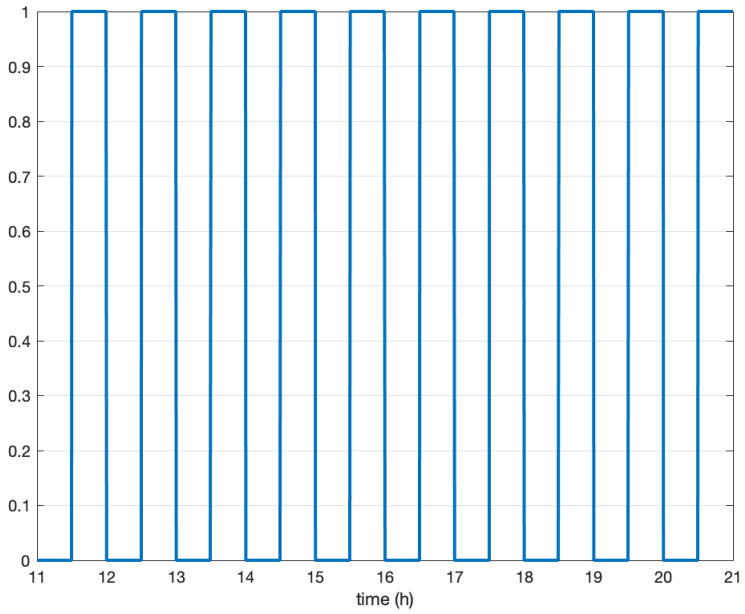

Figure 5.2: Operating mode alternation along the day

The output of outlet air temperature, specific humidity ratio and silica-gel water uptake are shown in Figure 5.3.
It can be noticed how the trend, for all the three parameters, during the first minutes (within first adsorption cycle) is different: this is the result of the initial conditions setting. Afterwards, the behaviour is always similar for each cycle, with variations of the maximum and minimum values.
Considering the outlet air temperature during adsorption, it is rapidly cooled down from the temperature reached at the end of the previous regeneration cycle (in general included in the range 33.5-36 °C), to a temperature level around 24.3-26.8 °C. The minimum outlet temperature is equal to 23.3 °C and it is reached at 20.30, when the ambient temperature is at the lowest level in the functioning period considered. The maximum temperature, instead, is almost the same along the day, around 36 °C, except for the last hour considered, in which the external temperature is at the minimum level and the relative humidity is low.
The outlet air specific humidity presents its maximum value (16.8 $g_v kg_a^{-1}$) around

19.43, when the ambient temperature is high (31.7 °C) and the relative humidity is at its maximum value (47%), corresponding to an inlet specific humidity of 13.8 $g_v kg_a^{-1}$. The minimum value instead is equal to 6.61 $g_v kg_a^{-1}$ achieved around 12.09 during adsorption, with external conditions coinciding with an air temperature of 31 °C and relative humidity equal to 36%, meaning the inlet specific humidity is equal to 10.1 $g_v kg_a^{-1}$.
Concerning the water uptake, the highest value, equal to 0.13 $kg_w kg_s^{-1}$, is obtained around the end of the adsorption cycle starting at 19.00, when the relative humidity of ambient air is at its maximum (47%). The minimum value (0.06 $kg_w kg_s^{-1}$), instead coincides with the end of the regeneration started at 11.30.

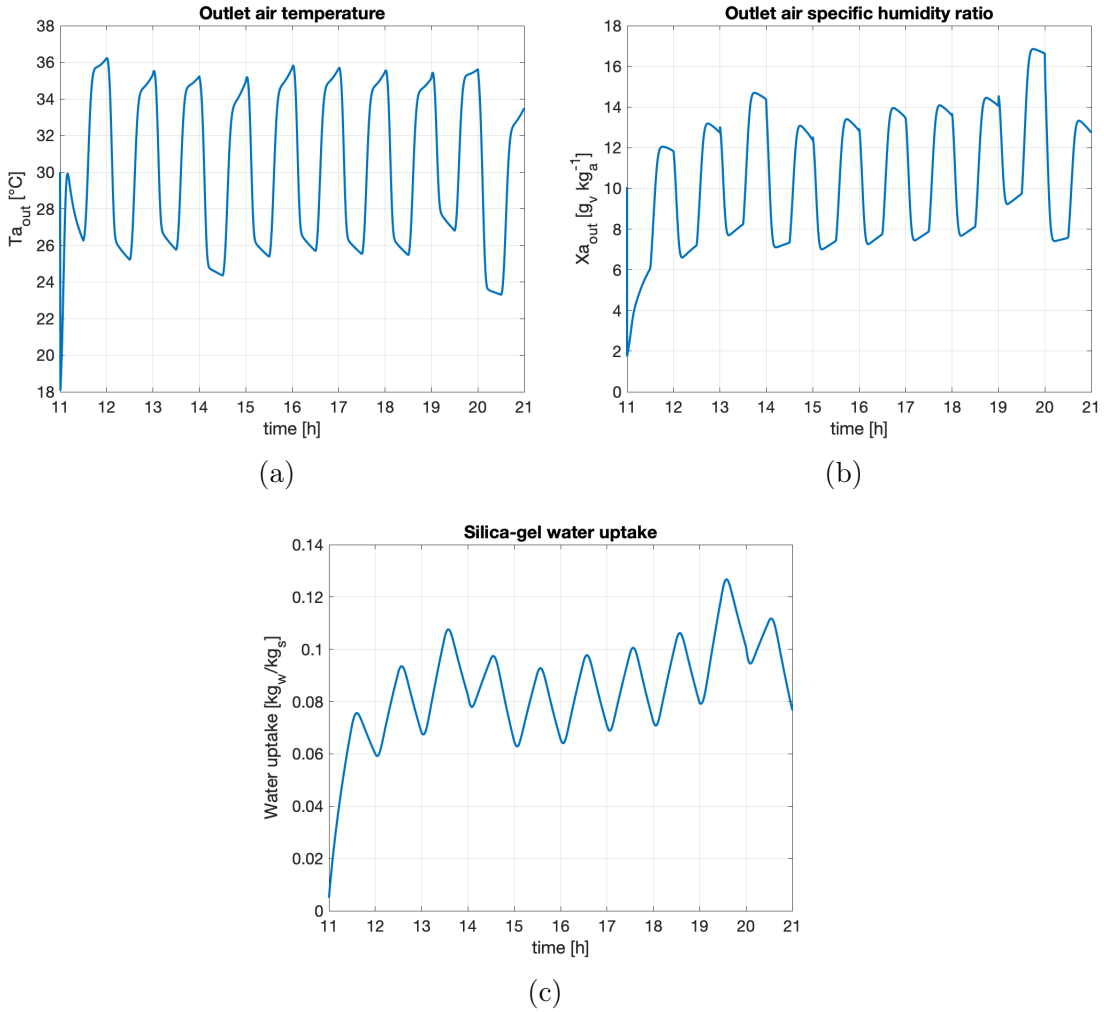

Figure 5.3: Temperature (a), specific humidity ratio (b) of outlet air and silica-gel water uptake (c)

At this point, the output of the entire system is presented, with the intention of understanding, at each time step, the characteristics of the air entering the indoor environment. This means the outlet conditions of both the heat exchangers, in

adsorption mode, are considered. In fact, as previously explained, the two adsorption batteries work simultaneously in opposite modes: when the first heat exchanger is in adsorption mode, the other one is undertaking the silica-gel regeneration.
The resulting outlet air temperature and specific humidity ratio are reported in Figure 5.4.

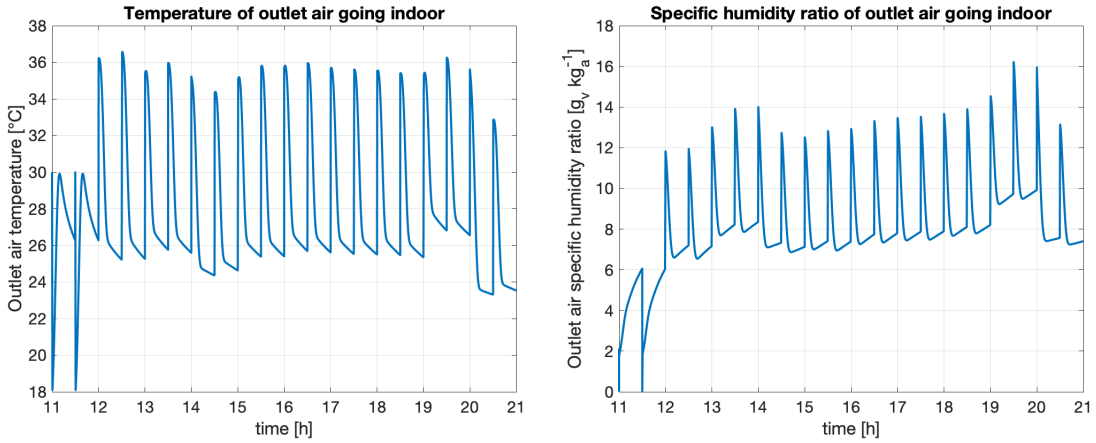

Figure 5.4: Outlet air temperature and specific humidity ratio

The maximum and minimum values of both the parameters are the same already discussed. It can be noticed that at the beginning of each adsorption cycle, the outlet air temperature and specific humidity are high. This occurs because adsorption is immediately subsequent to regeneration, meaning it takes a while to shift to the new functioning mode. In particular, the water flowing in the tubes of heat exchanger has to change its temperature level from 50 °C to 20 °C. Since air with high temperature and specific humidity can not be supplied indoor, a solution could be found in lowering the air flow rate, in waiting before inverting the air streams direction for few minutes or in introducing a pre-cooling before sending the air flow to the indoor environment.

The cooling power, together with both sensible and latent contributions, and its correspondent average values are reported in Figure 5.5, Figure 5.6 and Figure 5.7. The power peaks during the first functioning hour are due to the setting of the initial conditions of the model, meaning the water flowing in the tubes is at a uniform temperature equal to the one imposed for the inlet flow (15 °C), the silica-gel is at the temperature of the inlet air stream and its water uptake is at the set initial value, the air stream temperature and specific humidity ratio are at the conditions of external environment at each Δz.
Considering the results obtained for the sensible cooling power, excluding the first

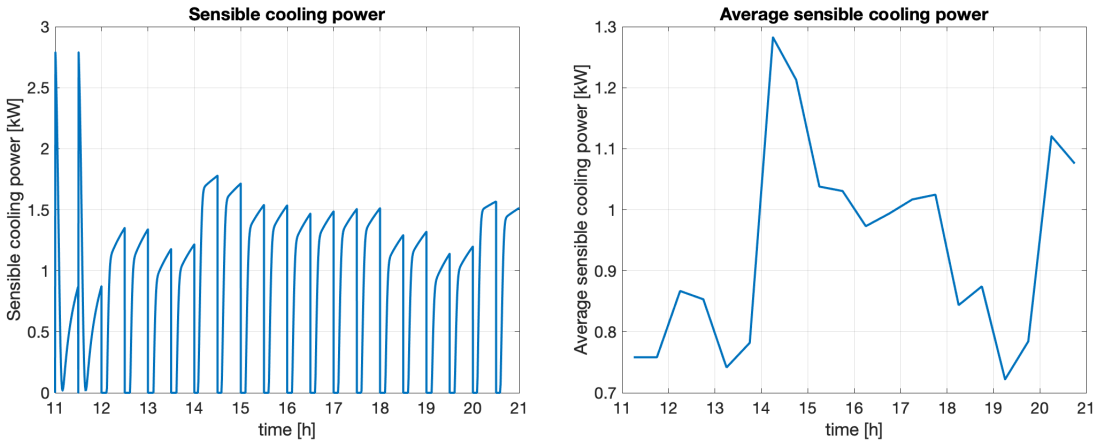

Figure 5.5: Sensible cooling power

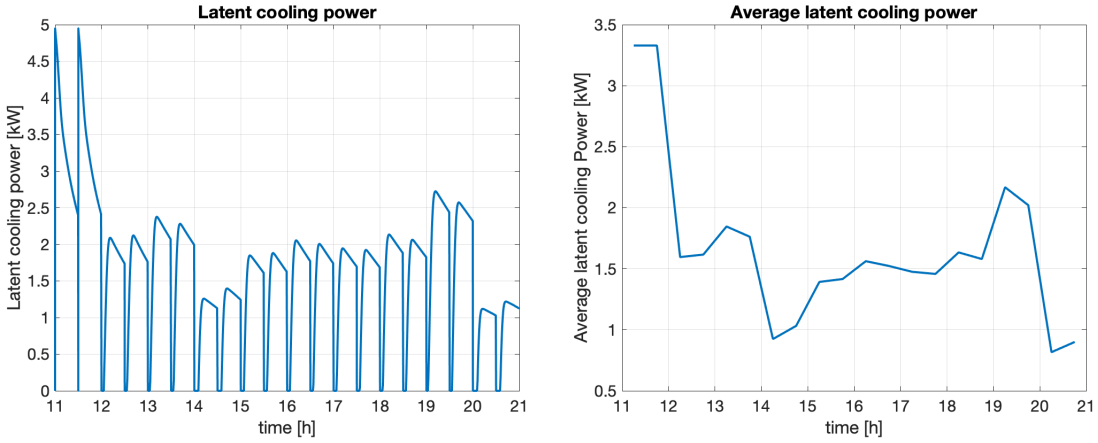

Figure 5.6: Latent cooling power

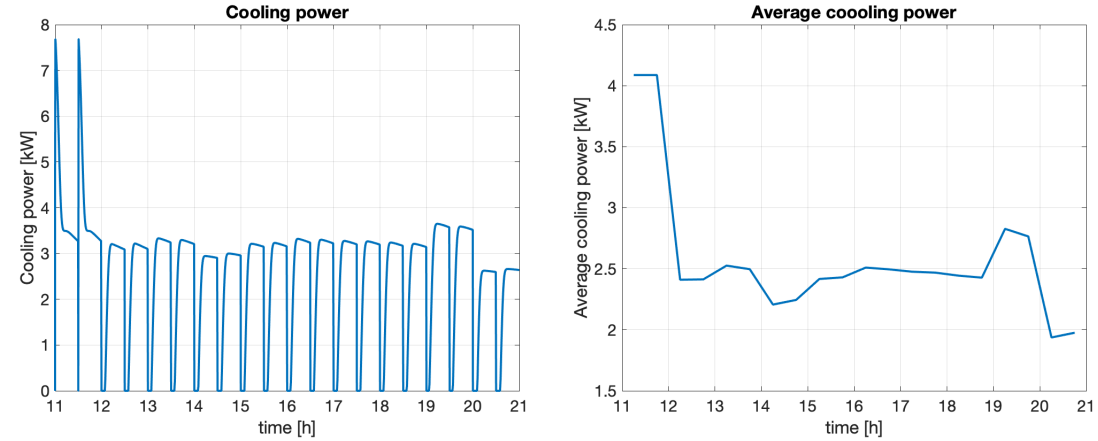

Figure 5.7: Total cooling power

hour, its maximum value, equal to 1.78 kW, is reached between 14.00 and 15.00, when the external ambient temperature is the highest and the relative humidity is the lowest. This means that the air stream entering the heat exchanger is characterized by a lower moisture content, in fact the latent cooling power during this hour is reduced, and, so, the system can provide more sensible cooling power. Moreover, the temperature of the air stream is at the highest level, so, a larger temperature difference occurs between air and cold water, allowing a greater heat exchange. This translates also to a high average value of sensible cooling power, that, between 14.00 and 15.00 coincides with 1.28 kW. The minimum values of sensible cooling power, instead, are obtained between 13.00 and 14.00 (1.18 kW) and in the hour going from 19.00 to 20.00 (1.14 kW). During these two hours, the ambient air relative humidity is at its maximum values (respectively equal to 42% and 47%), meaning the latent cooling power share will be higher, while, the sensible one is at its lowest level. The equivalent average sensible power, in these two hours, are equal to 0.74 kW and 0.72 kW, respectively, with a reduction of about 59% with respect to the maximum average value.

Concerning the latent cooling power, it has already been said that, when the external air relative humidity is higher, the latent cooling power increases, since the moisture content of air raises. Its maximum values are in the hours during which the sensible cooling power is minimum, and correspond to 2.38 kW between 13.00 and 14.00 and to 2.72 kW between 19.00 and 20.00, with average values respectively equal to 1.85 kW and 2.17 kW. The lowest values, instead, are obtained between 14.00 and 15.00, with 1.26 kW, (when sensible cooling power is maximum and external air relative humidity is at its minimum) and between 20.00 and 21.00, with 1.12 kW. This last result is due to the fact that the external relative humidity is low (equal to 35%), but also the ambient temperature is the coldest considered in the functioning period. The minimum average latent cooling power is correspondent to 0.82 kW and it is achieved between 20.00 and 21.00, with a reduction of 69.9% with respect to the maximum average value.

The resultant cooling power mainly follows the trend of latent cooling power, since it represents the major contribution, and, so, it presents its maximum value, 3.65 kW, between 19.00 and 20.00, when also the latent cooling power presents its maximum. The correspondent average value is equal to 2.83 kW. Similarly, the minimum value is obtained between 20.00 and 21.00, when also the latent cooling power is minimum, with a value of 2.62 kW and a consequent average cooling power of 1.94 kW (decrease of 32.9% with respect to the maximum average value).

5.2.1 Influence of switch time

The purpose of this section is to understand how the performance of the system varies as the switch time changes.
The switch times used are the following: 15 minutes, 30 minutes, 1 hour. The performance is evaluated analyzing the resulting average outlet temperature, cooling power and moisture removal.

Average outlet air temperature

The average temperature, for each adsorption cycle, of the air exiting the system and directed to the indoor environment, for all the switch times considered, is reported in Figure 5.8.

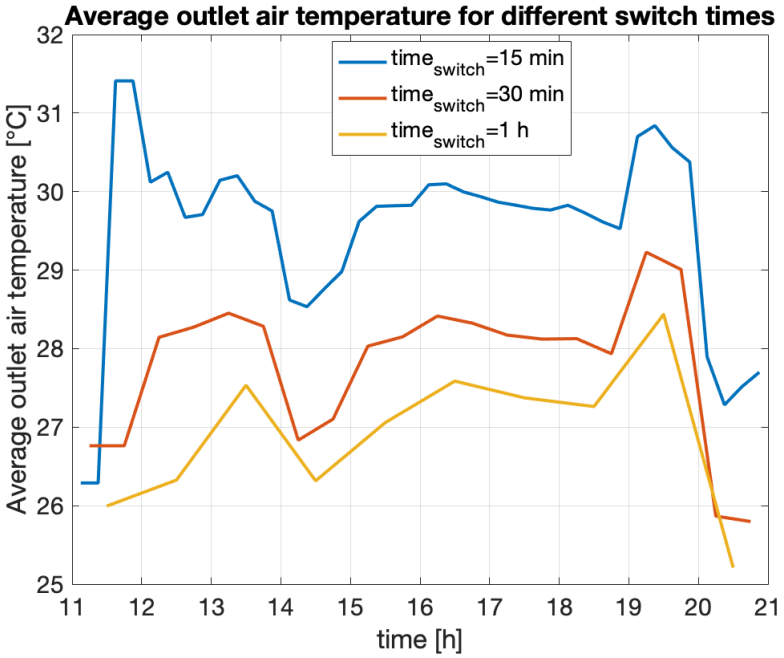

Figure 5.8: Average outlet air temperature for different switch times

It has to be considered that, as previously explained, the adsorption outlet air temperature, during the first minutes, shows a peak due to the fact that adsorption is immediately subsequent to regeneration. This justifies the high average values resulting in Figure 5.8. Apart from this observation, it can be noticed that the average outlet air temperature significantly changes as the switch time varies. During the central hours, the average temperature, for a switch time equal to 15 minutes, presents a value around 30 °C, while, when the switch time is doubled, the temperature lowers until a value around 28 °C. Increasing the switch time to 1 hour, the average outlet air temperature is further reduced, reaching a value approximately

equal to 27.5 °C. This decrease is a consequence of the fact that the outlet air temperature during adsorption, rapidly reduces and then settles around a certain value. This means that, lengthening the adsorption duration, increases the time in which the outlet air is at a lower temperature.
The trend along time, instead, is the same for all the cases assessed; the discrepancies are due to the fact that the average values are calculated for each adsorption cycle, whose duration changes between 15 minutes to 1 hour.

Moisture removal

The average moisture removal as a function of time and switch time is reported in Figure 5.9.

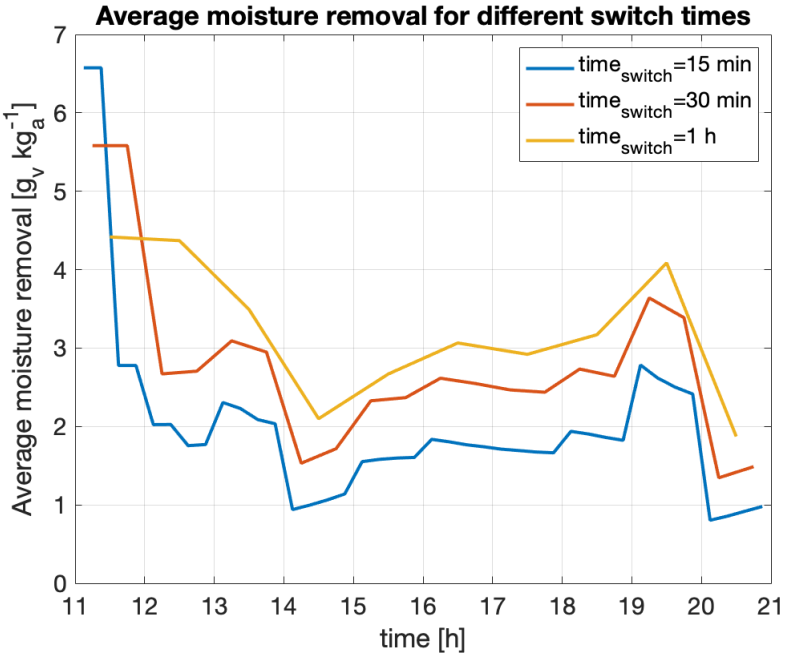

Figure 5.9: Average air moisture removal

Considering the trends obtained, they have similar behaviours over time, but the average moisture removal curve relating to the switch time of 15 minutes is below the others. In fact, passing from 15 minutes to 30 minutes, the average moisture removal increases as the peaks of the outlet air specific humidity due to the alternation with regeneration are less in number: in one hour, there are four peaks in the case of a switch time equal to 15 minutes and 2 peaks when the switch time is doubled. Moreover, the outlet air specific humidity is, in general, higher with lower switch times, because silica-gel is further from being completely regenerated, decreasing the useful effect of moisture removal. The maximum average moisture removal with

switch time set to 15 minutes is equal to 2.78 $g_v kg_a^{-1}$, while, for a switch time of 30 minutes, it is correspondent to 3.64 $g_v kg_a^{-1}$ (30.9% higher) and it reaches 4.01 for a switch time of 1 hour. Evaluating the daily average of moisture removal, it is equal to 2.0 $g_v kg_a^{-1}$, with 15 minutes for the switch time and to 2.8 $g_v kg_a^{-1}$ when the switch time coincides with 30 minutes (40.0% greater). Imposing a switch time of 1 hour, instead, the daily average moisture removal coincides with 3.2 $g_v kg_a^{-1}$, corresponding to an increment of 14.3%.
So, increasing the switch time, the moisture removal grows, but as the duration of the adsorption cycle raises, the adsorbent starts to approach saturation. This means that further increasing the switch time, the average moisture removed will converge to a certain value.

Cooling power

The sensible, latent and total cooling power over time, for each switch time analyzed are reported in Figure 5.10.
The results obtained reflect what has been previously said for average outlet air temperature and moisture removal. In fact, the sensible cooling power, dependent on the difference in temperature between inlet and outlet air, is higher for larger switch times, as the outlet temperature lowers as the switch time increases. The latent cooling power, instead, follows the trend of the average moisture removal, meaning, it is higher, for greater switch times. The total cooling power trend, again, is more similar to the one of the latent cooling power, since it represents the more significant contribution.
Considering the sensible cooling power, its maximum average value (not considering the first two cycles) passes from 0.90 kW, when the switch time corresponds to 15 minutes, to 1.28 kW, for the switch time equal to 30 minutes (42.0% higher than the case with the minimum switch time) and, then to 1.41 kW when the switch time is set to 1 hour (56.7% greater than the simulation with the minimum switch time assessed). The average values (considering the entire simulation along the day), raising the switch time from 15 minutes to 1 hour are respectively equal to 0.63 kW, 0.94 kW and 1.11 kW (1.76 times higher than the case with the switch time equal to 15 minutes).
Concerning the latent cooling power, its maximum average value, starting from the minimum switch time, passes from 1.66 kW to 2.17 kW (33.1% higher than the case with the minimum switch time) and, then to 2.44 kW when the switch time is set to 1 hour (32.6% greater than the simulation with the minimum switch time assessed). The average values (during the hours considered), raising the switch time from 15

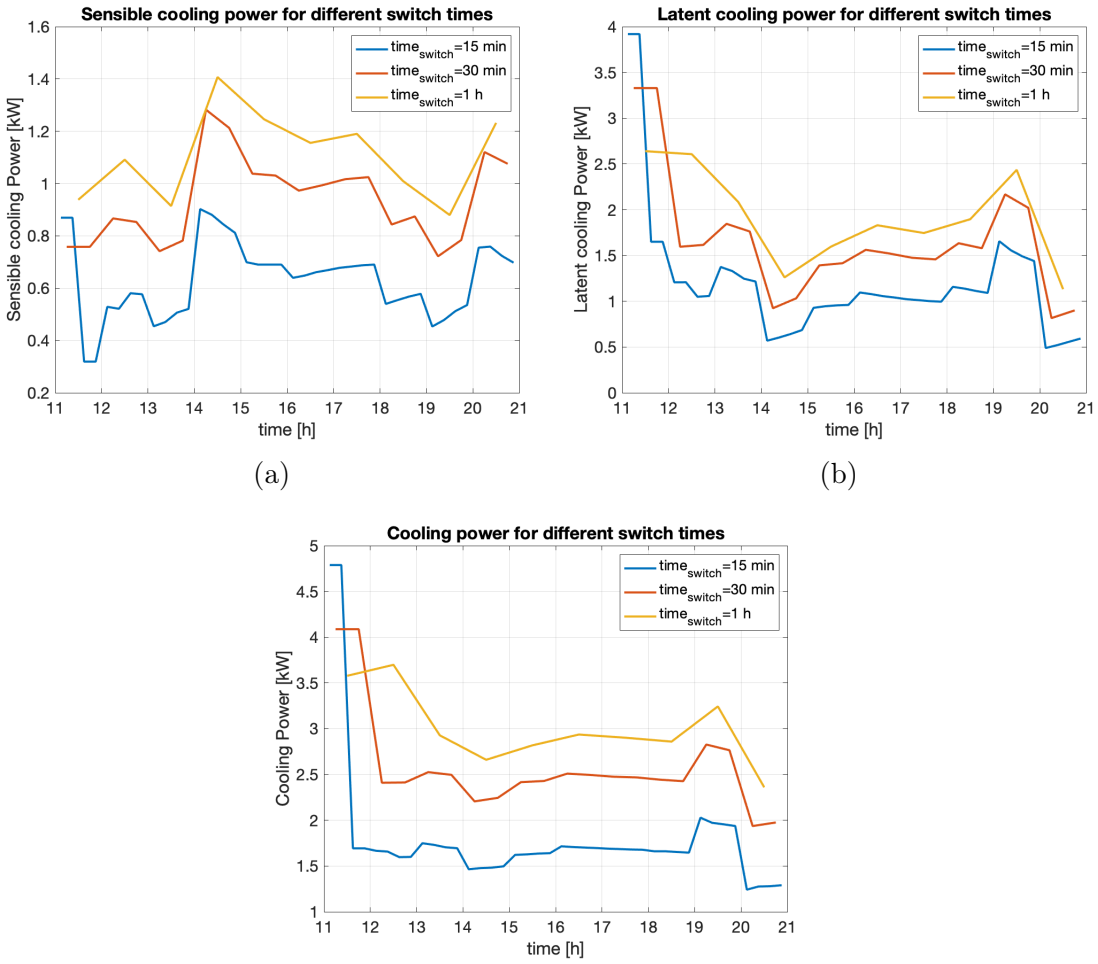

Figure 5.10: Sensible (a), latent (b) and total (c) cooling power as switch time varies

minutes to 1 hour are respectively equal to 1.21 kW, 1.67 kW and 1.92 kW, with an increase between the minimum and the maximum value of 58.7%.
The maximum values of total cooling power for the switch time passing from 15 minutes to 1 hour are equal to 2.02 kW, 2.83 kW and 3.24 kW. The average values, instead, correspond to 1.80 kW, 2.58 kW and 3.00 kW, with an increase of 66.7% between 15 minutes and 1 hour of switch time.

5.2.2 Influence of air flow rate

In this step, the performance of the system is investigated varying the air flow rates. The air flow rate used are the following: 0.1 m^3s^{-1} (360 m^3h^{-1}), 0.2 m^3s^{-1} (720 m^3h^{-1}) and 0.3 m^3s^{-1} (1080 m^3h^{-1}). The average outlet air temperature, moisture removal and cooling power are analyzed.

Average outlet air temperature

The average outlet air temperature of the system destined to the indoor environment, as the flow rate varies, is shown in Figure 5.11.

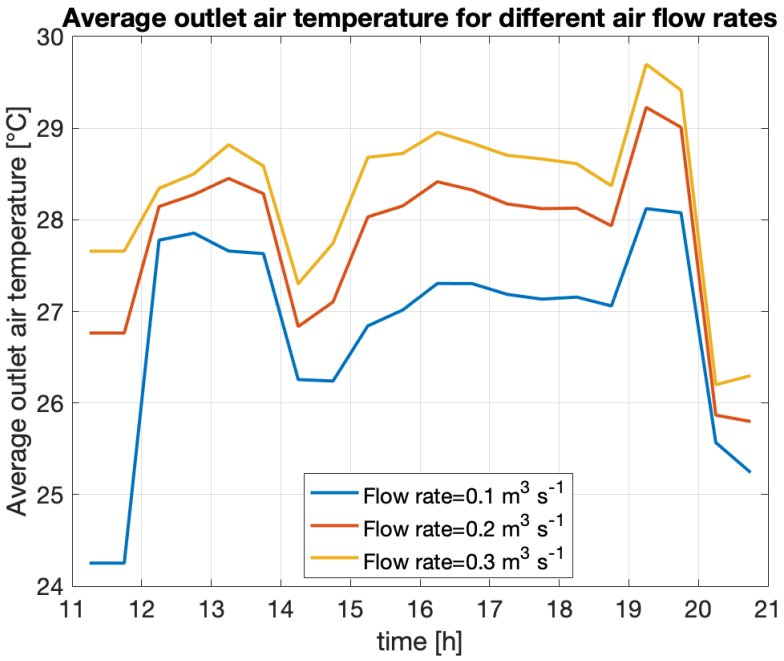

Figure 5.11: Average outlet air temperature for different air flow rates

Similarly of what has been said for the switch time variation, the outlet average air temperature is high because of the contribution of the first minutes of each adsorption cycle, during which the temperature is still affected by the previous regeneration cycle.

It can be noticed that the curves are slightly different, in particular, the one referred to an air flow rate of 0.2 m^3s^{-1} and 0.3 m^3s^{-1} are close to each other. Only when the air flow rate is reduced until 0.1 m^3s^{-1}, the average temperature is moderately lower. The average value during the operating time is 26.8 °C when the air flow rate is equal to 0.1 m^3s^{-1}, 27.8 °C for an air flow rate of 0.2 m^3s^{-1} (3.73% higher with respect to the previous case)and 28.3 °C with the air flow rate corresponding to 0.3 m^3s^{-1} (1.80% higher than the case with an air flow rate of 0.2 m^3s^{-1}). This behaviour is due to the fact that for lower air flow rates, the amount of air entering the adsorption battery is reduced and, so, a smaller quantity of air has to be cooled down, so the heat exchange is more effective. As the air flow rate grows, this effect become less significant, since the curves tend to coincide.

Moisture removal

The average moisture removal for the air flow rates selected is reported in Figure 5.12.

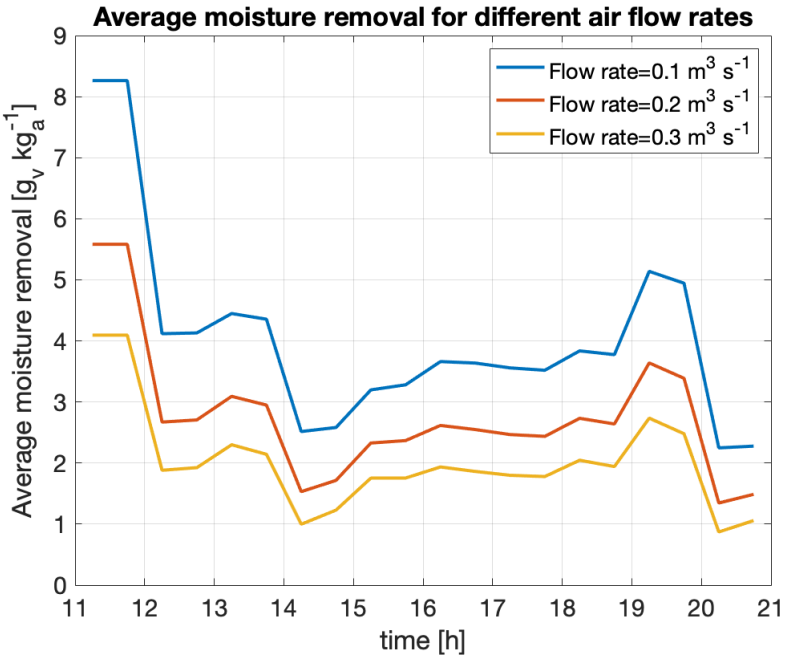

Figure 5.12: Average air moisture removal for different air flow rates

Again, there is a more significant difference between the output related to the lowest air flow rate and the intermediate one, while, the curves corresponding to 0.2 m^3s^{-1} and 0.3 m^3s^{-1} are closer.
The peak value (not considering the first two adsorption cycles) for an air flow rate of 0.1 m^3s^{-1} is equal to 5.14 $g_v kg_a^{-1}$, it decreases to 3.64 $g_v kg_a^{-1}$ (29.2% lower), when the air flow rate coincides with 0.2 m^3s^{-1} and it further reduces to 2.74 $g_v kg_a^{-1}$ when the air flow rate is correspondent to 0.3 m^3s^{-1}, with a reduction of 46.7% with respect to the case with 0.1 m^3s^{-1}. The average moisture removal values over the functioning time, instead, for the air flow rate increasing from 0.1 m^3s^{-1} to 0.3 m^3s^{-1} are respectively equal to 4.10 $g_v kg_a^{-1}$, 2.80 $g_v kg_a^{-1}$ and 2.00 $g_v kg_a^{-1}$. This corresponds to a reduction in the average moisture removal of 51.2% increasing the air flow rate from 0.1 m^3s^{-1} to 0.3 m^3s^{-1}. Instead, raising the air flow rate only from 0.1 m^3s^{-1} to 0.2 m^3s^{-1} the decrease is equal to 31.7%. This behaviour is due to the fact that when the air flow rate is equal to 0.1 m^3s^{-1} there is a lower quantity of air crossing the heat exchanger, meaning more moisture can be removed from the inlet air stream.

Cooling power

The sensible, latent and total cooling power over the functioning time of the system, for each air flow rate analyzed is reported in Figure 5.13.

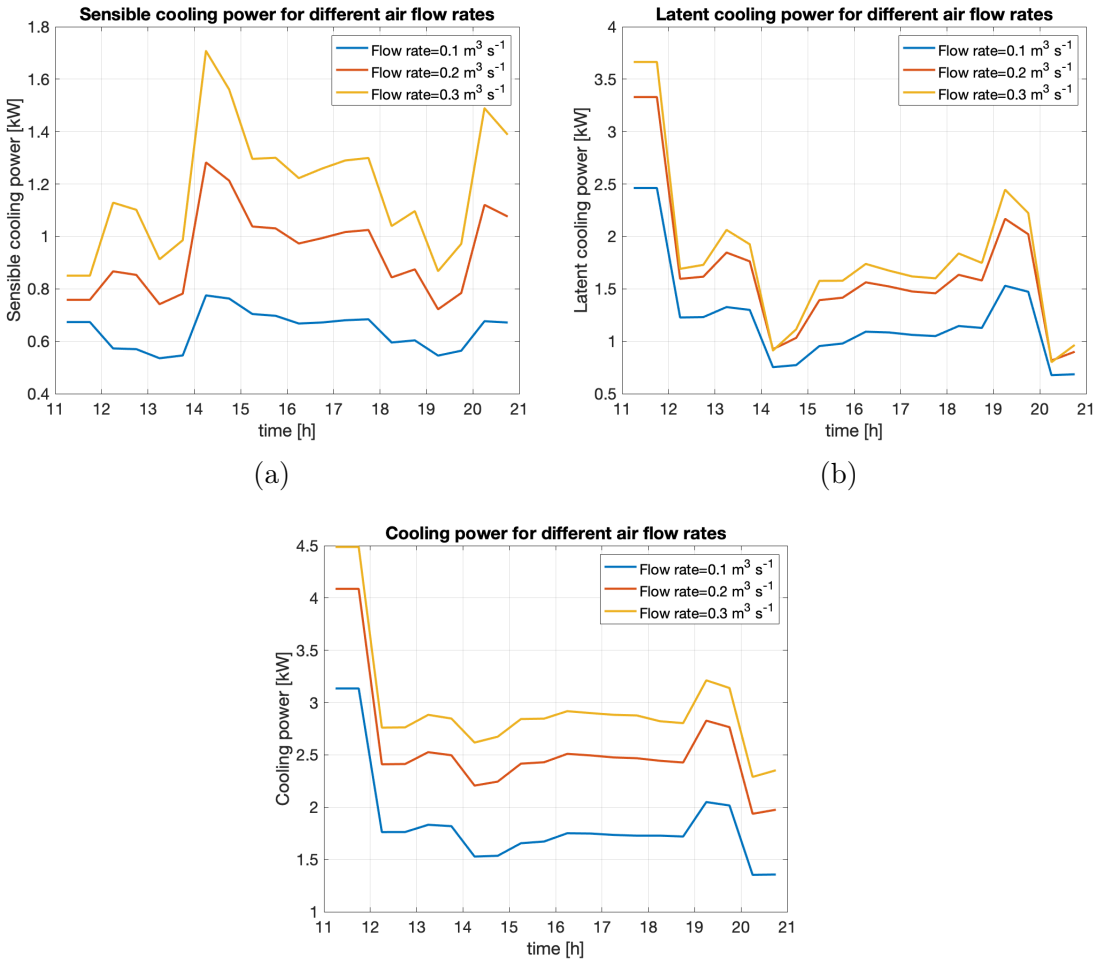

Figure 5.13: Sensible (a), latent (b) and total (c) cooling power as air flow rate varies

Considering the resulting sensible cooling power, it significantly changes as the air flow rate varies. Even though the average outlet air temperature curves were close to each other, the sensible cooling power is, instead, different in the three cases because it is calculated multiplying the sensible contribution of the enthalpy difference between inlet and outlet air by the air flow rate, which, then, has a considerable role in the final result. The maximum average sensible cooling power (excluding the first two adsorption cycles), obtained with the maximum air flow rate considered (0.3 $m^3 s^{-1}$), is equal to 1.71 kW, while, decreasing the air flow rate to 0.2 $m^3 s^{-1}$, it corresponds to 1.28 kW (24.7% lower). Finally, imposing an air flow rate equal

to 0.1 m^3s^{-1}, the maximum average sensible cooling power obtained corresponds to 0.78 kW (54.4% lower than the case with the maximum air flow rate). The average values during the functioning time of the system for air flow rates coinciding with 0.1 m^3s^{-1}, 0.2 m^3s^{-1} and 0.3 m^3s^{-1} are respectively equal to 0.64 kW, 0.94 kW (46.9% higher), 1.18 kW (about 1.8 times higher than that corresponding to the minimum flow rate).

Concerning the latent cooling power, even if the average moisture removal for the minimum air flow rate considered is the largest, the correspondent latent cooling power is the lowest because of the relevant contribution of the air flow rate value in the cooling power calculation. When the air flow rate is set to 0.2 m^3s^{-1} and to 0.3 m^3s^{-1}, the output curves are closer to each other, because the lower moisture removed with a flow rate of 0.3 m^3s^{-1}, is compensated by the higher value of flow rate. The maximum value of latent cooling power (starting from 12.00) reached with an air flow rate of 0.3 m^3s^{-1} is equal to 2.45 kW; for a flow rate of 0.2 m^3s^{-1} it corresponds to 2.17 kW (reduced by 11.4%), while, with a flow rate coinciding with 0.1 m^3s^{-1}, the maximum average latent cooling power is equal to 1.70 kW (34.4% lower than the case with flow rate correspondent to 0.3 m^3s^{-1}). The average values during the functioning time of the system for air flow rates coinciding with 0.1 m^3s^{-1}, 0.2 m^3s^{-1} and 0.3 m^3s^{-1} are respectively equal to 1.22 kW, 1.67 kW (36.9% higher) and 1.83 kW (50.0% greater than that corresponding to the minimum flow rate).

The maximum resulting total average cooling power coincides with the simulation using the maximum flow rate (0.3 m^3s^{-1}), while the minimum is obtained through a flow rate of 0.1 m^3s^{-1}. The maximum values from each flow rate analyzed are equal to 2.05 kW (with the air flow rate set to 0.1 m^3s^{-1}), 2.83 kW (for the flow rate corresponding to 0.2 m^3s^{-1}) and 3.21 kW (when the air flow rate is maximum). The average value during the entire system operating time is equal to 1.85 kW when the air flow rate is the lowest considered, to 2.58 kW for the air flow coinciding with 0.2 m^3s^{-1} (increment of 39.5%) and to 2.97 kW when the air flow rate is equal to 0.3 m^3s^{-1} (60.5% greater with respect to the case with the minimum air flow rate).

Chapter 6

Conclusions

The aim of this thesis work was to build a numerical model for the adsorption battery of HySun in order to simulate its functioning and understand which are the better working conditions.
The parametric analysis allowed to analyze how the performance of the system varies as some conditions change. The results showed that higher lengths of the heat exchanger and regeneration temperatures as well as lower cold water temperatures and air flow velocities permit to remove more moisture from air, so, it can be concluded that these conditions are more suitable in humid climates, where a greater amount of water vapor needs to be removed from air in order to obtain more comfortable conditions in the indoor environment.
Instead, in dry climates, where less average moisture removal is needed to match the user requirements, it is more convenient to use a shorter heat exchanger, lower regeneration temperatures and cold water temperatures and higher velocities, since these settings result in a better performance of the system in terms of COP (both thermal and electric, except for the thermal COP of regeneration temperature).
Afterwards, the dynamic simulations have been accomplished during a typical summer day in Turin in order to understand how the system works in a real operating environment, meaning with variable inlet air conditions. In this analysis the system has been considered entirely, meaning not only a single adsorption battery, but both the batteries working in parallel, with the purpose of assessing the outlet conditions of air actually destined to the indoor environment.
The results showed a critical aspect: the characteristics of air, at the beginning of each adsorption cycle, cannot match the indoor requirements in terms of both air temperature and specific humidity. This occurs because regeneration and adsorption, in each battery, are immediately consecutive, so, the water temperature needs some time to switch to the new set point. This means that a pre-cooling of air,

before releasing it into the indoor environment, has to be introduced. Moreover, the fact that the outlet specific humidity is still high at the end of regeneration, for the switch times considered, means that silica-gel is not completely regenerated. This can be overcome by further extending the switch time or by reducing the length of the heat exchanger, since the ambient conditions in which the system is placed present a low relative humidity.

6.1 Future works

The model used for the dynamic simulations can be exploited in order to accomplish additional simulations in different climates and with diverse configurations. Additionally, it can be exploited to carry out simulations with the aim of implementing control and regulation strategies, since the computational time to run the model is relatively low (less than 11 seconds for the simulation along the functioning hours selected, considering both the adsorption batteries).
Moreover, the RE-COGNITION project has as one of its main objectives in the integration on a large-scale of Renewable Energy Sources (RES) in buildings. In this context, HySun has been designed as a system in which heat and cold power can be supplied by diverse technologies, including RES technologies such as thermal collectors, heat pump (which can be driven by a local PV system), waste heat, cooling towers, ground water. So, the model built can be integrated with simulators for the different technologies involved in order to investigate the system performance changing the various hot and cold sources.

Bibliography

[1] Ali Alahmer and Salman Ajib. Solar cooling technologies: State of art and perspectives. *Energy Conversion and Management*, 214:112896, 2020.

[2] Carrie Carlson Alex Ebben. Activated Alumina Overview, FEECO International, Inc. https://feeco.com/activated-alumina-overview/, 2021.

[3] Zeid A ALOthman. A review: fundamental aspects of silicate mesoporous materials. *Materials*, 5(12):2874–2902, 2012.

[4] Nimibofa Ayawei, Augustus Newton Ebelegi, and Donbebe Wankasi. Modelling and interpretation of adsorption isotherms. *Journal of chemistry*, 2017, 2017.

[5] R Boukhanouf, HG Ibrahim, A Alharbi, and M Kanzari. Investigation of an evaporative cooler for buildings in hot and dry climates. *journal of clean energy technologies*, 2(3):221–225, 2014.

[6] Britannica. The Editors of Encyclopaedia, Silica gel, Encyclopaedia Britannica, 16 aug. 2013, https://www.britannica.com/science/silica-gel.

[7] Craig Brown. Activated carbon, Pureflow, Inc. https://www.pureflowinc.com/wp-content/uploads/2018/07/summertn-activatedcarbon-digital.pdf, 2018.

[8] Elyse Canosa. Adsorbents for pollution reduction in cultural heritage collections, 2019.

[9] Eliodoro Chiavazzo. Lecture notes of the course: Energy storage, politecnico di torino, 2020.

[10] European Commission. 2030 climate & energy framework, https://ec.europa.eu/clima/policies/strategies/2030, 2021.

[11] Ioannis Moschos et al. Dimosthenis Ioannidis. Deliverable 1.4 - re-cognition system architecture (v.1), https://re-cognition-project.eu/dissemination/deliverables/, 2019.

[12] MD Donohue and GL Aranovich. Adsorption hysteresis in porous solids. *Journal of colloid and interface science*, 205(1):121–130, 1998.

[13] MD Donohue and GL Aranovich. Classification of gibbs adsorption isotherms. *Advances in colloid and interface science*, 76:137–152, 1998.

[14] Mahmoud B Elsheniti, Osama A Elsamni, Raya K Al-dadah, Saad Mahmoud, Eman Elsayed, and Khaled Saleh. Adsorption refrigeration technologies. *Sustainable air conditioning systems*, pages 71–95, 2018.

[15] TS Ge, YJ Dai, and RZ Wang. Performance study of silica gel coated fin-tube heat exchanger cooling system based on a developed mathematical model. *Energy Conversion and Management*, 52(6):2329–2338, 2011.

[16] TS Ge, YJ Dai, RZ Wang, and ZZ Peng. Experimental comparison and analysis on silica gel and polymer coated fin-tube heat exchangers. *Energy*, 35(7):2893–2900, 2010.

[17] Dieter M Herlach, Thomas Palberg, Ina Klassen, Stefan Klein, and Raphael Kobold. Overview: Experimental studies of crystal nucleation: Metals and colloids. *The Journal of chemical physics*, 145(21):211703, 2016.

[18] IEA. Cooling, IEA, Paris, https://www.iea.org/reports/cooling, 2020.

[19] IEA. Tracking Buildings 2020, IEA, Paris, https://www.iea.org/reports/tracking-buildings-2020, 2020.

[20] Mrinal Jagirdar and Poh Seng Lee. Mathematical modeling and performance evaluation of a desiccant coated fin-tube heat exchanger. *Applied energy*, 212:401–415, 2018.

[21] Y Jiang, TS Ge, RZ Wang, and LM Hu. Experimental investigation and analysis of composite silica-gel coated fin-tube heat exchangers. *International Journal of Refrigeration*, 51:169–179, 2015.

[22] Linda K et al. Lawrie. Development of global typical meteorological years (tmyx), http://climate.onebuilding.org, 2019.

[23] Trevor M Letcher. *Chemical thermodynamics for industry*. Royal Society of Chemistry, 2004.

[24] Ang Li, Kyaw Thu, Azhar Bin Ismail, and Kim Choon Ng. A heat transfer correlation for transient vapor uptake of powdered adsorbent embedded onto the fins of heat exchangers. *Applied Thermal Engineering*, 93:668–677, 2016.

[25] Paolo Gregorio Michele Calì. *Termodinamica*. Società Editrice Esculapio, 1996.

[26] Kim Choon Ng, HT Chua, CY Chung, CH Loke, T Kashiwagi, A Akisawa, and Bidyut Baran Saha. Experimental investigation of the silica gel–water adsorption isotherm characteristics. *Applied Thermal Engineering*, 21(16):1631–1642, 2001.

[27] Ahmad A Pesaran and Anthony F Mills. Moisture transport in silica gel packed beds—i. theoretical study. *International Journal of Heat and Mass Transfer*, 30(6):1037–1049, 1987.

[28] United Nations Environment Programme. Global status report for buildings and construction: Towards a zero-emission, efficient and resilient buildings and construction sector, Nairobi, 2020.

[29] RE-COGNITION. About RE-COGNITION, https://re-cognition-project.eu/about-re-cognition/, 2019.

[30] RE-COGNITION. HYSun - a solar hybrid cooling technology, https://re-cognition-project.eu/2020/07/24/hysun-a-solar-hybrid-cooling-technology/, 2019.

[31] Douglas M Ruthven. *Principles of adsorption and adsorption processes*. John Wiley & Sons, 1984.

[32] Ying Sheng, Yufeng Zhang, Na Deng, Lei Fang, Jinzhe Nie, and Lijun Ma. Experimental analysis on performance of high temperature heat pump and desiccant wheel system. *Energy and buildings*, 66:505–513, 2013.

[33] Marco Simonetti. Lecture notes of the course: Technology for renewable energy sources, politecnico di torino, 2019.

[34] SimplyCooler. Bry-air adsorption coolers. http://simplycooler.co.uk/bry-air-adsorption-coolers/, 2021.

[35] KSW Sing. Reporting physisorption data for gas/solid systems with special reference to the determination of surface area and porosity (provisional). *Pure and applied chemistry*, 54(11):2201–2218, 1982.

[36] XY Sun, YJ Dai, TS Ge, Y Zhao, and RZ Wang. Experimental and comparison study on heat and moisture transfer characteristics of desiccant coated heat exchanger with variable structure sizes. *Applied Thermal Engineering*, 137:32–46, 2018.

[37] Swep. Absorption chillers, https://www.swep.net/refrigerant-handbook/10.-systems/asdf1/, 2019.

[38] David B Thompson. Numerical methods 101-convergence of numerical models. *USGS Staff–Published Research*, page 115, 1992.

[39] Hao Wu, Fabrice Salles, and Jerzy Zajac. A critical review of solid materials for low-temperature thermochemical storage of solar energy based on solid-vapour adsorption in view of space heating uses. *Molecules*, 24(5):945, 2019.

[40] J. Yeom, M.A. Shannon, and T. Singh. Micro-coolers. In *Reference Module in Materials Science and Materials Engineering*. Elsevier, 2017.

[41] Yao Zhao, YJ Dai, TS Ge, XY Sun, and RZ Wang. On heat and moisture transfer characteristics of a desiccant dehumidification unit using fin tube heat exchanger with silica gel coating. *Applied Thermal Engineering*, 91:308–317, 2015.

Appendix A

Matlab code

```
clear
close all
clc


%% Air properties & functions

% Prandtl number - air
Pr_a=0.7055;                                    % [-]
% Thermal conductivity - air
k_a=0.027;                                      % [W/m/K]
% Nusselt number - air
Nu_air=@(Re)0.722.*Re.^0.43.*Pr_a.^0.3;         % [-]
% Number of Sherwood
Sher=@(Re,Nsc)0.664.*Re.^0.5.*Nsc.^0.33;                        % [-]
% Air specific humidity
x_a=@(RH,p_sat)0.622.*RH.*p_sat./(101325-RH.*p_sat);            % [kg_v/kg_a]
%Relative humidity
RH=@(xa,Psat) xa./(0.622+xa)*101325./Psat;                      % [-]
% Air density
rho_air=@(T)352.98./(T+273.15);                                 % [kg/m^3]
% Dynamic viscosity of air
mu_air=@(T)(T+273.15-300)./50.*23.6.*1e-7+184.6.*1e-7;          % [Pa*s]
% Specific heat of air
cp_air=@(x)1884.*x+1005.*(1-x);                                 % [J/kgK]
%Air enthalpy
h_air=@(x,T)1e3*(1.006*T+x*(2501+1.86*T));                      % [J/kg]
h_sens=@(T)1e3*1.006*T;                                         % [J/kg]
h_lat=@(x,T)1e3*x*(2501+1.86*T);                                % [J/kg]
% Saturation pressure of water vapor
p_sat=@(T)0.0004677.*T.^4+0.02444.*T.^3+1.359.*T.^2+45.98.*T+604.6;  % [Pa]
% Molecular diffusivity water-air
Dm_wa=@(T)1.735.*1e-9.*((T+273.15).^1.685)./1.01325;            % [m^2/s]
%Air velocity
vv=0.8;                                                         % [m/s]


%% Water properties & functions

% Prandtl number - water
Pr_w=6.9;                                       % [-]
% Nusselt number - water
Nu_w=@(Re)0.023.*Re.^0.8.*Pr_w.^0.4;            % [-]


%% Silica-gel properties & functions

% Sio2 emptiness degree
eps_p=0.35;                                                     % [-]
% Diffusivity
D0=1.6e-6;                                                      % [m^2/s]
% Tortuosity factor
tao_s=1;                                                        % [-]
% SiO2 density
rho_s=1129;                                                     % [kg/m^3]
%Silica-gel thermal conductivity
k_s=0.2;                                                        % [W/mK]
% Average radius for RD silica gel spheres
```

```
r_ave=100e-10;                                                    % [m]
% Superficial diffusivity
Dsup=@(T,Hads)D0.*exp(-0.947.*Hads./(T+273.15));                  % [m^2/s]
%Knudsen diffusivity
Dknudsen=@(T)r_ave.*22.86.*(T+273.15).^0.5;                       % [m^2/s]
% Silica gel specific heat
cp_sio2=@(w)4178.*w+921;                                          % [J/kgK]
% Relative humidity Si02 at the equilibrium
RH_eq=@(T,w)-2.49434e-3.*T+5.29632e-5.*T.^2+5.65527.*w+...        % [-]
   3.60887e-2.*w.*T-7.13679e-5.*w.*T.^2-24.9044.*w.^2-...
   0.112424.*T.*w.^2+54.8088.*w.^3-1.23558e-7.*T.^3;
% Heat of adsorption
H_ads=@(w)(3500-13400.*w).*(w<=0.05)+(2950-1400.*w).*(w>0.05);    % [kJ/kgK]

%% Other materials properties

% Copper thermal conductivity
k_cu=365;                         % [W/m/K]
%Aluminum thermal conductivity
k_al=290;                         % [W/m/K]


%% Geometrical configuration of adsorption battery

% Battery width
wd=0.5;                           % [m]
% Battery height
ht=0.5;                           % [m]
% Battery cross area
Ab=wd*ht;                         % [m^2]
%Battery length
LL=0.2;                           % [m]
%Battery volume
V_b=Ab*LL;                        % [m^3]
% Fin thickness
delta=1e-4;                       % [m]
%Fin pitch
fp=2.5e-3;                        % [m]
% Fins number
Nf=wd/fp;                         % [-]
%Trasversal pipes pitch
Xt=25e-3;                         % [m]
%Longitudinal pipes pitch
Xl=21.65e-3;                      % [m]
%Fin length
lf=Xt/2;                          % [m]
%Pipes pitch
Nr=floor(LL/Xl);                  % [-]
Nv=floor(ht/Xt);                  % [-]
%Pipes number
Np=Nr*Nv;                         % [-]
% Pipes outer diameter
Do=9.52e-3;                       % [m]
% Pipes inner diameter
Di=Do-2*0.45e-3;                  % [m]
% Silica-gel layer thickness
delta_s=0.55e-3;                  % [m]
%Fins area
Af=2*Nf*(ht*LL-Np*Do^2/4*pi)+2*(wd+LL)*delta;                     % [m^2]
```

```
% Pipes area
Ap=Np*(wd-Nf*delta)*Do*pi;                                          % [m^2]
%Total area (fins+pipes)
A_tot=Af+Ap;                                                        % [m^2]
% Minimum free-flow area
Ao=Ab-Nv*wd*(Do+2*delta_s)...                                       % [m^2]
    -Nf*(delta+2*delta_s)*(ht-Nv*(Do+2*delta_s));
% Ratio of minimum free flow area to frontal area
sig=Ao/Ab;                                                          % [-]
% Ratio of heat exchange area on air side to heat exchanger volume
alpha=A_tot/V_b;                                                    % [-]
%Hydraulic diameter
Dh=4*sig/alpha;                                                     % [m]
%Silica-gel volume
Vol_s=2*Nf*delta_s*(ht*LL-Np*Do^2/4*pi)...
    +Np*((Do+delta_s)^2-Do^2)*pi*(wd-Nf*(delta+2*delta_s));         % [m^3]
% Total exchange per volume of the battery
a_f=A_tot/V_b;                                                      % [1/m]
% Void volume
V_void=V_b-Vol_s-Nf*(wd*LL-Np*Do^2/4*pi)*delta-Np*Do^2/4*pi*wd;     % [m^3]
%Water pipes cross area
A_w=Di^2/4*pi;                                                      % [m^2]
% Total pipes length
lp=wd*Np;                                                           % [m]
% Pipes internal area
Ai=Di*pi*lp;                                                        % [m^2]


%% Solution

% Space discretization
dz=3e-3;              % [m]
zz=(0:dz:LL)';

%Cycle definition
%Period counter
pp=0;
% index
kk=1;
%Adsorption cycle duration
ads_time=1;                     % [h]
%Regeneration cycle duration
rig_time=ads_time;                % [h]
%Total cycle duration
cycle_time=ads_time+rig_time;     % [h]
%Definition of one period
period=cycle_time*3600;           % [s]
%Number of periods
np=2;                             % [-]

% Time domain
tend=period*np-1;                 % [s]
% Time step
dt=1;                             % [s]
%Time vector
time=0:dt:tend;

%Initial condition - functioning mode
```

```
rig(1)=Dutycycle(ads_time,time(1),period,pp);


% Input data

if rig(1)==0

%Inlet air relative humidity
RHi=0.7;                  % [-]
%Inlet air temperature
Tamb=30;                  % [¬∞C]
% Temperature of the air entering the battery
Ta_in=Tamb;               % [¬∞C]
%Inlet air mass flow rate
Ga=vv*rho_air(Ta_in)*Ab;
% Water temperature entering the water pipes
Tm_s=20;                  % [¬∞C]
%Initial silica-gel water uptake
W0=0.005;                 % [kg_w/kg_s]
% Initial temperature of the silica gel
Ts0=Ta_in;                % [¬∞C]


else

%Inlet air relative humidity
RHi=0.7;                  % [-]
%Inlet air temperature
Tamb=30;                  % [¬∞C]
% Temperature of the air entering the battery
Ta_in=Tamb;               % [¬∞C]
%Inlet air mass flow rate
Ga=vv*rho_air(Ta_in)*Ab;
% Water temperature entering the water pipes
Tm_s=50;                  % [¬∞C]
%Initial silica-gel water uptake
W0=0.005;                 % [kg_w/kg_s]
% Initial temperature of the silica gel
Ts0=Ta_in;                % [¬∞C]

end

% Temperature of the water entering the heAt exchanger
Tw_in=Tm_s;

% Specific humidity of inlet air
xa_in=x_a(RHi,p_sat(Ta_in));

% Initialization old arrays
xa_old=xa_in*ones(size(zz));
w_old=W0*ones(size(zz));
Ta_old=Ta_in*ones(size(zz));
Ts_old=Ts0*ones(size(zz));
Tw_old=Tw_in*ones(size(zz));

% Initialization new arrays
xa_new=xa_old;
```

```
w_new=w_old;
Ts_new=Ts_old;
Ta_new=Ta_old;
Tw_new=Tw_old;

%Inizialization solution
Ta=ones(length(zz),length(time));
xx=ones(length(zz),length(time));
ww=ones(length(zz),length(time));
Tw=ones(length(zz),length(time));
Ts=ones(length(zz),length(time));

%Imposing initial conditions
Ta(:,1)=Ta_new;
xx(:,1)=xa_new;
ww(:,1)=w_new;
Ts(:,1)=Ts_new;
Tw(:,1)=Tw_new;


%Parameters initialization
deltah(1)=0;
fan=0;
pump=0;
cc=0;
hp=0;
ht=0;
HP(1)=0;
Cool(1)=0;
deltax(1)=0;
deltaT(1)=0;
wm(1)=W0;
dx=0;

for ii=2:length(time)

    if time(ii)==period+period*pp
        pp=pp+1;
    end

   rig(ii)=Dutycycle(ads_time,time(ii),period,pp);

if rig(ii)==0

    Tm_s=20;                                        % [¬∞C]
    %Water mass flow rate
    Gw=0.08;                                        % [kg/s]
    xa_in=x_a(RHi,p_sat(Ta_in));                    % [kg_v/kg_a]

else

    Tm_s=50;                                        % [¬∞C]
    %Water mass flow rate
    Gw=0.05;                                        % [kg/s]
    xa_in=x_a(RHi,p_sat(Ta_in));                    % [kg_v/kg_a]

end
```

```
%% Air Properties

% Air density
rho_a=rho_air(Ta_old);                              % [kg/m^3]
% Air dynamic viscosity
mu_a=mu_air(Ta_old);                                % [Pa*s]
% Air Reynolds number
Re_a=rho_a.*vv.*Dh./mu_a;                           % [-]
%Friction factor - distributed losses through the hx
ff=64./Re_a(1);                                     % [-]
% Distributed losses through the hx
PD=ff*vv^2/2*rho_a(1)*LL/Dh;                        % [Pa]
%Air velocity vector
v_air=vv*ones(size(zz));                            % [m/s]
%  Nusselt number - air
Nu_a=Nu_air(Re_a);                                  % [-]
% Air specific heat
cp_a=cp_air(xa_old);                                % [J/kg/K]
% Air heat transfer coefficient - air side
h_a=k_a./Dh.*Nu_a;                % [W/m^2/K]

%% Water properties

if rig(ii)==0
    % water kinematic viscosity
    kv_w=1e-6;                                      % [m^2/s]
    %Water thermal conductivity
    k_w=0.598;                                      % [W/mK]
    %Water density
    rho_w=998;                                      % [kg/m^3]
    %Water specific heat
    cp_w=4181;                                      % [J/kgK]
else
    kv_w=0.556e-6;
    k_w=0.651;
    rho_w=982;
    cp_w=4186;
end

%Water flow velocity
v_w=Gw/rho_w/A_w;                                   % [m/s]
% Water Reynolds number
Re_w=v_w*Di/kv_w;                                   % [-]
%Water convective heat transfer coefficient
h_w=Nu_w(Re_w).*k_w./Di;                            %  [W/m^2K]
% Water pipes friction factor  - distributed losses
fw=(-1.8*log(6.9/Re_w+(0/Di/3.7)^1.11))^-2;         % [-]
%Water side pressure drop
PDw=fw*0.5*v_w^2*rho_w*wd*Np/Di+Nr*(Nv-1)*2.5*v_w^2/2*rho_w;    %[Pa]


%% Silica gel water content

% Sio2 area per volume
a_s=A_tot/Vol_s;                                    %[m^2/m^3]
% Moisture content equilibrium value between air and the solid
x_eq=x_a(RH_eq(Ts_old,w_old),p_sat(Ts_old));        % [kgv/kga]
```

```
% Adsorption heat
Had=H_ads(w_old).*1e3;                              % [J/kg_w]
% Molecular diffusivity water-air
Dm=Dm_wa(Ta_old);                                   % [m^2/s]
% Schmidt number
Sc=mu_a./rho_a./Dm;                                 % [-]
% Sherwood number
Sh=Sher(Re_a,Sc);                                   % [-]
% Mass transfer coefficient
hm=Dm.*rho_a./Dh.*Sh;                               % [kg/m^2s]
% Knudsen diffusivity
Dkn=Dknudsen(Ts_old);                               % [m^2/s]
% Superficial diffusivity
Ds=Dsup(Ts_old,Had./1000);                          % [m^2/s]
% Diffusion global coefficient
D_eff=(Ds+eps_p./tao_s.*1./(1./Dm+1./Dkn)).*rho_a.*2./delta_s; %[m^2/s]
% Global mass transfer coefficient
Kg=hm.*D_eff./(hm+D_eff);                           % [kg/s/m^2]
% Battery void fraction
eps=V_void/(V_void+Vol_s);                          % [-]
%Silica-gel bulk density
rho_bulk=eps_p*rho_a(1)+(1-eps_p)*rho_s;            % [kg/m^3]

% Solution
w_new=w_old+dt./rho_bulk.*Kg.*a_s.*(xa_old-x_eq);
ww(:,ii)=w_new;
%Average water uptake
wm(ii)=mean(w_new);


%% Air - water mass balance

%Solution matrix building
A1=v_air./dz/eps;
A2=Kg.*a_s./rho_a/eps;
sub_mass=-dt.*A1;
main_mass=(1+dt.*(A1+A2));
Ma=spdiags([sub_mass main_mass],-1:0,length(zz),length(zz));
Qa=(xa_old+dt.*A2.*x_eq);

%Boundary conditions
Ma(1,1)=1;
Ma(1,2)=0;
Qa(1)=xa_in;

%Solution
xa_new=Ma\Qa;
xx(:,ii)=xa_new;
deltax(ii)=xa_in-xa_new(end);

%% Air thermal balance

% Building the matrix
B1=v_air./dz/eps;
B2=h_a.*a_f./rho_a./cp_a/eps;
sub_th=-dt.*B1;
main_th=(1+dt*(B1+B2));
Mb=spdiags([sub_th main_th],-1:0,length(zz),length(zz));
```

```
    Qb=Ta_old+dt.*B2.*Ts_old;

    % Boundary conditions
    Mb(1,1)=1;
    Mb(1,2)=0;
    Qb(1)=Ta_in;

    % Solution
    Ta_new=Mb\Qb;
    Ta(:,ii)=Ta_new;
    deltaT(ii)=Ta_in-Ta_new(end);


    %% Silica gel thermal balance

    %  Silica-gel specific heat
    cp_s=cp_sio2(w_old);                                % [J/kg/K]

    %Fin efficiency coefficients
    mm=sqrt(2.*h_a./k_cu./delta);                       % [1/m]
    eta_f=tanh(mm.*lf)./mm./lf;                         % [-]
    %Global fin efficiency
    eta_0=1-Af/A_tot*(1-eta_f);                         % [-]
    %Inner thermal resistance - water side
    Ri=1./h_w./Ai;                                      % [K/W]
    % Pipes thermal resistance
    Rmid=log(Do/Di)./2./pi./lp./k_cu;                   % [K/W]
    % Silica-gel thermal resistance
    Ro=delta_s./k_s/A_tot./eta_0;                       % [K/W]
    % total thermal resistance
    RR=Ri+Rmid+Ro;                                      % [K/W]
    %Global heat exchange coefficient
    UU=1./A_tot./RR;                                    % [W/m^2K]

    %Coefficients
    C1=Had.*Kg.*a_s./rho_s./cp_s/(1-eps);
    C2=h_a.*a_f./rho_s./cp_s/(1-eps);
    C3=UU.*a_f./rho_s./cp_s/(1-eps);

    % Solution
    Ts_new=(Ts_old+dt.*C1.*(xa_old-
x_eq)+dt.*C2.*Ta_old+dt.*C3.*Tw_old)./(1+dt.*C2+dt.*C3);
    Ts(:,ii)=Ts_new;


    %% Water loop thermal balance

    %Building the matrix
    D1=Gw./rho_w./Ab/dz;
    D2=UU.*a_f./rho_w./cp_w;
    sub_w=-(dt*D1)*ones(size(zz));
    main_w=(1+dt.*D1+dt.*D2);
    Md=spdiags([sub_w main_w],-1:0,length(zz),length(zz));

    % Boundary conditions
    Md(1,1)=1;
    Md(1,2)=0;
```

```
    % Solution
    Qd=Tw_old+dt.*D2.*Ts_old;
    Qd(1)=Tm_s;
    Tw_new=Md\Qd;
    Tw(:,ii)=Tw_new;


%% Updating values

    w_old=w_new;
    xa_old=xa_new;
    Ta_old=Ta_new;
    Ts_old=Ts_new;
    Tw_old=Tw_new;

%% Parameters calculation

    if pp==1

    tt(kk)=time(ii);

    % Air enthalpy variation
    deltah(kk)=(h_air(xa_in,Ta_in)-h_air(xa_new(end),Ta_new(end)));
    deltah_sens(kk)=h_sens(Ta_new(1))-h_sens(Ta_new(end));
    deltah_lat(kk)=h_lat(xa_new(1),Ta_new(1))...
        -h_lat(xa_new(end),Ta_new(end));

    %Air fan efficiency
    eta_fan=0.45*0.95;                  % [-]
    %Water pump efficiency
    eta_pump=0.65*0.95;                 % [-]
    % Air fan -  electric power
    FP=PD*Ga/rho_a(1)/eta_fan;          %[W]


    if rig(ii)==0

        if deltax(ii)>0
            dx=dx+deltax(ii)*dt;
        end

        if deltah(kk)>0
        %Total cooling power
        Cool(kk)=deltah(kk)*Ga;
        else
        Cool(kk)=0;
        end

        if deltah_sens(kk)>0
        %Sensible cooling power
        Cool_sens(kk)=deltah_sens(kk)*Ga;
        else
        Cool_sens(kk)=0;
        end

        if deltah_lat(kk)>0
```

```
        %Latent cooling power
        Cool_lat(kk)=deltah_lat(kk)*Ga;
        else
        Cool_lat(kk)=0;
        end

    %Integrated cooling power
    cc=cc+Cool(kk)*dt/3600;                    % [Wh]
    %Temperature difference at the heat pump evaporator
    DT=5;                                      % [¬∞C]
    %Heat pump COP
    COP_hp=(Tm_s-DT+273)/(Tamb-Tm_s+DT)*0.5;     % [-]
    % Heat pump required electric energy
    HP(kk)=Gw*cp_w*(Tw_new(end)-Tm_s)/COP_hp;    % [W]
    %Pump electric power - adsorption
    PP_ads=PDw*Gw/rho_w/eta_pump;          %[W]
    %Regeneration heat
    Heat(kk)=0;


    else

    Cool(kk)=0;
    Cool_sens(kk)=0;
    Cool_lat(kk)=0;
    %Temperature difference at the heat pump condenser
    DT=5;
    COP_hp=(Tm_s+DT+273)/(Tm_s+DT-Tamb)*0.5;
    HP(kk)=Gw*cp_w*(-Tw_new(end)+Tm_s)/COP_hp;
    %Pump electric power - regeneration
    PP_reg=PDw*Gw/rho_w/eta_pump;           %[W]
    Heat(kk)=Gw*cp_w*(Tm_s-Tw_new(end));

    end

    %Integrated values
    fan=fan+PD*Ga/rho_a(1)/eta_fan*dt/3600;    % [Wh]
    pump=pump+PDw*Gw/rho_w/eta_pump*dt/3600;   % [Wh]
    hp=hp+HP(kk)*dt/3600;                      % [Wh]
    ht=ht+Heat(kk)*dt/3600;                    % [Wh]

    %Instant electric COP
    COP_inst(kk)=Cool(kk)/(PP_ads+FP+HP(kk));     % [-]

    kk=kk+1;

    end
end

%Average electric COP
COP_ave=cc/(fan+hp+pump);                      % [-]
%Thermal COP
COP_th=cc/ht;                                  % [-]
%Average moisture removed
avedx=dx/ads_time/3600;                       % [kg_v/kg_a]
```